

# MEASURING QUANTUM STATE IN PHASE SPACE

KONRAD BANASZEK

Rozprawa doktorska przygotowana  
w Instytucie Fizyki Teoretycznej  
Uniwersytetu Warszawskiego  
pod kierunkiem Prof. Krzysztofa  
Wódkiewicza



Wydział Fizyki  
Uniwersytet Warszawski  
Warszawa 1999



# Contents

<b>1</b>	<b>Introduction</b>	<b>3</b>
<b>2</b>	<b>Phase space representations of quantum state</b>	<b>9</b>
2.1	Wigner function . . . . .	9
2.2	Quasidistribution functions . . . . .	11
2.3	Quantum interference in phase space . . . . .	13
2.4	Deconvolution . . . . .	15
2.5	Multimode quasidistributions . . . . .	16
2.6	Quasidistribution functionals . . . . .	17
<b>3</b>	<b>Homodyne techniques for quantum state measurement</b>	<b>21</b>
3.1	Balanced homodyne detector . . . . .	22
3.2	Double homodyne detection . . . . .	25
3.3	Optical homodyne tomography . . . . .	27
3.4	Random phase homodyne detection . . . . .	30
<b>4</b>	<b>Direct probing of quantum phase space</b>	<b>33</b>
4.1	Wigner function and photon statistics . . . . .	34
4.2	Phase space picture . . . . .	36
4.3	Generalization . . . . .	38
4.4	Multimode approach . . . . .	40
4.5	Examples of photocount statistics . . . . .	42
<b>5</b>	<b>Practical aspects</b>	<b>47</b>
5.1	Photon count generating function . . . . .	48
5.2	Statistical error . . . . .	48
5.3	Compensation of detector losses . . . . .	50
5.4	Mode mismatch . . . . .	55

<b>6</b>	<b>Experiment</b>	<b>59</b>
6.1	Principle . . . . .	60
6.2	Setup . . . . .	60
6.3	Results . . . . .	62
6.4	Discussion . . . . .	63
<b>7</b>	<b>Statistical uncertainty in photodetection measurements</b>	<b>67</b>
7.1	Statistical analysis of experiment . . . . .	69
7.2	Phase-insensitive detection of a light mode . . . . .	73
7.2.1	Direct photon counting . . . . .	74
7.2.2	Random phase homodyne detection . . . . .	78
7.3	Consequences for quantum state measurement . . . . .	81
<b>8</b>	<b>Conclusions</b>	<b>85</b>
	<b>Bibliography</b>	<b>87</b>

# Chapter 1

## Introduction

The development of quantum mechanics was connected with one of the greatest conceptual leaps in theoretical physics. In order to describe properly microscopic phenomena, it was necessary to abandon the classical notion of a physical property, and to resort to a completely new formalism representing microobjects. This formalism lies at the heart of quantum mechanics. It makes a clear distinction between the state of a physical system, and the performed observation. The state is characterized by a wave function, whose time evolution is governed by an appropriate equation of motion (e.g. the Schrödinger equation for a nonrelativistic particle). If we want to relate the state to quantities observed in an experiment, we need to use the second element of the quantum mechanical formalism, i.e. the representation of the measuring apparatus in terms of operators acting on the wave function. According to the Born interpretation, quantum mechanics provides probabilistic predictions concerning the behaviour of a quantum system [1]. Quantum description of an experiment specifies only the chance that the measurement will yield a given outcome. In order to verify such predictions, we need to repeat the measurement many times on identically prepared systems, and then to compare the histogram of experimental outcomes with the probability distribution calculated from the theory. The result of a single measurement cannot be described in a deterministic way. This randomness seems to be a very fundamental feature of the microworld. So far, all attempts to introduce deterministic description of microscopic phenomena have failed, and experiments have ruled out whole classes of theories alternative to quantum mechanics.

Pictorially speaking, the click on a measuring apparatus is only a faint shadow of the quantum state, which stays hidden behind the scene, though being the main actor. However, one might ask if it is possible to reveal experimentally the complete information on the state of a quantum system. This cannot be the case if we are given only a single copy of the system. Any measurement consists in a certain kind of interaction between the system and the detecting apparatus. This interaction maps some properties of the measured system onto the state of the apparatus, and makes them accessible to our cognition. After the measurement, the state of the system is perturbed by the interaction with the detector, and it is no longer described by the original wave

function. For example, observation of the position of a particle by scattering photons inevitably modifies its momentum. The deleterious character of quantum measurement was realized very early in the development of quantum mechanics, and it is closely related to the Heisenberg uncertainty principle [2]. Thus, our system can be detected only once, and we cannot gain more information by repeating the measurement. One might try to circumvent this difficulty by designing a single measurement that would yield complete information on the quantum state. Such a measurement would map each possible state of the system onto a different, fully distinguishable state of the apparatus. This means that all the final states of the apparatus would have to be mutually orthogonal, even these corresponding to nonorthogonal initial states of the measured system. Of course, this would violate unitarity of quantum evolution, and such a measurement does not exist. One could also consider cloning of quantum states, i.e. an operation that would generate two or more identical copies from a given system. Then, one could increase the amount of information by performing measurements on the reproduced copies. Such a strategy fails because of the no-cloning theorem [3], which is a simple consequence of the quantum superposition principle.

Nevertheless, no principles of quantum mechanics prevent us from characterizing the quantum state of an *ensemble* of physical systems. By repeating the measurement many times on individual copies, we may arrive at reliable information on the properties of the ensemble. The aim of quantum state measurement can be formulated in technological terms: suppose we have a machine producing identically prepared copies of a quantum system. When delivering this output for some application, we should be able to provide its specification, which on the most complete level means a full characterization of the quantum state. Such a problem, apart from interesting fundamental aspects, is currently of practical interest in many areas of science. This is due to extensive studies devoted presently to preparation, manipulation, and control of quantum systems. The motivation of this research is to overcome current technological limitations by exploiting fully possibilities offered by quantum mechanics. Let us mention just few examples. The yield of chemical reactions can be increased by controlling the quantum state of reactants [4]. Application of so-called squeezed states of light improves precision of interferometric measurements, which can be used to enhance sensitivity of gravitational wave detectors [5]. Coherent preparation and manipulation of entangled multiparticle systems can be used to solve computational problems intractable by classical computers [6]. An important matter in developing these and other technologies is the possibility to gain extensive and reliable information on the state of quantum systems. The ultimate tool for this purpose is the measurement of the complete quantum state.

When characterizing ensembles, we usually need to take into account the possibility of statistical fluctuations, and to describe their state using the more general concept of the density matrix rather than a wave function. From the formal point of view, the task of characterizing the quantum state can be accomplished by a set of appropriately chosen measurements, which would extract unambiguous information on all the elements of the density matrix. The crucial

question, however, is: how to do this in practice? The challenge of quantum state measurement has several important aspects. The first one is design and realisation of measurement schemes that yield complete characterization of the quantum state. Further, there is a nontrivial task of extracting precise information on the quantum state from data collected in a realistic, imperfect experimental setup. Finally, we have said above that expectation values of a sufficiently large set of observables contain complete information on the density matrix. The problem is that true expectation values are obtained only in the limit of the infinite number of measurements. In a real laboratory we always deal with *finite* ensembles, and this is our source of information on the quantum state, which we would like to use as efficiently as possible.

In quantum optics and related fields, several examples of simple quantum systems have been thoroughly studied, including a single light mode, a trapped ion, and a diatomic molecule. A lot of interest has been paid to detection of subtle quantum statistical effects. It was therefore natural that the domain of quantum state measurement has grown mainly on the ground of advances in quantum optics. In 1993, the group of Michael Raymer at the University of Oregon demonstrated complete experimental characterization of the quantum state of a single light mode by means of optical homodyne tomography [7]. This seminal experiment was followed by extensive research in the field of quantum state measurement. Over past several years, we have witnessed a series of beautiful experiments with various quantum systems [8]. The vibrational state of a diatomic molecule has been reconstructed from measurements of the time-dependent fluorescence spectrum [9]. Optical homodyne tomography has been applied to reconstruct a whole gallery of squeezed states of light [10]. The motional state of a trapped ion has been characterized using a very sophisticated technique based on the monitoring of the fluorescence [11]. The tomographic method has been used to measure the transverse motional state of an atomic beam [12]. All these experiments were tightly connected with the rapid theoretical development of the domain of quantum state measurement. Numerous measurement schemes have been proposed and analysed in detail. In particular, the role of statistical uncertainty has been discussed, and various approaches to reconstructing quantum state representations from experimental data have been described.

The subject of this thesis is the measurement of the quantum state in the phase space. The concept of the phase space provides a bridge between the quantum mechanical formalism and classical physics. Predictions of quantum mechanics have essentially statistical character. As a rule, one can predict only probabilities of obtaining specific outcomes of a measurement. Such a situation can be encountered in classical mechanics as well. For example, if we deal with an ensemble of classical systems, properties of a single copy can be defined only in statistical terms. The state of the ensemble is characterized by a phase space distribution, which describes the probability of occupying a given volume element by the system. One may wonder whether this intuitive picture of fluctuations has its counterpart in quantum physics. The answer to this question is not straightforward. It is possible to convert the quantum mechanical formalism into a form which resembles a classical statistical theory. The first phase space representation

of the quantum state was introduced in 1932 by Wigner [13]. However, such a phase space representation is not unique: noncommutativity of quantum observables leads to abundance of quantum analogs of the phase space distribution, and none of them captures all the properties of the classical object [14]. This is a manifestation of the fact that quantum mechanics is essentially different from a classical theory. Nevertheless, quantum phase space quasidistributions contain complete information on the quantum state. The family of quasidistribution functions provides a convenient framework for studying many quantum optical problems. It is also a useful tool in visualising quantum coherence and interference phenomena.

For a long time, quantum quasidistribution functions have been considered mainly as a quite odd theoretical concept rather than a quantity which can be measured in a feasible experimental scheme. This perspective changed completely with the demonstration of optical homodyne tomography, which brought quasidistributions, in particular the Wigner function, to the realm of a physical laboratory. Optical homodyne tomography is based on the observation that marginal distributions of the Wigner function of a light mode can be measured by means of homodyne detection. The inverse problem, i.e. the retrieval of the Wigner function from its projections, is similar to the procedure used in medical imaging, where the spatial distribution of the tissue is reconstructed from absorption measured across the body. Practical implementation of the reconstruction algorithm is a rather complex and delicate matter: the back-projection transformation is singular, and its application to experimental data has to be accompanied by a special filtering procedure. Demonstration of optical homodyne tomography was a successful combination of a precise quantum optical measurement with sophisticated data processing.

In this work we develop a novel, entirely different approach to measuring quasidistribution functions of light. We exploit the fact that the value of a quasidistribution at a given point of the phase space is itself a well defined quantum observable. Motivated by this representation, we propose and demonstrate an optical scheme for measuring *directly* quasidistribution functions. This method, based on photon counting, avoids the detour via complex numerical reconstruction algorithm. The basic elements of our measurement scheme are very simple. The light mode whose quantum state we want to measure is interfered with an auxiliary coherent probe field, and a photon counting detector is used to measure the photocount statistics of the superposed fields. We show that a simple arithmetic operation performed on the measured photocount statistics yields directly the value of the quasidistribution at a point defined by the amplitude and the phase of the probe field. By changing these two parameters of the probe field, we may scan the complete phase space, and obtain the full representation of the quantum state of the measured light mode. We demonstrate an experimental realisation of this scheme, and present measurements of the Wigner function for several quantum states of light. The experimental part of this thesis has been performed in Division of Optics, Institute of Experimental Physics, Warsaw University, in collaboration with Prof. Czesław Radzewicz.

We shall study here in detail various aspects of the direct scheme for measuring quasidistribution functions. On the practical side, there is a question about the role of typical experimental

imperfections. We shall analyse how the result of the measurement is affected by such factors as non-unit detection efficiency and imperfect interference visibility. We shall also provide estimates for statistical error, which are necessary to design an accurate experiment, and to specify confidence of the experimental outcome. These theoretical results will be an important tool for quantitative analysis of the performed experiment. In addition, our discussion of practical aspects has interesting consequences in the recently disputed problem of compensating for detector losses in photodetection measurements. Over past several years, there were conflicting claims concerning the possibility of removing deleterious effects of imperfect detection by appropriate numerical processing of experimental data [15, 16, 17]. Our measurement scheme provides a testing ground for this problem. We will show that in general no compensation for detection losses is possible, unless some *a priori* knowledge about the measured quantum state is given. Discussion of this problem reveals the fundamental role of statistical uncertainty in realistic quantum measurements, which results from the fact that in a laboratory we always deal with finite ensembles.

An attractive feature of the presented approach to measuring quasidistribution functions of a single light mode is the direct link between the measured observable and the quantum state representation. One may wonder whether this approach can be applied in other situations. We shall describe here a generalization of the measurement scheme to multimode radiation. We shall demonstrate that multimode quasidistribution functions are also directly related to the photocount statistics, and that they can be determined in an equally simple way. Although our interest in this thesis will be confined to detection of optical radiation, it should be noted that the idea underlying our measurement scheme has proven to be fruitful in the measurement of the vibrational state of a trapped ion [11]. It has also motivated measurement schemes for a cavity mode [18] and a diatomic molecule [19].

This thesis is organized as follows. In Chap. 2 we review phase space representations of the quantum state. Starting from the definition of the Wigner function, we show how this distribution can be unified with other phase space representations, and we discuss properties of generalized *s*-ordered quasidistribution functions. In Chap. 3 we review briefly previous work on measuring the quantum state of light. We present two techniques which have been realized in experiments: optical homodyne tomography and balanced homodyne detection. Next, in Chap. 4, we introduce the direct method for measuring quasidistribution functions of light. We present the phase space picture of the measurement, and we develop the multimode theory of the scheme. Various practical aspects of the proposed measurement are discussed in Chap. 5, including the effects of imperfect detection, and the possibility of compensation for detector losses. In Chap. 6 we present experimental realization of the proposed scheme, and demonstrate the direct measurement of the Wigner function of a single light mode. The issue of statistical uncertainty in photodetection measurements is discussed from a more general point of view in Chap. 7. We show that the statistical noise sometimes limits available information on the quantum state. Finally, Chap. 8 concludes the thesis. Major part of original results presented in this thesis has been

published in the following articles:

- K. Banaszek and K. Wódkiewicz,  
*Direct probing of quantum phase space by photon counting*,  
*Phys. Rev. Lett.* **76**, 4344 (1996).
- K. Banaszek and K. Wódkiewicz  
*Accuracy of sampling quantum phase space in a photon counting experiment*,  
*J. Mod. Opt.* **44**, 2441 (1997).
- K. Banaszek, C. Radzewicz, K. Wódkiewicz, and J. S. Krasiński,  
*Direct measurement of the Wigner function by photon counting*,  
*Phys. Rev. A* **60**, 674 (1999).
- K. Banaszek,  
*Statistical uncertainty in quantum-optical photodetection measurements*,  
*J. Mod. Opt.* **46**, 675 (1999).

## Acknowledgements

First and foremost, I thank my supervisor, Prof. Krzysztof Wódkiewicz, for guiding me throughout my PhD studies, and for providing numerous comments and suggestions on drafts of this thesis. It has been both a pleasure and a privilege to share his enthusiasm for scientific research. I am also indebted to Prof. Czesław Radzewicz and Prof. Jerzy S. Krasiński, with whom I collaborated on the experiment, for teaching me how things *really* work. My special thanks go to Prof. Kazimierz Rzążewski and Prof. Jan Mostowski. I owe them my first encounters with quantum optics.

Some of the results presented in this thesis were obtained during my stay in Laser Optics and Spectroscopy Group at Imperial College, London. I would like to thank the Head of the Group, Prof. Peter L. Knight FRS, as well as all its members, for making my stay so fruitful and enjoyable. In understanding foundations of quantum state measurement, I have benefited a lot from the visit at Università di Pavia, and collaboration with Prof. G. Mauro D'Ariano, Dr. Matteo Paris, and Dr. Massimiliano Sacchi.

Finally, I would like to thank the Foundation for Polish Science for the Domestic Grant for Young Scholars.

# Chapter 2

## Phase space representations of quantum state

In the standard formulation of quantum mechanics, the quantum state is characterized by a vector from the Hilbert space describing the physical system. The state vector is related to measurable quantities by evaluating expectation values with operators which represent observables. This formalism is very far from a classical, intuitive picture of statistical fluctuations. Nevertheless, there is a possibility to transform the standard quantum mechanical formalism into the form which resembles a classical statistical theory. Such a representation is particularly useful in investigating the classical limit of quantum mechanics. The fundamental role in this approach is played by quasidistribution functions, which can be regarded as quantum analogs of a phase space probability distribution. However, due to noncommutativity of quantum observables, the phase space representation of the quantum state is not unique, and it is not possible to have in quantum mechanics a phase space distribution that has all the properties of the classical one.

### 2.1 Wigner function

In 1932, Eugene Wigner [13] introduced a quantum analog of the classical phase space probability distribution. For a particle travelling along one dimension, the Wigner function is related to the wave function  $\psi(x)$  through the formula:

$$W(q, p) = \frac{1}{2\pi\hbar} \int dx \psi^*(q + x/2) e^{ipx/\hbar} \psi(q - x/2), \quad (2.1)$$

and it completely characterizes the quantum state. The integral of  $W(q, p)$  over  $q$  and  $p$  is one, which follows from the normalization of the wave function. Expectation values of quantum observables can be obtained from the Wigner function by integrating it with appropriate Wigner-Weyl expressions representing these observables [14]. Furthermore, marginals of the Wigner function yield quantum mechanical distributions for the position and the momentum. However,

the Wigner function has one property which manifests that quantum mechanics is distinct from a classical statistical theory: the Wigner function can take negative values. We shall see later that this property is closely related to quantum interference phenomena.

Difficulties with defining the quantum phase space distribution have their origin in the non-commutativity of quantum observables. As the position and momentum operators do not commute, we cannot introduce a joint distribution of these two observables. This problem is closely related to the issue of the ordering of observables, which appears when passing from classical to quantum mechanics. For example, the classical expression  $qp$  has the following nonequivalent quantum counterparts:  $\hat{q}\hat{p}$ ,  $\hat{p}\hat{q}$ , or  $\frac{1}{2}(\hat{q}\hat{p} + \hat{p}\hat{q})$ . The Wigner function corresponds to a specific, symmetric ordering of the position and momentum operators, called the Weyl ordering [20]. We will now transform Eq. (2.1) to the form which shows explicitly relation between the Wigner function and the symmetric ordering of the position and momentum operators. For this purpose, let us introduce an additional delta function and represent it in an integral form:

$$\begin{aligned} W(q, p) &= \frac{1}{2\pi\hbar} \int dx \int dy e^{ipx/\hbar} \delta(y - q - x/2) \psi^*(y) \psi(y - x) \\ &= \frac{1}{(2\pi\hbar)^2} \int dx \int dy \int dk e^{ipx/\hbar} e^{i(y-q-x/2)k/\hbar} \psi^*(y) \psi(y - x) \\ &= \frac{1}{(2\pi\hbar)^2} \int dx \int dk e^{i(px-kq)/\hbar} \int dy e^{ikx/2\hbar} \psi^*(y) e^{ik(y-x)/\hbar} \psi(y - x). \end{aligned} \quad (2.2)$$

In the last expression, the integral over  $y$  can be written as the quantum expectation value:

$$\int dy e^{ikx/2\hbar} \psi^*(y) e^{ik(y-x)/\hbar} \psi(y - x) = \langle \psi | e^{i(k\hat{q} - \hat{p}x)/\hbar} | \psi \rangle. \quad (2.3)$$

This quantity is a function of two real parameters  $k$  and  $x$ . By differentiating over  $k$  and  $x$  we may obtain moments of the position and momentum operators. These moments are ordered symmetrically in  $\hat{q}$  and  $\hat{p}$ , which follows from the form of the exponent in Eq. (2.3). The function  $\langle \psi | e^{i(k\hat{q} - \hat{p}x)/\hbar} | \psi \rangle$  is called the Wigner-Weyl ordered characteristic function for the position and the momentum. Coming back to Eq. (2.2), we finally arrive at the formula

$$W(q, p) = \frac{1}{(2\pi\hbar)^2} \int dx \int dk e^{i(px-kq)/\hbar} \langle \psi | e^{i(k\hat{q} - \hat{p}x)/\hbar} | \psi \rangle \quad (2.4)$$

which shows that the Wigner function is the Fourier transform of the symmetrically ordered characteristic function for the position and the momentum. Eq. (2.4) can be used to evaluate the Wigner function corresponding to a mixed state described by the density matrix  $\hat{\rho}$ . In such a case, we have to replace  $\langle \psi | e^{i(k\hat{q} - \hat{p}x)/\hbar} | \psi \rangle$  by  $\text{Tr}(\hat{\rho} e^{i(k\hat{q} - \hat{p}x)/\hbar})$ . Equivalently, the Wigner function of a mixed state can be obtained from a weighted sum of the Wigner functions describing the pure components of the mixed state.

For a harmonic oscillator, it is convenient to introduce a pair of dimensionless annihilation and creation operators, defined by the equations:

$$\hat{a} = \frac{1}{\sqrt{2}}(\lambda^{-1}\hat{q} + i\lambda\hbar^{-1}\hat{p}), \quad \hat{a}^\dagger = \frac{1}{\sqrt{2}}(\lambda^{-1}\hat{q} - i\lambda\hbar^{-1}\hat{p}) \quad (2.5)$$

where  $\lambda$  is a natural length scale defined by the mass and the frequency of the oscillator. Analogously, the two real parameters of the Wigner function can be combined into a single complex argument  $\alpha = (\lambda^{-1}q + i\lambda\hbar^{-1}p)/\sqrt{2}$ . The Wigner function in this parameterization is given by

$$W(\alpha) = \frac{1}{\pi^2} \int d^2\zeta e^{\zeta^* \alpha - \zeta \alpha^*} \langle e^{\zeta \hat{a}^\dagger - \zeta^* \hat{a}} \rangle \quad (2.6)$$

where the integration is performed over the whole complex plane and the angular brackets  $\langle \dots \rangle$  denote the quantum expectation value. Let us note, that the normalization constant in Eq. (2.6) has changed compared to Eq. (2.4). This is because the integration measure over the phase space is now equal to  $d^2\alpha = dq dp/2\hbar$ .

The physical system which we shall describe in the phase space representation, is optical radiation. In the standard procedure of quantization, the electromagnetic field is decomposed into a set of independent modes. Each of these modes is characterized by a pair of creation and annihilation operators, which satisfy bosonic commutation relations for a harmonic oscillator. When only one of the modes is excited, we may describe its quantum state using the Wigner function defined in Eq. (2.6). In the classical limit, the parameter  $\alpha$  characterizes the complex amplitude of the field, expressed in dimensionless units. We may also use the single-mode description if our measuring apparatus is sensitive only to a selected mode of the detected radiation.

## 2.2 Quasidistribution functions

As it is clearly seen from Eq. (2.6), the Wigner function corresponds to the characteristic function with the symmetric ordering of the creation and annihilation operators. In principle, we could consider also other orderings, for example normal or antinormal. In the normal ordering all creation operators are placed before annihilation operators, and vice versa for the antinormal ordering. Thus, we could think of replacing the quantum expectation value in Eq. (2.6) by the normally ordered characteristic function  $\langle e^{\zeta \hat{a}^\dagger} e^{-\zeta^* \hat{a}} \rangle$ , or by the antinormally ordered one  $\langle e^{-\zeta^* \hat{a}} e^{\zeta \hat{a}^\dagger} \rangle$ . These and other possibilities can be written jointly in a very elegant way by introducing an exponential factor, which defines the ordering of the creation and annihilation operators. This idea leads to the concept of more general  $s$ -parameterized quasiprobability distributions. The one-parameter family of quasidistribution functions is given by the following formula [21]:

$$W(\alpha; s) = \frac{1}{\pi^2} \int d^2\zeta e^{s|\zeta|^2/2 + \zeta^* \alpha - \zeta \alpha^*} \langle e^{\zeta \hat{a}^\dagger - \zeta^* \hat{a}} \rangle. \quad (2.7)$$

The real parameter  $s$  is associated with the ordering of the field bosonic operators through the exponential factor  $\exp(s|\zeta|^2/2)$ . In particular, it can which can be easily checked using the Baker-Campbell-Haussdorf formula that three values  $s = 1, 0$ , and  $-1$  generate the normal, symmetric and antinormal ordering, respectively.

The definition given by Eq. (2.7) unifies the Wigner function with other, independently developed quantum analogs of a phase space distribution. For instance, normal ordering corresponds to the so-called  $P$  function, introduced by Glauber [22] and Sudarshan [23]. This function serves as a weight function in the diagonal coherent state representation for the density matrix  $\hat{\rho}$ :

$$\hat{\rho} = \int d^2\alpha P(\alpha) |\alpha\rangle\langle\alpha|. \quad (2.8)$$

On the other hand, antinormal ordering yields the distribution known as the Husimi [24] or  $Q$  function [25, 26], which is given by the diagonal elements of the density matrix in the coherent state basis:

$$Q(\alpha) = \frac{1}{\pi} \langle \alpha | \hat{\rho} | \alpha \rangle. \quad (2.9)$$

Properties of various  $s$ -parameterized quasidistribution functions are quite different. This can be seen using the three examples of the  $P$  function, the Wigner function, and the  $Q$  function. The  $P$  function is highly singular for nonclassical states of light. For example, it is given by derivatives of the delta function for eigenstates of the photon number operator  $\hat{a}^\dagger \hat{a}$ . The Wigner function is well behaved for all states, but it may take negative values. Finally the  $Q$  function is always positive definite, which follows directly from Eq. (2.9). The fact that quasidistribution functions with lower ordering are more regular reflects a general relation linking any two differently ordered quasidistributions via convolution with a Gaussian function in the complex phase space:

$$W(\alpha; s') = \frac{2}{\pi(s - s')} \int d^2\beta \exp\left(-\frac{2|\alpha - \beta|^2}{s - s'}\right) W(\beta; s), \quad (2.10)$$

where  $s > s'$ . Thus the lower the ordering, the smoother the quasidistribution is, and fine details of the function are not easily visible. The Gaussian exponent appearing in the above equation can be formally regarded as a propagator for the diffusion equation, with the ordering parameter playing the role of the time. Following this analogy, we may write a differential equation for quasidistribution functions corresponding to a given quantum state:

$$\frac{\partial}{\partial s} W(\alpha; s) = -\frac{1}{2} \frac{\partial^2}{\partial \alpha \partial \alpha^*} W(\alpha; s). \quad (2.11)$$

Let us note that the above equation differs from the standard diffusion equation by the minus sign. This difference originates from the fact, that the “diffusion” of quasidistributions follows in the direction of decreasing  $s$ .

In our calculations a normally ordered representation of the quasidistribution functions will be very useful. Introducing normal ordering of the creation and annihilation operators in Eq. (2.7) allows to perform the integral explicitly, which yields:

$$W(\alpha; s) = \frac{2}{\pi(1-s)} \left\langle : \exp\left(-\frac{2}{1-s}(\hat{a}^\dagger - \alpha^*)(\hat{a} - \alpha)\right) : \right\rangle. \quad (2.12)$$

Thus the  $s$ -ordered quasidistribution function at a complex phase space point  $\alpha$  is given by the expectation value of the operator

$$\hat{W}(\alpha; s) = \frac{2}{\pi(1-s)} : \exp\left(-\frac{2}{1-s}(\hat{a}^\dagger - \alpha^*)(\hat{a} - \alpha)\right) : \quad (2.13)$$

Using the operator identity [27]

$$: \exp[(e^{i\zeta} - 1)\hat{v}^\dagger \hat{v}] : = \exp(i\zeta \hat{v}^\dagger \hat{v}) \quad (2.14)$$

valid for an arbitrary bosonic annihilation operator  $\hat{v}$ , we may transform Eq. (2.13) to the following expression:

$$\hat{W}(\alpha; s) = \frac{2}{\pi(1-s)} \left(\frac{s+1}{s-1}\right)^{(\hat{a}^\dagger - \alpha^*)(\hat{a} - \alpha)}. \quad (2.15)$$

The operator appearing in the exponent is the displaced photon number operator  $\hat{n} = \hat{a}^\dagger \hat{a}$ . Using the standard displacement operator  $\hat{D}(\alpha) = \exp(\alpha \hat{a}^\dagger - \alpha^* \hat{a})$ , we may write  $\hat{W}(\alpha; s)$  as [28, 29]:

$$\begin{aligned} \hat{W}(\alpha; s) &= \frac{2}{\pi(1-s)} \hat{D}(\alpha) \left(\frac{s+1}{s-1}\right)^{\hat{n}} \hat{D}^\dagger(\alpha) \\ &= \frac{2}{\pi(1-s)} \sum_{n=0}^{\infty} \left(\frac{s+1}{s-1}\right)^n \hat{D}(\alpha) |n\rangle \langle n| \hat{D}^\dagger(\alpha). \end{aligned} \quad (2.16)$$

The last form is simply the spectral decomposition of  $\hat{W}(\alpha; s)$ . The eigenvectors are displaced Fock states  $\hat{D}(\alpha) |n\rangle$ , and the corresponding eigenvalues are  $[(s+1)/(s-1)]^n$  times the front normalization factor  $2/\pi(1-s)$ . It is instructive to see, how the properties of the quasidistributions are reflected by the spectrum of  $\hat{W}(\alpha; s)$ . First, let us note that for  $s \rightarrow 1$ , the factor  $(s+1)/(s-1)$  is divergent; this corresponds to the singular character of the  $P$  representation. For  $0 < s < 1$  the set of eigenvalues is unbounded; therefore, the corresponding quasidistributions also may exhibit singular behaviour. The operator  $\hat{W}(\alpha; s)$  becomes bounded for  $s \leq 0$ , and the highest value, i.e.  $s = 0$ , corresponds to the Wigner function. Even when  $\hat{W}(\alpha; s)$  is bounded, its eigenvalues corresponding to odd  $ns$  can be negative. The highest value of  $s$  for which all the eigenvalues are nonnegative is  $s = -1$ , which corresponds to the  $Q$  function.

## 2.3 Quantum interference in phase space

We will now discuss, using a simple example, how quantum interference phenomena are visualised in the phase space representation. A quantum analog of a classical field with well defined amplitude and phase is the coherent state  $|\alpha_0\rangle$ , defined as an eigenstate of the annihilation operator  $\hat{a}|\alpha_0\rangle = \alpha_0|\alpha_0\rangle$ . This equivalence originates from the fact, that full quantum theory of

photodetection gives for coherent states the same predictions as semiclassical theory with quantized detector and classical electromagnetic fields [30]. Coherent states are represented in the phase space by Gaussians

$$\hat{W}^{|\alpha_0\rangle}(\alpha; s) = \frac{2}{\pi(1-s)} \exp\left(-\frac{2}{1-s}|\alpha - \alpha_0|^2\right). \quad (2.17)$$

Quantum mechanics allows one to combine two such classical-like state, for example  $|\alpha_0\rangle$  and  $|-\alpha_0\rangle$  into a coherent superposition

$$|\psi\rangle = \frac{1}{\sqrt{2(1 + e^{-2|\alpha_0|^2})}}(|\alpha_0\rangle + |-\alpha_0\rangle). \quad (2.18)$$

States of this type illustrate quantum coherence and interference between classical-like components, and are often called quantum optical Schrödinger cats [31]. In contrast to coherent states, they exhibit a variety of nonclassical properties [32]. The quasidistribution function of the superposition  $|\psi\rangle$  is given by the formula

$$\begin{aligned} W^{|\psi\rangle}(\alpha; s) = & \frac{1}{\pi(1-s)(1 + e^{-2|\alpha_0|^2})} \left[ \exp\left(-\frac{2}{1-s}|\alpha - \alpha_0|^2\right) \right. \\ & + \exp\left(-\frac{2}{1-s}|\alpha + \alpha_0|^2\right) \\ & \left. + 2 \exp\left(\frac{2s}{1-s}|\alpha_0|^2\right) \exp\left(-\frac{2}{1-s}|\alpha|^2\right) \cos\left(\frac{4\text{Im}(\alpha_0\alpha^*)}{1-s}\right) \right]. \end{aligned} \quad (2.19)$$

The first two terms in the square brackets describe the two coherent components. The last term results from quantum interference between these components. It contains an oscillating factor  $\cos[4\text{Im}(\alpha_0\alpha^*)/(1-s)]$ . It is seen that the frequency of the oscillations grows with the distance between the coherent components. The envelope of this oscillating term is defined by the Gaussian  $\exp[-2|\alpha|^2/(1-s)]$ , which is centered exactly half way between the interfering states.

Fig. 2.1 shows quasidistributions plotted for three different values of the ordering parameter  $s$ . The Wigner function contains an oscillating component originating from the interference between the coherent states. This component is much smaller for  $s = -0.1$  and it is completely smeared out in the  $Q$  function, which can hardly be distinguished from that of a statistical mixture of two coherent states. This is because the whole interference term is multiplied by the factor  $\exp[2s|\alpha_0|^2/(1-s)]$ , which quickly tends to zero with decreasing  $s$ . Let us note that the larger is the distance between the components, the faster this factor vanishes. The decay of the interference component can be formally viewed as a result of diffusion, described by Eq. (2.11). Decreasing the ordering parameter  $s$  makes the whole quasidistribution blurred, and this effect is particularly deleterious to the quickly oscillating pattern.

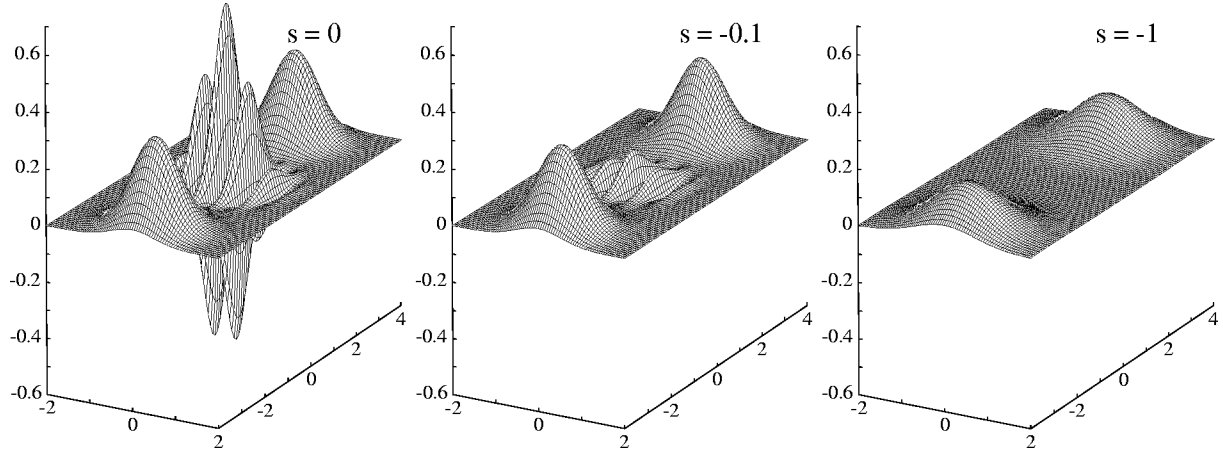


Figure 2.1: Quasidistributions representing the Schrödinger cat state for  $\alpha_0 = 3i$ , depicted for the ordering parameters  $s = 0, -0.1$ , and  $-1$ .

## 2.4 Deconvolution

We have seen, using the example of the Schrödinger cat state, that signatures of quantum interference can be visible better in quasidistribution functions with higher ordering. Thus, what is interesting, is the inversion of Eq. (2.10), i.e. deconvolution of a lower-ordered quasidistribution function. This task is quite difficult. Let us first note that in general the integral in Eq. (2.10) fails to converge if we take  $s < s'$ . Instead, we may use the Fourier transforms of the quasidistribution functions

$$\tilde{W}(\zeta; s) = \int d^2\beta e^{\zeta\beta^* - \zeta^*\beta} W(\beta; s) = e^{s|\zeta|^2/2} \langle e^{\zeta\hat{a}^\dagger - \zeta^*\hat{a}} \rangle. \quad (2.20)$$

Transition to a higher ordered quasidistribution consists now simply in multiplication by an exponent:

$$\tilde{W}(\zeta; s') = e^{(s'-s)|\zeta|^2/2} \tilde{W}(\zeta; s), \quad (2.21)$$

and evaluation of the inverse Fourier transform. The complete expression of  $W(\alpha; s')$  in terms of a lower ordered quasidistribution has the form:

$$W(\alpha; s') = \frac{1}{\pi^2} \int d^2\zeta e^{(s'-s)|\zeta|^2/2 + \zeta^*\alpha - \zeta\alpha^*} \int d^2\beta e^{\zeta\beta^* - \zeta^*\beta} W(\beta; s). \quad (2.22)$$

Anticipating for a moment the connection of the quasidistributions with experiment, let us suppose that we are given an experimentally determined quasidistribution  $W(\beta; s)$ , and that we are trying to apply the deconvolution procedure described by Eq. (2.22). Usually, values of  $W(\beta; s)$  will be affected by errors originating from statistical uncertainty and various experimental imperfections. These errors make the deconvolution a very delicate matter. The crucial problem is that the Fourier transform  $\tilde{W}(\zeta; s)$  has to be multiplied by an *exploding* factor  $e^{(s'-s)|\zeta|^2/2}$ . Experimental errors of  $W(\beta; s)$  can generate long, slowly decaying high-frequency components in its

Fourier transform. Multiplication by an exploding exponent enormously amplifies contribution of these fluctuations, which leads to huge errors of the reconstructed  $W(\alpha; s)$ . Therefore, deconvolution of experimentally determined quasidistributions according to Eq. (2.22) is practically impossible.

## 2.5 Multimode quasidistributions

The concept of quasidistribution functions can be generalized in a straightforward manner to multimode radiation. In analogy to Eq. (2.7), we need to take the symmetrically ordered multimode characteristic function, and to evaluate its Fourier transform with an appropriately chosen Gaussian factor which defines the ordering:

$$W(\alpha_1, \dots, \alpha_M; s) = \frac{1}{\pi^{2M}} \int d\zeta_1 \dots d\zeta_M \exp \left( \sum_{i=1}^M \frac{s}{2} |\zeta_i|^2 + \zeta_i^* \alpha_i - \zeta_i \alpha_i^* \right) \left\langle \exp \left( \sum_{i=1}^M \zeta_i \hat{a}_i^\dagger - \zeta_i^* \hat{a}_i \right) \right\rangle. \quad (2.23)$$

Introducing normal ordering allows one to perform the integrals, which yields an explicit normally ordered representation:

$$W(\alpha_1, \dots, \alpha_M; s) = \left( \frac{2}{\pi(1-s)} \right)^M \left\langle : \exp \left( -\frac{2}{1-s} \sum_{i=1}^M (\hat{a}_i^\dagger - \alpha_i^*)(\hat{a}_i - \alpha_i) \right) : \right\rangle. \quad (2.24)$$

Using Eq. (2.14), we may represent the quasidistribution functions as:

$$W(\alpha_1, \dots, \alpha_M; s) = \left( \frac{2}{\pi(1-s)} \right)^M \left\langle \left( \frac{s+1}{s-1} \right)^{\sum_{i=1}^M (\hat{a}_i^\dagger - \alpha_i^*)(\hat{a}_i - \alpha_i)} \right\rangle. \quad (2.25)$$

The expression  $\sum_{i=1}^M (\hat{a}_i^\dagger - \alpha_i^*)(\hat{a}_i - \alpha_i)$  appearing in the exponent is simply the phase space displaced operator of the *total* number of photons. In analogy to the single-mode case, we may write the multimode quasidistributions as an expectation value of the operator involving the multimode displacement operator

$$\hat{D}(\{\alpha_i\}) = \exp \left( \sum_{i=1}^M \alpha_i \hat{a}_i^\dagger - \alpha_i^* \hat{a}_i \right), \quad (2.26)$$

and the total photon number operator, defined as

$$\hat{N} = \sum_{i=1}^M \hat{n}_i \quad (2.27)$$

where  $\hat{n}_i = \hat{a}_i^\dagger \hat{a}_i$ . The explicit expressions are:

$$\begin{aligned} W(\alpha_1, \dots, \alpha_M; s) &= \left( \frac{2}{\pi(1-s)} \right)^M \left\langle \hat{D}(\{\alpha_i\}) : \exp \left( -\frac{2\hat{N}}{1-s} \right) : \hat{D}^\dagger(\{\alpha_i\}) \right\rangle \\ &= \left( \frac{2}{\pi(1-s)} \right)^M \left\langle \hat{D}(\{\alpha_i\}) \left( \frac{s+1}{s-1} \right)^{\hat{N}} \hat{D}^\dagger(\{\alpha_i\}) \right\rangle. \end{aligned} \quad (2.28)$$

## 2.6 Quasidistribution functionals

The representation given in Eq. (2.28) suggests generalization of the multimode quasidistribution functions to the form independent of the specific decomposition into modes. Such generalized quasidistributions are functionals of the electromagnetic field. Instead of using a finite set of annihilation and creation operators, we will now deal with the full description of the electromagnetic field, involving the operator fields  $\hat{\mathbf{E}}(\mathbf{r}, t)$  and  $\hat{\mathbf{H}}(\mathbf{r}, t)$ . In order to simplify the notation, we shall fix the time  $t$ , and omit it in the subsequent formulae. The definition of quasidistribution functionals involves two operators: the coherent displacement operator  $\hat{\mathcal{D}}$ , and the operator of the total number of photons  $\hat{\mathcal{N}}$ . The action of the displacement operator is straightforward: it adds a classical amplitude to the field operators according to the formula

$$\begin{aligned} \hat{\mathcal{D}}[\mathbf{E}(\mathbf{r}), \mathbf{H}(\mathbf{r})]\hat{\mathbf{E}}(\mathbf{r})\hat{\mathcal{D}}^\dagger[\mathbf{E}(\mathbf{r}), \mathbf{H}(\mathbf{r})] &= \hat{\mathbf{E}}(\mathbf{r}) - \mathbf{E}(\mathbf{r}) \\ \hat{\mathcal{D}}[\mathbf{E}(\mathbf{r}), \mathbf{H}(\mathbf{r})]\hat{\mathbf{H}}(\mathbf{r})\hat{\mathcal{D}}^\dagger[\mathbf{E}(\mathbf{r}), \mathbf{H}(\mathbf{r})] &= \hat{\mathbf{H}}(\mathbf{r}) - \mathbf{H}(\mathbf{r}). \end{aligned} \quad (2.29)$$

In order to find an explicit formula for quasidistribution functionals, we need to express the total photon number operator  $\hat{\mathcal{N}}$  in terms of the electric and magnetic field. We shall start from the standard decomposition of the electromagnetic field into plane waves with periodic boundary conditions in a box of the volume  $V$ :

$$\hat{\mathbf{E}}(\mathbf{r}) = i \sum_{l\sigma} \sqrt{\frac{\hbar\omega_l}{2\epsilon_0 V}} \mathbf{e}_{l\sigma} (\hat{a}_{l\sigma} e^{i\mathbf{k}_l \cdot \mathbf{r}} - \hat{a}_{l\sigma}^\dagger e^{-i\mathbf{k}_l \cdot \mathbf{r}}) \quad (2.30)$$

$$\hat{\mathbf{H}}(\mathbf{r}) = -\frac{i}{c\mu_0} \sum_{l\sigma} \sqrt{\frac{\hbar\omega_l}{2\epsilon_0 V}} \mathbf{e}_{l\sigma} \times \frac{\mathbf{k}_l}{|\mathbf{k}_l|} (\hat{a}_{l\sigma} e^{i\mathbf{k}_l \cdot \mathbf{r}} - \hat{a}_{l\sigma}^\dagger e^{-i\mathbf{k}_l \cdot \mathbf{r}}). \quad (2.31)$$

Here the indices  $l$  and  $\sigma$  label respectively the wave vectors  $\mathbf{k}_l$  and the polarizations  $\mathbf{e}_{l\sigma}$ , and  $\omega_l = c|\mathbf{k}_l|$  is the frequency of an  $l$ th mode. Our goal is to represent the sum

$$\hat{\mathcal{N}} = \sum_{l\sigma} \hat{a}_{l\sigma}^\dagger \hat{a}_{l\sigma} \quad (2.32)$$

using  $\hat{\mathbf{E}}(\mathbf{r})$  and  $\hat{\mathbf{H}}(\mathbf{r})$ . For this purpose we shall take Fourier transforms of these fields:

$$\int d^3\mathbf{r} \hat{\mathbf{E}}(\mathbf{r}) e^{-i\mathbf{k}_l \cdot \mathbf{r}} = i \sqrt{\frac{\hbar\omega_l V}{2\epsilon_0}} \sum_{\sigma} (\mathbf{e}_{l\sigma} \hat{a}_{l\sigma} - \mathbf{e}_{-l\sigma} \hat{a}_{-l\sigma}^\dagger) \quad (2.33)$$

$$\int d^3r \hat{\mathbf{H}}(\mathbf{r}) e^{-i\mathbf{k}_l \cdot \mathbf{r}} = -i\sqrt{\frac{\hbar\omega_l V}{2\mu_0}} \sum_{\sigma} \left( \mathbf{e}_{l\sigma} \times \frac{\mathbf{k}_l}{|\mathbf{k}_l|} \hat{a}_{l\sigma} - \mathbf{e}_{-l\sigma} \times \frac{\mathbf{k}_{-l}}{|\mathbf{k}_{-l}|} \hat{a}_{-l\sigma}^{\dagger} \right). \quad (2.34)$$

Here on the right-hand sides we have used the fact that  $\mathbf{k}_{-l} = -\mathbf{k}_l$ . The product of the Fourier transforms taken for  $\mathbf{k}_l$  and  $\mathbf{k}_{-l}$  can be expressed as:

$$\int d^3r \int d^3r' \hat{\mathbf{E}}(\mathbf{r}) \hat{\mathbf{E}}(\mathbf{r}') e^{-i\mathbf{k}_l \cdot (\mathbf{r} - \mathbf{r}')} = \frac{\hbar\omega_l V}{2\epsilon_0} \sum_{\sigma\sigma'} (\mathbf{e}_{l\sigma} \hat{a}_{l\sigma} - \mathbf{e}_{-l\sigma} \hat{a}_{-l\sigma}^{\dagger}) (\mathbf{e}_{l\sigma'} \hat{a}_{l\sigma'}^{\dagger} - \mathbf{e}_{-l\sigma'} \hat{a}_{-l\sigma'}), \quad (2.35)$$

and

$$\begin{aligned} & \int d^3r \int d^3r' \hat{\mathbf{H}}(\mathbf{r}) \hat{\mathbf{H}}(\mathbf{r}') e^{-i\mathbf{k}_l \cdot (\mathbf{r} - \mathbf{r}')} \\ &= \frac{\hbar\omega_l V}{2\mu_0} \sum_{\sigma\sigma'} \left( \mathbf{e}_{l\sigma} \times \frac{\mathbf{k}_l}{|\mathbf{k}_l|} \hat{a}_{l\sigma} - \mathbf{e}_{-l\sigma} \times \frac{\mathbf{k}_{-l}}{|\mathbf{k}_{-l}|} \hat{a}_{-l\sigma}^{\dagger} \right) \left( \mathbf{e}_{l\sigma'} \times \frac{\mathbf{k}_l}{|\mathbf{k}_l|} \hat{a}_{l\sigma'}^{\dagger} - \mathbf{e}_{-l\sigma'} \times \frac{\mathbf{k}_{-l}}{|\mathbf{k}_{-l}|} \hat{a}_{-l\sigma'} \right) \\ &= \frac{\hbar\omega_l V}{2\mu_0} \sum_{\sigma\sigma'} (\delta_{\sigma\sigma'} \hat{a}_{l\sigma} \hat{a}_{l\sigma'}^{\dagger} + \mathbf{e}_{l\sigma} \mathbf{e}_{-l\sigma'} \hat{a}_{l\sigma} \hat{a}_{-l\sigma'} + \mathbf{e}_{-l\sigma} \mathbf{e}_{l\sigma'} \hat{a}_{-l\sigma}^{\dagger} \hat{a}_{l\sigma'}^{\dagger} + \delta_{\sigma\sigma'} \hat{a}_{-l\sigma}^{\dagger} \hat{a}_{-l\sigma'}). \end{aligned} \quad (2.36)$$

We shall now add the expressions for the electric and magnetic fields multiplied by the factors  $\epsilon_0/2\hbar\omega_l V$  and  $\mu_0/2\hbar\omega_l V$  respectively. This yields:

$$\int d^3r \int d^3r' \left( \frac{\epsilon_0}{2} \hat{\mathbf{E}}(\mathbf{r}) \hat{\mathbf{E}}(\mathbf{r}') + \frac{\mu_0}{2} \hat{\mathbf{H}}(\mathbf{r}) \hat{\mathbf{H}}(\mathbf{r}') \right) \frac{e^{-i\mathbf{k}_l \cdot (\mathbf{r} - \mathbf{r}')}}{\hbar\omega_l V} = \sum_{\sigma} \frac{1}{2} (\hat{a}_{l\sigma} \hat{a}_{l\sigma}^{\dagger} + \hat{a}_{-l\sigma}^{\dagger} \hat{a}_{-l\sigma}). \quad (2.37)$$

This formula is close to the standard expression for the energy of the electromagnetic field. Indeed, we could obtain it via multiplication of both the sides by  $\hbar\omega$ , and summation over  $l$ . However, we are now interested in a different quantity, namely the total number of photons, and we need to perform the summation with the factor  $\hbar\omega$  in the denominator of the left hand side. In this way we obtain:

$$\sum_{l\sigma} \frac{1}{2} (\hat{a}_{l\sigma} \hat{a}_{l\sigma}^{\dagger} + \hat{a}_{l\sigma}^{\dagger} \hat{a}_{l\sigma}) = \int d^3r \int d^3r' \left( \frac{\epsilon_0}{2} \hat{\mathbf{E}}(\mathbf{r}) \hat{\mathbf{E}}(\mathbf{r}') + \frac{\mu_0}{2} \hat{\mathbf{H}}(\mathbf{r}) \hat{\mathbf{H}}(\mathbf{r}') \right) K(\mathbf{r} - \mathbf{r}'). \quad (2.38)$$

In the second term of the left-hand side we have changed the summation index  $-l \rightarrow l$ . The integral kernel  $K(\mathbf{r} - \mathbf{r}')$  appearing on the right-hand side is given by:

$$K(\mathbf{r}) = \sum_l \frac{e^{-i\mathbf{k}_l \cdot \mathbf{r}}}{\hbar\omega_l V}. \quad (2.39)$$

We shall evaluate it in the continuous limit, when the sum over  $l$  can be replaced by a three-dimensional integral over the wave vector  $\mathbf{k}$ . In this limit, there occurs a singularity at  $\mathbf{r} = 0$ , which is a result of the slowly decaying integrand with large  $\mathbf{k}$ . We shall regularize the integral

by introducing the upper cut-off  $k_{\max}$  for the wave number. Physically, this means that we do not take into account photons with energy larger than  $\hbar c k_{\max}$ . The regularized kernel can be evaluated in a straightforward manner:

$$\begin{aligned} K(\mathbf{r}) &= \frac{1}{(2\pi)^3 \hbar c} \int d^3 \mathbf{k} \frac{e^{-i\mathbf{kr}}}{|\mathbf{k}|} = \frac{1}{(2\pi)^2 \hbar c} \int_0^{k_{\max}} dk k \int_0^\pi d\vartheta \sin \vartheta e^{-ik|\mathbf{r}| \cos \vartheta} \\ &= \frac{1}{2\pi^2 \hbar c} \frac{1 - \cos k_{\max} |\mathbf{r}|}{\mathbf{r}^2}. \end{aligned} \quad (2.40)$$

It is easily seen that truncation of the wave vector magnitude has removed singularity of the kernel  $K(\mathbf{r})$  occurring at  $\mathbf{r} = 0$ .

On the left-hand side of Eq. (2.38), we have a symmetrically ordered product of the creation and annihilation operators  $\frac{1}{2}(\hat{a}_{l\sigma} \hat{a}_{l\sigma}^\dagger + \hat{a}_{l\sigma}^\dagger \hat{a}_{l\sigma})$ . In order to obtain the total photon number operator, we need to introduce the normal ordering of the right-hand side of Eq. (2.38). Using this expression, we can easily define quasidistribution functionals of the electromagnetic field. There is a small difficulty arising from the fact that we now deal with the infinite number of degrees of freedom. In Eq. (2.24), we cannot pass to infinity with the number of modes in the normalization prefactor  $[2/\pi(1-s)]^M$ . We shall solve this difficulty by absorbing the normalization prefactor into the functional integration measure over the fields  $\mathbf{E}$  and  $\mathbf{H}$ . Thus, we define the quasidistribution functional as:

$$\mathcal{W}[\mathbf{E}(\mathbf{r}), \mathbf{H}(\mathbf{r}); s] = \left\langle \hat{\mathcal{D}}[\mathbf{E}(\mathbf{r}), \mathbf{H}(\mathbf{r})] : \exp \left( -\frac{2\hat{\mathcal{N}}}{1-s} \right) : \hat{\mathcal{D}}^\dagger[\mathbf{E}(\mathbf{r}), \mathbf{H}(\mathbf{r})] \right\rangle. \quad (2.41)$$

This definition can be written explicitly using the electromagnetic field operators with the help of the derived expression for the total photon number operator as:

$$\begin{aligned} \mathcal{W}[\mathbf{E}(\mathbf{r}), \mathbf{H}(\mathbf{r}); s] &= \left\langle : \exp \left[ -\frac{2}{1-s} \int d^3 \mathbf{r} \int d^3 \mathbf{r}' K(\mathbf{r} - \mathbf{r}') \left( \frac{\epsilon_0}{2} [\hat{\mathbf{E}}(\mathbf{r}) - \mathbf{E}(\mathbf{r})][\hat{\mathbf{E}}(\mathbf{r}') - \mathbf{E}(\mathbf{r}')] \right. \right. \right. \\ &\quad \left. \left. \left. + \frac{\mu_0}{2} [\hat{\mathbf{H}}(\mathbf{r}) - \mathbf{H}(\mathbf{r})][\hat{\mathbf{H}}(\mathbf{r}') - \mathbf{H}(\mathbf{r}')] \right) \right] : \right\rangle. \end{aligned} \quad (2.42)$$

The integral kernel appearing in the above formula is given by Eq. (2.39).



# Chapter 3

## Homodyne techniques for quantum state measurement

Over the last decade, the domain of quantum state measurement has passed a long way from first theoretical proposals to well understood experimental realizations. Complete presentation of the current state of this field would require a separate book, encompassing a wide range of experimental techniques and concepts of data analysis. In this chapter we shall set the scene for further parts of the thesis by describing briefly earlier works on measuring the quantum state of light. We shall restrict our attention to detection of optical radiation, and describe two techniques which have been successfully realized in experiments: double homodyne detection and optical homodyne tomography.

Double homodyne detection allows one to measure the  $Q$  function of a light mode. It was demonstrated in 1986 by Walker and Caroll [33]. Their experiment had as a main purpose the demonstration of a homodyne measurement near the quantum noise limit, and it later attracted attention as a complete characterization of the quantum state. As we discussed in the previous chapter, the  $Q$  function is a positive definite distribution, and it exhibits only faint traces of quantum interference. Optical homodyne tomography was realized first by Smithey *et al.* in 1993 [7]. This technique is capable of measuring the Wigner function. Apparently, this fact added extra excitement to the development of homodyne tomography, as the Wigner function is a nonclassical distribution function which may take negative values resulting from quantum interference.

Both these techniques are based on the same experimental apparatus, namely the balanced homodyne detector. This device provides information on phase-sensitive properties of light. In the quantum mechanical formalism, it performs the measurement of a family of observables called *quadratures*. We shall start this chapter with a description of the balanced homodyne detector in Sec. 3.1. The double homodyne detection scheme is discussed in Sec. 3.2. We show that this scheme can be used to measure two noncommuting observables at the cost of introducing extra noise to the measurement. Sec. 3.3 is devoted to optical homodyne tomography. It describes

the physical principle of the method, as well as mathematical transformations involved in the processing of experimental data.

### 3.1 Balanced homodyne detector

Standard photodetection is insensitive to phase properties of optical radiation. This is because the observed signal depends only on the operator of the number of photons  $\hat{n} = \hat{a}^\dagger \hat{a}$ . Nevertheless, we may use a photodetector to measure phase-dependent quantities by superposing the measured beam with an auxiliary coherent field using a beam splitter. The auxiliary field has the name of the *local oscillator*. When measuring such a superposition, the signal from the photodetector will be described by an expression involving terms linear in  $\hat{a}$  and  $\hat{a}^\dagger$ . Thus, it carries information on the phase properties of the measured field. This is the basic idea of homodyne detection.

In quantum optics, homodyne detection has played an important role in investigating the squeezed states of light. These states exhibit interesting noise properties in certain phase-dependent observables. More specifically, for a single light mode we may introduce a family of quadrature observables dependent on the phase  $\theta$ :

$$\hat{x}_\theta = \frac{e^{i\theta} \hat{a}^\dagger + e^{-i\theta} \hat{a}}{\sqrt{2}}. \quad (3.1)$$

It is easy to check that the commutator of two quadratures corresponding to phases which differ by  $\pi/2$  is  $[\hat{x}_\theta, \hat{x}_{\theta+\pi/2}] = i$ . Consequently, variances of these two observables satisfy the uncertainty relation in the form  $\Delta x_\theta \Delta x_{\theta+\pi/2} \geq 1/2$ . For coherent states, this variance is evenly distributed over all the quadratures, and it equals to  $\Delta x_\theta = 1/\sqrt{2}$ . Squeezed states are such states of the electromagnetic field, which for a certain phase  $\theta$  have the variance smaller than the coherent state level. These states cannot be described within classical theory of radiation, and the squeezing is clearly a non-classical property. Squeezed states can find application in very precise interferometric measurements [5].

Of course, it is obvious from the definition of quadratures that their measurement requires a phase-sensitive technique, such as homodyne detection. In practice, we need to take into account various experimental imperfections. One of them is the excess noise of the local oscillator field. This noise adds to the observed level of fluctuations, and it may mask subtle quantum effects related to squeezing. Fortunately, there is a possibility to subtract the local oscillator noise by using the so-called balanced scheme. In the balanced homodyne detection scheme, depicted in Fig. 3.1, the signal field is superposed using a 50:50 beam splitter with the local oscillator. Two photodetectors monitor the output ports of the beam splitter, and the recorded signal is the difference of the detector photocurrents. In this way, we cancel the effect of local oscillator noise when measuring the variance of the difference photocurrent.

Moreover, theoretical description of the balanced homodyne detector shows that this setup, in an idealized limit, is the optical realization of the quantum measurement of the quadrature op-

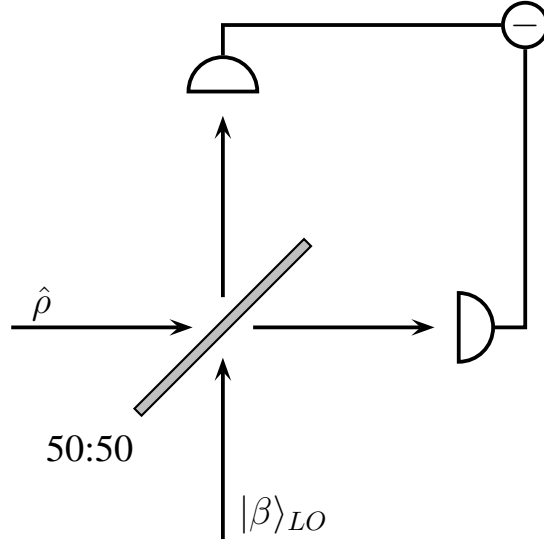


Figure 3.1: The balanced homodyne setup. The signal field, described by a density matrix  $\hat{\rho}$ , is combined with a coherent local oscillator  $|\beta\rangle_{LO}$ . The two outgoing fields are measured using photodetectors. The difference of their counts is the statistical data recorded in the experiment.

erator  $\hat{x}_\theta$ . The idealization is based on two assumptions: the unit efficiency of the photodetectors and the classical limit of the local oscillator. The latter condition can be easily satisfied in an experiment. Also, efficiency of photodetectors used in a homodyne setup can be close to 100%. If we rely on these two assumptions, theoretical analysis of the balanced scheme becomes quite compact. More detailed studies can be found in Ref. [34, 35, 36].

Let us describe the signal field with the annihilation operator  $\hat{a}$ , and the local oscillator field with  $\hat{b}$ . These two fields, superposed on a 50:50 beam splitter, yield two outgoing modes. In general, combination of the modes at a beam splitter is given by an SU(2) transformation [37]. For a 50:50 beam splitter, we may simplify this transformation to the matrix

$$\begin{pmatrix} \hat{c} \\ \hat{d} \end{pmatrix} = \frac{1}{\sqrt{2}} \begin{pmatrix} 1 & 1 \\ 1 & -1 \end{pmatrix} \begin{pmatrix} \hat{a} \\ \hat{b} \end{pmatrix}, \quad (3.2)$$

where  $\hat{c}$  and  $\hat{d}$  are the annihilation operators of the outgoing fields. We assume that the local oscillator is in a coherent state  $|\beta\rangle_{LO}$ , and the quantum state of the mode  $\hat{a}$  is given by the density matrix  $\hat{\rho}$ .

The quantity we are interested in is the difference of photocurrents generated by the detectors monitoring the modes  $\hat{c}$  and  $\hat{d}$ . On the microscopic level, these photocurrents consist of a discrete number of electrons  $n_1$  and  $n_2$ . In a real experiment, this discreteness is not observed due to the large average number of the generated photoelectrons. The observable measured in balanced

homodyne detection is the difference of the electron number  $\Delta N = n_1 - n_2$ . The probability  $p(\Delta N)$  of obtaining a specific value for  $\Delta N$  can be easily derived using the standard theory of photoelectric detection. It is given by the expression:

$$p(\Delta N) = \sum_{n_1 - n_2 = \Delta N} \text{Tr}\{\hat{\varrho} \otimes |\beta\rangle\langle\beta|_{LO} : e^{-\hat{c}^\dagger \hat{c}} \frac{(\hat{c}^\dagger \hat{c})^{n_1}}{n_1!} e^{-\hat{d}^\dagger \hat{d}} \frac{(\hat{d}^\dagger \hat{d})^{n_2}}{n_2!} : \}. \quad (3.3)$$

In further calculations, it is more convenient to deal with the generating function for the probability distribution  $p(\Delta N)$ . The generating function is obtained by evaluating the Fourier transform:

$$\begin{aligned} Z(\xi) &= \sum_{\Delta N = -\infty}^{\infty} e^{i\xi\Delta N} p(\Delta N) \\ &= \text{Tr}\{\hat{\varrho} \otimes |\beta\rangle\langle\beta|_{LO} : \exp[(e^{i\xi} - 1)\hat{c}^\dagger \hat{c} + (e^{-i\xi} - 1)\hat{d}^\dagger \hat{d}] : \}. \end{aligned} \quad (3.4)$$

In this way, we managed to get rid of the troublesome constrained sum with the condition  $n_1 - n_2 = \Delta N$ . We can now remove the normal ordering symbol by making use of the operator identity given in Eq. (2.14). This yields:

$$Z(\xi) = \text{Tr}\{\hat{\varrho} \otimes |\beta\rangle\langle\beta|_{LO} e^{i\xi(\hat{c}^\dagger \hat{c} - \hat{d}^\dagger \hat{d})}\} = \text{Tr}\{\hat{\varrho} \otimes |\beta\rangle\langle\beta|_{LO} e^{i\xi(\hat{a}^\dagger \hat{b} + \hat{a} \hat{b}^\dagger)}\}. \quad (3.5)$$

When the local oscillator is in a strong coherent state, the bosonic operators  $\hat{b}, \hat{b}^\dagger$  in the exponent  $e^{i\xi(\hat{a}^\dagger \hat{b} + \hat{a} \hat{b}^\dagger)}$  can be replaced by *c*-numbers  $\beta, \beta^*$ . In this regime, it is also convenient to rescale the difference photocurrent  $\Delta N$ , which grows as the first power of the local oscillator amplitude. Dividing  $\Delta N$  by  $|\beta|$ , we obtain a quantity which is independent of the magnitude  $|\beta|$  in the regime of the classical local oscillator. We shall introduce an extra factor of  $1/\sqrt{2}$ , and define the homodyne variable as  $x = \Delta N/\sqrt{2}|\beta|$ . This variable can be treated as a continuous one, as the local oscillator amplitude is very large. The rescaling of the homodyne variable corresponds to changing the parameter of the generating function according to  $\lambda = \xi\sqrt{2}|\beta|$ . In the new parameterization, the generating function takes the form:

$$Z_\theta(\lambda) = \left\langle \exp\left(\frac{i\lambda}{\sqrt{2}}(e^{i\theta}\hat{a}^\dagger + e^{-i\theta}\hat{a})\right) \right\rangle = \langle e^{i\lambda\hat{x}_\theta} \rangle, \quad (3.6)$$

where  $\theta$  is the phase of the local oscillator:  $\beta = |\beta|e^{i\theta}$ . We have added here a subscript  $\theta$  to the generating function  $Z_\theta(\lambda)$  to stress that the measured observable depends on the local oscillator phase. Using the last form of the  $Z_\theta(\lambda)$ , we may easily obtain the probability distribution  $p_\theta(x)$  for the homodyne variable  $x$  by evaluating the inverse Fourier transform. Let us note that we should now integrate over all real values  $\lambda$  because of the introduced rescaling. The inverse Fourier transform yields:

$$p_\theta(x) = \frac{1}{2\pi} \int_{-\infty}^{\infty} d\lambda e^{-i\lambda x} \langle e^{i\lambda\hat{x}_\theta} \rangle = \langle \delta(x - \hat{x}_\theta) \rangle = \langle |x\rangle_\theta \langle x| \rangle. \quad (3.7)$$

This expression clearly shows, that balanced homodyne detection is the measurement of the quadrature operator  $\hat{x}_\theta$ . The probability of obtaining the result  $x$  is given by the projection on the corresponding eigenstate of the quadrature operator, defined as  $\hat{x}_\theta|x\rangle_\theta = x|x\rangle_\theta$ .

## 3.2 Double homodyne detection

In homodyne detection, we have to select the phase of the local oscillator, which defines the measured quadrature. Simultaneous measurement of different quadratures is not possible, because they correspond to noncommuting observables: it is easy to check that for example  $[x_\theta, x_{\theta+\pi/2}] = i$ . However, we may try to circumvent this difficulty by splitting first the input beam on a 50:50 beam splitter and performing *two* homodyne measurements on the outgoing fields. This is the idea of double homodyne detection. The corresponding setup is shown in Fig. 3.2. The signal field, described by an annihilation operator  $\hat{a}$ , is divided using the 50:50 beam splitter BS. The two outgoing beams are measured with two separate balanced homodyne detectors. The phases of local oscillators can be independently adjusted in each of the arms of the setup, which allows one to measure two arbitrary quadratures of the fields leaving the beam splitter BS. For simplicity, let us choose the two local oscillator phases to be 0 and  $\pi/2$ , and to denote the corresponding quadratures by  $\hat{q} = \hat{x}_0$  and  $\hat{p} = \hat{x}_{\pi/2}$ . These two quantities commute to the imaginary unit  $[\hat{q}, \hat{p}] = i$ , and they are optical analogs of the position and the momentum operators for a particle.

In the quantum description of the setup, we need to take into account the vacuum field entering through the unused input port of the beam splitter BS dividing the signal field. This vacuum field is denoted with the annihilation operator  $\hat{v}$  in Fig. 3.2. The quadratures measured at the two homodyne detectors are given by the combinations

$$\hat{q}_1 = \frac{1}{\sqrt{2}}(\hat{q}_a + \hat{q}_v), \quad \hat{p}_2 = \frac{1}{\sqrt{2}}(\hat{p}_a - \hat{p}_v) \quad (3.8)$$

where the indices  $a$  and  $v$  denote quadrature operators corresponding the signal and the vacuum mode respectively. The form of these combinations follows directly from Eq. (3.2), describing transformation of the field operators at a 50:50 beam splitter.

The probability distribution  $p(q_1, p_2)$  for the outcomes of the measurement is now defined on the two-dimensional space spanned by the variables  $q_1$  and  $p_2$ . Analogously to the previous section, it will be more convenient to use the generating function  $Z(\lambda_1, \lambda_2)$ , which depends now on two parameters  $\lambda_1$  and  $\lambda_2$ :

$$Z(\lambda_1, \lambda_2) = \int d\lambda_1 \int d\lambda_2 e^{i\lambda_1 q_1 + i\lambda_2 p_2} p(q_1, p_2). \quad (3.9)$$

The generating function describing the joint measurement of the quadratures  $\hat{q}_1$  and  $\hat{p}_2$  is given by a straightforward generalization of Eq. (3.6):

$$\begin{aligned} Z(\lambda_1, \lambda_2) &= \langle \exp(i\lambda_1 \hat{q}_1 + i\lambda_2 \hat{p}_2) \rangle_{a,v} \\ &= \exp\left(-\frac{1}{8}(\lambda_1^2 + \lambda_2^2)\right) \left\langle \exp\left(\frac{i}{\sqrt{2}}(\lambda_1 \hat{q}_a + \lambda_2 \hat{p}_a)\right) \right\rangle_a. \end{aligned} \quad (3.10)$$

In the second line we have evaluated explicitly the quantum expectation value over the vacuum mode. The joint probability distribution  $p(q_1, p_2)$  can be obtained from the double inverse Fourier

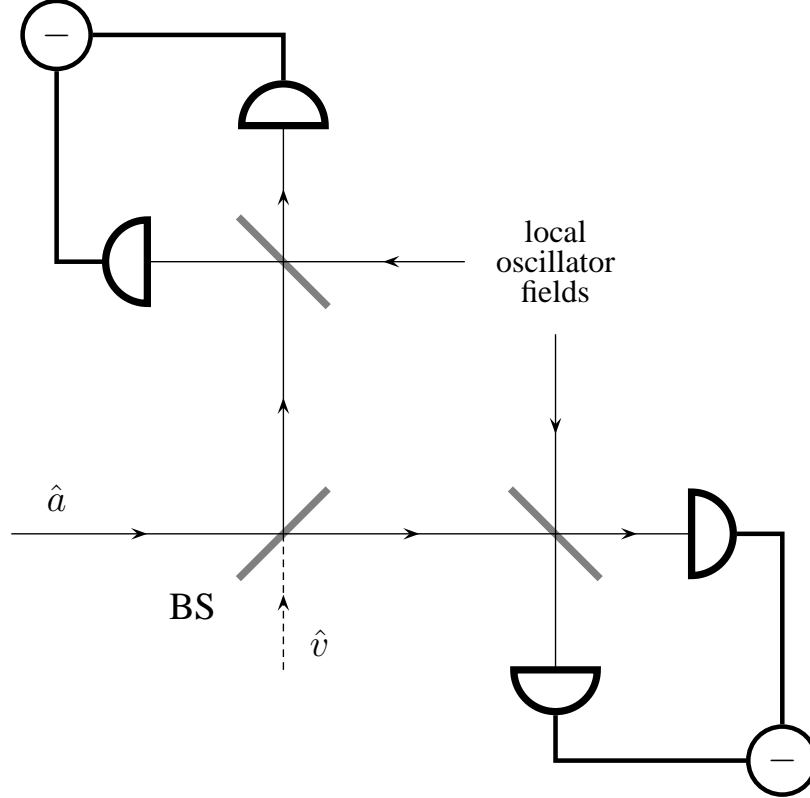


Figure 3.2: Double homodyne detection setup. The signal field, denoted by the annihilation operator  $\hat{a}$ , is divided using a 50:50 beam splitter BS. The two outgoing fields fall onto balanced homodyne detectors. The local oscillator phases are adjusted such that two conjugate quadratures are measured. In the quantum mechanical description of the setup, one has to take into account the vacuum field  $\hat{v}$  entering through the unused input port of the beam splitter BS.

transform of the generating function. We shall rearrange this expression to the form:

$$\begin{aligned} p(q_1, p_2) &= \frac{1}{(2\pi)^2} \int d\lambda_1 \int d\lambda_2 e^{-i\lambda_1 q_1 - i\lambda_2 p_2} Z(\lambda_1, \lambda_2) \\ &= \frac{1}{\pi^2} \int d^2\zeta e^{-|\zeta|^2/2 + \zeta^*(q_1 + ip_2) - \zeta(q_1 - ip_2)} \langle e^{\zeta \hat{a}^\dagger - \zeta^* \hat{a}} \rangle_a \end{aligned} \quad (3.11)$$

where we have substituted  $\zeta = (i\lambda_1 - \lambda_2)/2$ . The last expression can be directly related to the definition of quasidistribution functions in Eq. (2.7), with  $\alpha = q_1 + ip_2$ , and  $s = -1$ . Thus, the joint probability distribution of homodyne events measured in double homodyne detection is equal to the  $Q$  function of the mode  $\hat{a}$ :

$$p(q_1, p_2) = Q_a(q_1 + ip_2). \quad (3.12)$$

One may wonder how this formula changes when we inject an arbitrary state in the second input port of the beam splitter BS dividing the signal field. In this case  $Z(\lambda_1, \lambda_2)$  can be factorized

to the product of the symmetrically ordered characteristic functions for the position and the momentum:

$$Z(\lambda_1, \lambda_2) = \left\langle \exp \left( \frac{i}{\sqrt{2}} (\lambda_1 \hat{q}_a + \lambda_2 \hat{p}_a) \right) \right\rangle_a \left\langle \exp \left( \frac{i}{\sqrt{2}} (\lambda_1 \hat{q}_v + \lambda_2 \hat{p}_v) \right) \right\rangle_v. \quad (3.13)$$

The inverse Fourier transform maps the product of the symmetrically ordered characteristic functions onto a convolution of the corresponding Wigner functions. After a simple calculation, we obtain:

$$p(q_1, p_2) = 2 \int dq \int dp W_a(q, p) W_v(\sqrt{2}q_1 - q, \sqrt{2}p_2 - p), \quad (3.14)$$

where  $W_a(q, p)$  and  $W_v(q, p)$  are the Wigner functions describing the quantum state of the fields incident on the beam splitter BS.

The above results illustrates the operational approach to the joint measurement of the position and the momentum [38, 39]. These two observables do not commute and they cannot be measured simultaneously. Nevertheless, we may introduce an auxiliary system, called the “quantum ruler”, and measure two commuting combinations of positions and momenta. Such a pair of combinations has been defined in Eq. (3.8). These two operational observables can be detected simultaneously, and their measurement yields a joint two-dimensional probability distribution of two variables which can be related to the position and the momentum. The resulting operational phase space distribution is given by a convolution of the Wigner functions of the measured system and the ruler. Double homodyne detection is an optical realisation of this approach, with the role of the quantum ruler played by the vacuum field. The vacuum field is described by the gaussian Wigner function, and the double homodyne detection yields a smeared Wigner function of the signal field, which coincides with the  $Q$  function.

Double homodyne detection has been realized experimentally by Walker and Caroll [33]. A thorough discussion of this technique can be found in the article by Walker [40]. The same experimental scheme has been applied in the operational measurement of the quantum phase [41], and it was shown later that the phase distribution measured in this scheme corresponds to the radially integrated  $Q$  function [42, 43].

### 3.3 Optical homodyne tomography

In contrast to the  $Q$  function, the Wigner function does not have the operational meaning of a probability distribution, simply because it may take negative values. Therefore, one cannot design an experiment, in which the joint statistics of two real variables would be described by the Wigner function. Nevertheless, one-dimensional projections of the Wigner function are positive definite. Furthermore, these projections describe quadrature distributions according to the formula:

$$p_\theta(x) = \int dy W(x \cos \theta - y \sin \theta, x \sin \theta + y \cos \theta). \quad (3.15)$$

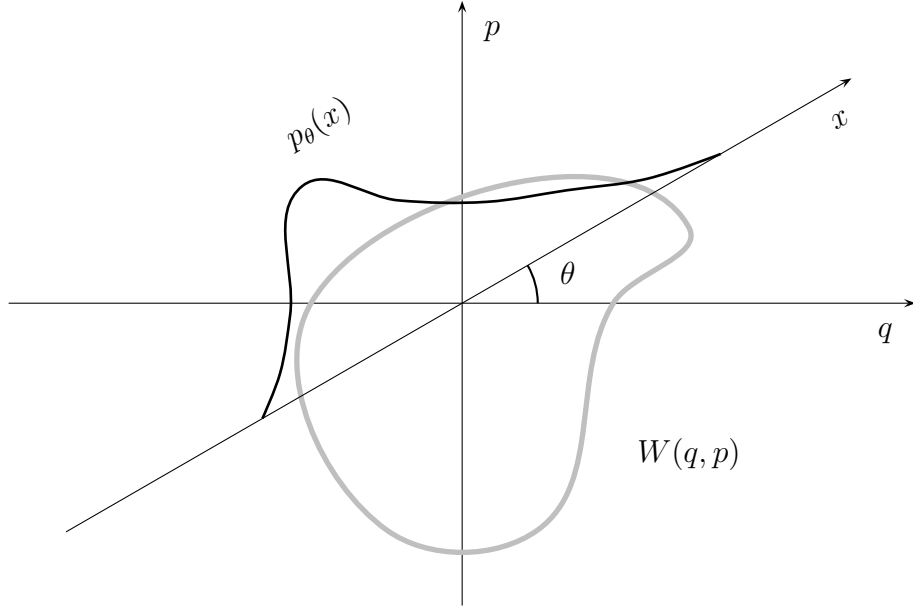


Figure 3.3: Quadrature distributions  $p_\theta(x)$  are one-dimensional projections of the Wigner function  $W(q, p)$ , obtained by integrating it along parallel stripes in the phase space.

This equation is a generalization of the marginal properties of the Wigner function for the position and the momentum. As we have seen in Sec. 3.1, quadrature distributions can be measured by means of a balanced homodyne detector. Thus we may obtain experimentally a family of one-dimensional projections of the Wigner function, depicted schematically in Fig. 3.3. What we would like to do, is to reconstruct from these “shadows” the two-dimensional Wigner function.

A very similar problem is encountered in medical tomography [44]. By measuring absorption of radiation across the body, we can obtain density of the tissue integrated along the direction of the measurement. These data are subsequently processed to reconstruct the full density distribution using numerical back-projections algorithms. In analogy to this technique, the method of reconstructing the Wigner function from homodyne statistics has been called *optical homodyne tomography*.

The relation between  $p_\theta(x)$  and  $W(q, p)$  defined in Eq. (3.15) can be viewed as a transformation between two-dimensional functions according to the formula:

$$p_\theta(x) = \int dq \int dp \delta(x - q \cos \theta - p \sin \theta) W(q, p), \quad (3.16)$$

which is known in the field of image processing as the *Radon transform*. A function  $W(q, p)$  of two real variables  $q$  and  $p$  is transformed into another function  $p_\theta(x)$  which depends on the angular variable  $\theta$  and a real variable  $x$ .

Inversion of the relation between the Wigner function and quadrature distributions becomes quite obvious, if we rewrite Eq. (3.15) in terms of the Fourier transforms of both the sides. The generating function for the quadrature distribution can be expressed using the Wigner function as:

$$\begin{aligned} Z_\theta(\lambda) &= \int dx e^{i\lambda x} p_\theta(x) \\ &= \int dx \int dy e^{i\lambda x} W(x \cos \theta - y \sin \theta, x \sin \theta + y \cos \theta) \\ &= \int dq \int dp e^{i\lambda(q \cos \theta + p \sin \theta)} W(q, p). \end{aligned} \quad (3.17)$$

The last expression is simply the Fourier transform of the Wigner function taken at the point  $(q \cos \theta, p \sin \theta)$ . Thus, the projection relation expressed in terms of the Fourier transforms consists in the change of the coordinate system, from the Cartesian one (Wigner function) to the polar one (quadrature distributions).

With this observation in hand, the way to invert Eq. (3.15) is straightforward: we need to write the Wigner function as the inverse Fourier transform, and to change the integration variables from Cartesian to polar. This allows us to insert the generating function for quadrature distributions:

$$W(q, p) = \frac{1}{(2\pi)^2} \int_{-\infty}^{\infty} |\lambda| d\lambda \int_0^\pi d\theta e^{-iq\lambda \cos \theta - ip\lambda \sin \theta} Z_\theta(\lambda). \quad (3.18)$$

Expressing  $Z_\theta(\lambda)$  in terms of quadrature distributions and performing the integral over  $\lambda$  yields:

$$W(q, p) = \frac{1}{2\pi^2} \int_{-\infty}^{\infty} dx \int_0^\pi d\theta p_\theta(x) \frac{d}{dx} P \frac{1}{x - q \cos \theta - p \sin \theta} \quad (3.19)$$

where  $P$  denotes the principal value. The above formula is known as *the inverse Radon transform*. It is clearly seen that this transformation is singular. Therefore, its numerical implementation is quite complicated. When processing experimental distributions  $p_\theta(x)$ , which are affected by statistical noise, one has to apply a regularization scheme.

The close link between the quadrature distributions and the Wigner function could be noted already during the discussion of the balanced homodyne detector. The first expression for  $Z_\theta(\lambda)$  in Eq. (3.6) is exactly the symmetrically ordered characteristic function that appears in Eq. (2.6), with  $\zeta = i\lambda e^{i\theta}/\sqrt{2}$ .

The first experimental realization of optical homodyne tomography has been demonstrated by Smithey *et al.* [7]. This seminal work has been followed by extensive theoretical and experimental research. The effects of imperfect detection were analysed [45], and it was shown that in such a case the inverse Radon transform yields a generalized quasidistribution function with the ordering parameter equal to  $-(1 - \eta)/\eta$ , where  $\eta$  is the efficiency of the photodetectors. Thus, detector losses result in blurring of the measured Wigner function. A more fundamental

problem related to optical homodyne tomography was the determination of other quantum state representations from homodyne statistics. In principle, once we have the Wigner function, we can evaluate the expectation value of any quantum observable  $\hat{O}$ , and obtain for example the density matrix in the Fock basis. However, it would be appealing to reconstruct the observables directly from the homodyne statistics, in order to avoid the detour via the singular inverse Radon transform. The formula needed for this purpose is of the form:

$$\langle \hat{O} \rangle = \int_{-\infty}^{\infty} dx \int_0^{\pi} d\theta f_{\hat{O}}(x, \theta) p_{\theta}(x), \quad (3.20)$$

where  $f_{\hat{O}}(x, \theta)$  is called the *pattern function* related to the observable  $\hat{O}$ . The problem of deriving pattern functions for the elements of the density matrix in the Fock basis was studied first by D'Ariano *et al.* [46]. It was later generalized to a more fundamental form [47, 48]. The statistical error of optical homodyne tomography has been thoroughly studied in a series of papers [49, 50, 51, 52]. On the experimental side, optical homodyne tomography has been demonstrated for cw fields [53], and a beautiful gallery of squeezed states of light has been presented [10]. An analogous tomographic method has been used to characterize transversal degrees of freedom of a laser beam [54].

### 3.4 Random phase homodyne detection

In the context of optical homodyne tomography, a new technique for measuring light has been developed. This technique is balanced homodyne detection with the phase  $\theta$  made a uniformly distributed random variable [55]. The distribution of events  $p_{\mathcal{R}}(x)$  observed in such a case is described by phase-averaged homodyne statistics:

$$p_{\mathcal{R}}(x) = \frac{1}{2\pi} \int_0^{2\pi} d\theta p_{\theta}(x) = \frac{1}{2\pi} \int_0^{2\pi} d\theta \langle |x\rangle_{\theta} \langle x| \rangle. \quad (3.21)$$

In this regime, the phase sensitivity of homodyne detection is completely lost, and the phase-averaged homodyne statistics  $p_{\mathcal{R}}(x)$  contains information only on phase-independent properties of the measured light. Nevertheless, random phase homodyne detection has some advantages compared to direct photodetection. First, ultrafast sampling time can be achieved by using the local oscillator field in the form of a short pulse. Second, information on the photon distribution is carried by two rather intense fields, which can be detected with substantially higher efficiency than the signal field itself. This feature has enabled an experimental demonstration of even-odd oscillations in the photon distribution of the squeezed vacuum state [56].

Let us now see, how the phase-averaged homodyne statistics depends on the photon distribution. We shall use the fact that eigenvectors of the quadrature operator  $\hat{x}_{\theta}$  can be obtained from the position eigenvectors  $|x\rangle$  by the unitary transformation  $|x\rangle_{\theta} = e^{i\theta\hat{a}^{\dagger}\hat{a}}|x\rangle$ . This unitary transformation is diagonal in the Fock basis, and  $e^{i\theta\hat{a}^{\dagger}\hat{a}}|n\rangle = e^{in\theta}|n\rangle$ . Introducing two decompositions

of the identity operator in the Fock basis, we have:

$$\begin{aligned}
 p_{\mathcal{R}}(x) &= \frac{1}{2\pi} \int_0^{2\pi} d\theta \sum_{m,n=0}^{\infty} \langle |m\rangle \langle m|x\rangle_{\theta\theta} \langle x|n\rangle \langle n| \rangle \\
 &= \sum_{m,n=0}^{\infty} \langle m|x\rangle \langle x|n\rangle \int_0^{2\pi} \frac{d\theta}{2\pi} e^{i(n-m)\theta} \langle |m\rangle \langle n| \rangle \\
 &= \sum_{m=0}^{\infty} |\langle m|x\rangle|^2 \langle |m\rangle \langle m| \rangle
 \end{aligned} \tag{3.22}$$

Thus, occupations of the Fock states given by the expectation values  $\langle |m\rangle \langle m| \rangle$  contribute to the phase-averaged homodyne statistics with the coefficients

$$|\langle m|x\rangle|^2 = \frac{1}{\sqrt{\pi} 2^m m!} H_m^2(x) e^{-x^2}, \tag{3.23}$$

where  $H_m(x)$  denote Hermite polynomials. These coefficients correspond to the position distributions for the eigenstates of the harmonic oscillator.

Integrating  $p_{\mathcal{R}}(x)$  with appropriate pattern functions, we may reconstruct the photon statistics of the measured field, as well as other phase independent observables. An alternative method of processing the phase-averaged homodyne statistics, based on maximum-likelihood estimation, has been described in Ref. [57].



# Chapter 4

## Direct probing of quantum phase space

Quasidistribution functions contain complete characterization of the quantum state. An interesting and nontrivial problem is how to determine quasidistributions from quantities which can be detected in a feasible experimental scheme. In the previous chapter, we have discussed two experimental techniques for measuring the quantum state of a light mode: double homodyne detection, and optical homodyne tomography. These techniques are based on detection of quadratures, which are continuous variables. The two-dimensional probability distribution observed in double homodyne detection yields directly the  $Q$  function of a light mode. In optical homodyne tomography, a family of one-dimensional projections of the Wigner function is measured and then processed numerically using the back-projection algorithm.

In this chapter, we shall present a different approach to measuring quasidistributions of a light mode. We have seen in Chap. 2 that quasidistributions at a specific point of the phase space are given by expectation values of certain Hermitian operators. We shall demonstrate that this definition leads to a novel optical scheme for measuring quasidistribution functions of light. This scheme is based on photon counting. In contrast to the homodyne techniques discussed in the previous chapter, it is essential in our approach that the signal obtained from the detector is discrete, and that it is described by an integer variable characterizing the number of absorbed photons.

Our starting point in Sec. 4.1 will be a simple relation between the Wigner function and the photon statistics. We show that this relation can be implemented using a simple optical setup, which allows one to determine quasidistributions from photon statistics. In Sec. 4.2 we discuss the proposed scheme using the phase space picture. This picture explains in an intuitive way how physical parameters of the setup determine the measured quantity. In Sec. 4.3 we generalize the relation linking the quasidistributions and the photon statistics. We also discuss effects of non-unit detector efficiency. The full multimode theory of the proposed setup is developed in Sec. 4.4. We show there that the direct method for measuring quasidistributions can be easily extended to multimode radiation. Finally, in Sec. 4.5 we discuss theoretically several examples of photon statistics which would be obtained from the photodetector when measuring quasidistribution

functions.

## 4.1 Wigner function and photon statistics

We will start from deriving a simple relation between the Wigner function at the origin of the complex phase space  $W(0)$  and the photon statistics. Let us take the operator (2.13) for  $\alpha = 0$  and  $s = 0$ , and expand it into a power series:

$$\begin{aligned}\hat{W}(0; 0) &= \frac{2}{\pi} : \exp(-2\hat{a}^\dagger \hat{a}) : \\ &= \frac{2}{\pi} \sum_{n=0}^{\infty} (-1)^n : e^{-\hat{a}^\dagger \hat{a}} \frac{(\hat{a}^\dagger \hat{a})^n}{n!} : \\ &= \frac{2}{\pi} \sum_{n=0}^{\infty} (-1)^n |n\rangle \langle n|. \end{aligned}\tag{4.1}$$

In the last step, we have used the normally ordered operator representation of the  $n$  photon number projection operator. The last expression contains a sum which assigns  $+1$  to even Fock states, and  $-1$  to odd Fock states. Therefore, the whole sum is simply the parity operator, and the Wigner function at the phase space origin is given, up to the front factor  $2/\pi$ , by its expectation value [58]. Taking the quantum average of Eq. (4.1) gives:

$$W(0) = \langle \hat{W}(0; 0) \rangle = \frac{2}{\pi} \sum_{n=0}^{\infty} (-1)^n p_n \tag{4.2}$$

where the value  $p_n$  appearing in this expansion is just the probability of counting  $n$  photons by an ideal photodetector. Thus the photon statistics allows one to evaluate the Wigner function at the origin of the phase space.

It would be appealing to generalize this relation to an arbitrary point of the phase space. In principle, the only thing we have to do is to shift the system or equivalently the frame of reference in the phase space. The problem is, how to realize this in practice for optical fields. We will show that this goal can be achieved using a very simple optical arrangement, and that in a certain limit the displacement transformation is realized.

Let us consider the setup presented in Fig. 4.1. We take the detected field to be a superposition of two single-mode fields, which we shall call the signal and the probe. The corresponding annihilation operators are denoted by  $\hat{a}_S$  and  $\hat{a}_P$  respectively. The superposition is realized by means of a beam splitter BS with the power transmission characterized by the parameter  $T$ . In general, the action of the beam splitter is described by an SU(2) transformation between the annihilation operators of the incoming and outgoing modes [37]. As the phase shifts appearing in this transformation can be eliminated by appropriate redefinition of the modes, the annihilation

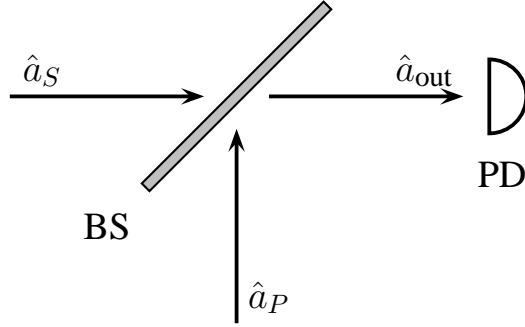


Figure 4.1: Experimental setup for measuring directly quasidistribution functions of a single light mode. BS denotes the beam splitter, PD is the photodetector, and the annihilation operators of the modes are indicated.

operator  $\hat{a}_{\text{out}}$  of the outgoing mode falling onto the detector surface can be assumed to be a combination

$$\hat{a}_{\text{out}} = \sqrt{T}\hat{a}_S - \sqrt{1-T}\hat{a}_P. \quad (4.3)$$

The photon statistics of the field  $\hat{a}_{\text{out}}$  is used to evaluate the alternating series according to Eq. (4.2). In this way we obtain the Wigner function of the outgoing mode at the origin of the phase space. This quantity depends on the quantum state of both the modes  $\hat{a}_S$  and  $\hat{a}_P$ . The Wigner function of the outgoing mode at the phase space origin is given in terms of the incoming modes by the expectation value of

$$\begin{aligned} \hat{W}_{\text{out}}(0; 0) &= \frac{2}{\pi} : \exp \left( -2\hat{a}_{\text{out}}^\dagger \hat{a}_{\text{out}} \right) : \\ &= \frac{2}{\pi} : \exp \left( -2T(\hat{a}_S^\dagger - \sqrt{(1-T)/T}\hat{a}_P^\dagger)(\hat{a}_S - \sqrt{(1-T)/T}\hat{a}_P) \right) : . \end{aligned} \quad (4.4)$$

This simple relation provides an interesting link between the detected quantity and the  $S$  mode. Let us consider the case when the probe field is a coherent state  $\hat{a}_P|\alpha\rangle = \alpha|\alpha\rangle$  uncorrelated with the signal mode. Performing the quantum average over the  $P$  mode in Eq. (4.4) is straightforward due to the normal ordering of the operators. Taking the expectation value over the signal and recalling the normally ordered definition of quasidistributions (2.12), we can recognize a quasidistribution of the signal field. Comparing its parameters, we obtain that the Wigner function (4.2) for the outgoing mode is proportional to an  $s = 1 - 1/T$  ordered quasidistribution function of the  $S$  mode:

$$W_{\text{out}}(0) = \frac{1}{T} W_S \left( \sqrt{\frac{1-T}{T}}\alpha; -\frac{1-T}{T} \right), \quad (4.5)$$

taken at the point  $\sqrt{(1-T)/T}\alpha$ . Thus our setup delivers directly the value of the signal quasidistribution function at the phase space point dependent on the amplitude and the phase of the

probe coherent state. Since both these parameters can be controlled experimentally without difficulties, we may simply scan the phase space by changing the amplitude and the phase of the probe field and thus determine the complete quasidistribution function. Eq. (4.5) shows that its ordering depends on the beam splitter transmission. For  $T$  near one the ordering is close to zero, which means that the measured quasidistribution approaches the Wigner function of the signal field. In contrast to optical homodyne tomography the Wigner function is measured directly and no sophisticated computer processing of the experimental data is necessary. The quantity measured in the experiment is proportional to the quasiprobability distribution at the phase space point depending only on the amplitude and phase of the probe state.

## 4.2 Phase space picture

The quantity measured in the setup discussed in the previous section has an interesting phase space interpretation for arbitrary states of the  $S$  and  $P$  modes. To show this, we shall disentangle the two-mode operator defined in Eq. (4.4) using the following Gaussian integral of normally ordered operators for the  $S$  and  $P$  modes:

$$\begin{aligned} \hat{W}_{\text{out}}(0; 0) &= \frac{4}{\pi^2} \int d^2\beta : \exp \left( -2(\sqrt{T}\beta^* - \hat{a}_P^\dagger)(\sqrt{T}\beta - \hat{a}_P) \right) : \\ &\quad \times : \exp \left( -2(\sqrt{1-T}\beta^* - \hat{a}_S^\dagger)(\sqrt{1-T}\beta - \hat{a}_S) \right) : . \end{aligned} \quad (4.6)$$

Under the assumption that the  $S$  and  $P$  modes are uncorrelated, we can evaluate separately expectation values over the signal and the probe modes. It is easily seen that these expectation values yield the values of Wigner functions of the signal and the probe modes  $W_S(\sqrt{1-T}\beta)$  and  $W_P(\sqrt{T}\beta)$ . Thus we obtain the following expression for the quantity detected by our setup:

$$\begin{aligned} W_{\text{out}}(0) &= \int d^2\beta W_S(\sqrt{1-T}\beta) W_P(\sqrt{T}\beta) \\ &= \frac{1}{1-T} \int d^2\beta W_S(\beta) W_P(\sqrt{T/(1-T)}\beta). \end{aligned} \quad (4.7)$$

This formula establishes a connection between the photon number parity of the outgoing mode and the Wigner functions of the  $S$  and  $P$  modes. The object of interest in the above formula is the Wigner function of the signal field  $W_S(\beta)$ . The quantity we obtain from the measurement is  $W_{\text{out}}(0)$ , which is given by the integral of  $W_S(\beta)$  with the function  $W_P(\sqrt{T/(1-T)}\beta)$ . Let us now see, what information on the signal state can be obtained from this integral.

In the case when the beam splitter splits the light equally, i.e. the power transmission is  $T = 50\%$ , we have  $\sqrt{T/(1-T)} = 1$  and  $W_{\text{out}}(0)$  is simply a doubled overlap of the signal and probe Wigner functions. If we take the probe field to be a coherent state with variable amplitude and phase, we obtain the  $Q$  function of the signal field. Analogously to double homodyne detection

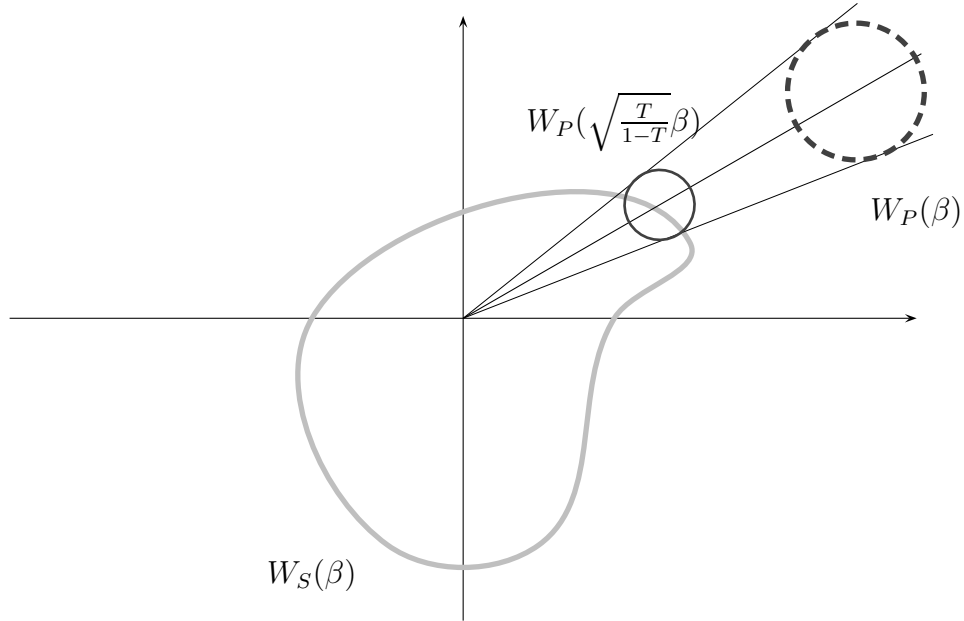


Figure 4.2: Phase space interpretation of the observable measured in the discussed setup. The Wigner function of the signal field  $W_S(\beta)$  is integrated with the rescaled Wigner function of the probe field  $W_P(\sqrt{\frac{T}{1-T}}\beta)$ . If the rescaling factor  $\sqrt{\frac{T}{1-T}}$  is larger than one, the probe Wigner function becomes effectively contracted in all directions. Of course, the rescaled Wigner function does not describe physical fields at any point of the setup.

discussed in Sec. 3.2, the probe Wigner function can be considered as a “quantum ruler”, which smoothes the signal Wigner function to a positive definite phase space distribution.

In a general case, the phase space parameterization of the probe Wigner function is rescaled by the factor  $\sqrt{T/(1-T)}$ . It is easy to see that this factor can take an arbitrary positive value depending on the beam splitter transmission. The most interesting region is for  $T > 1/2$ , where the scaling factor  $\sqrt{T/(1-T)}$  is greater than one. This situation is shown pictorially in Fig. 4.2. The scaling factor effectively “contracts” the probe Wigner function in all the directions simultaneously. Consequently, the area occupied by the rescaled probe Wigner function becomes smaller, and the integral in Eq. (4.7) provides more “local” information on the behaviour of the signal Wigner function  $W_S(\beta)$ . It is seen from the form of the scaling factor, that this effect of “contraction” grows unlimitedly with the beam splitter transmission tending to one.

In a particular case of the coherent probe field  $|\alpha\rangle$ , the  $P$  mode Wigner function is of the form

$$W_P(\beta) = \frac{2}{\pi} \exp(-2|\beta - \alpha|^2). \quad (4.8)$$

When  $T$  tends to one, the rescaled probe Wigner function  $W_P(\sqrt{T/(1-T)}\beta)$  approaches the form of the delta function, and the effect of smoothing becomes negligible. Thus, in the limiting

case of  $T \rightarrow 1$  the integral (4.7) yields the value the signal Wigner function at a single phase space point. However, it is seen from Eq. (4.5) that the rescaling of the probe Wigner function in the integral (4.7) has another consequence. When  $T$  tends to one, the factor multiplying the probe amplitude  $\alpha$  becomes very small. This effect is seen also in Fig. 4.2. Therefore, in order to scan the interesting region of the signal phase space we need to use a probe field of large intensity. From the mathematical point of view, the discussed limiting case involves two transitions: with  $T \rightarrow 1$  and  $|\alpha| \rightarrow \infty$ , such that the product  $\sqrt{(1-T)/T}\alpha$  is fixed. This product determines the point of the phase space at which the signal Wigner function is measured.

Let us stress that the rescaled Wigner function, not obeying the Heisenberg uncertainty principle, does not describe any fields appearing physically in the setup; it is a purely abstract object introduced in the phase space interpretation of our measurement scheme.

The integral representation derived in Eq. (4.7) shows a connection of our setup with the model scheme of a phase space measurement, discussed in Sec. 3.2. In this model scheme, a filter device—a “quantum ruler”—is introduced in addition to the system the measured phase space probability distribution is the convolution of the system and filter Wigner functions. Our scheme is more general, since the Wigner function of the filter can be rescaled by an arbitrary factor. Consequently the rescaled probe Wigner function does not have to obey the Heisenberg uncertainty principle and it may even approach the shape of a delta function, which leads to the direct measurement of the Wigner function.

### 4.3 Generalization

In the remaining discussion we will introduce two generalizations. First we will make our considerations more realistic by taking into account the imperfection of the photodetector. When the detector efficiency is  $\eta$ , the probability of counting  $n$  photons is given by the expectation value:

$$p_n = \left\langle : e^{-\eta \hat{a}_{\text{out}}^\dagger \hat{a}_{\text{out}}} \frac{(\eta \hat{a}_{\text{out}}^\dagger \hat{a}_{\text{out}})^n}{n!} : \right\rangle. \quad (4.9)$$

The second extension is the substitution of the factor  $(-1)^n$  in Eq. (4.2) by  $-(s+1)^n/(s-1)^{n+1}$ , where  $s$  is a real parameter. The origin and the role of the parameters  $\eta$  and  $s$  is different:  $\eta$  describes experimental limitations, while  $s$  is an artificial number introduced in the numerical processing of the measured data. With these two parameters we obtain the following simple generalization of the formula (4.4), when expressed in terms of the  $S$  and  $P$  modes

$$\begin{aligned} \hat{W}_{\text{out}}^{(\eta)}(0; s) &= \frac{2}{\pi(1-s)} \sum_{n=0}^{\infty} \left( \frac{s+1}{s-1} \right)^n : e^{-\eta \hat{a}_{\text{out}}^\dagger \hat{a}_{\text{out}}} \frac{(\eta \hat{a}_{\text{out}}^\dagger \hat{a}_{\text{out}})^n}{n!} : \\ &= \frac{2}{\pi(1-s)} : \exp \left( -\frac{2\eta}{1-s} \hat{a}_{\text{out}}^\dagger \hat{a}_{\text{out}} \right) : \end{aligned}$$

$$= \frac{2}{\pi(1-s)} : \exp \left( -\frac{2\eta T}{1-s} (\hat{a}_S^\dagger - \sqrt{(1-T)/T} \hat{a}_P^\dagger) (\hat{a}_S - \sqrt{(1-T)/T} \hat{a}_P) \right) : . \quad (4.10)$$

The third line of this equation suggests that the parameter  $s$  can be used to compensate the imperfectness of the photodetector. Indeed if we selected  $s = 1 - \eta$ , we would determine the expectation value of  $\exp(-2\hat{a}_{\text{out}}^\dagger \hat{a}_{\text{out}})$  : regardless of the detector efficiency. But in this case the factor multiplying the probability of counting  $n$  photons is  $(1 - 2/\eta)^n$  and its magnitude diverges to infinity with  $n \rightarrow \infty$ . Therefore we may expect problems with the convergence of the series. Even when the series is convergent, some singularities can be encountered in the processing of the experimentally measured photon statistics, which is affected by statistical fluctuations. Statistical noise may be a source of problems, as the increasing factor in Eq. (4.10) causes that an important contribution comes from the “tail” of the experimental counts distribution, which usually has a very poor statistics. The diverging factor  $[(s+1)/(s-1)]^n$  amplifies fluctuations in this tail, and consequently the final result has a huge statistical error. The simplest way to avoid all these problems is to assume that the factors multiplying the counts statistics are bounded, which is equivalent to the condition  $s \leq 0$ . We shall discuss thoroughly the effects of statistical noise in the next chapter. This discussion will fully confirm the present conclusion drawn from qualitative arguments that in principle it is not possible to compensate for detector losses, and that in general we should restrict the range of  $s$  to nonpositive values.

As before, let us consider the case when the coherent state  $|\alpha\rangle$  is employed as a probe. The expectation value of the generalized operator  $\hat{W}_{\text{out}}^{(\eta)}(0; s)$  is again given by the quasidistribution function of the signal mode:

$$\langle \hat{W}_{\text{out}}^{(\eta)}(0; s) \rangle = \frac{1}{\eta T} W_S \left( \sqrt{\frac{1-T}{T}} \alpha; -\frac{1-s-\eta T}{\eta T} \right). \quad (4.11)$$

Let us now analyze the ordering of this function. As we discussed in Sec. 2.4, although from a theoretical point of view an arbitrarily ordered distribution contains the complete characterization of the quantum state, experimental errors make it difficult to compute higher ordered distributions from the measured one. Thus what is interesting is the highest ordering achievable in our scheme. Analysis of the role of the parameter  $s$  is the simplest, since the greater its value, the higher is the ordering obtained. Because we have restricted its range to nonpositive values, it should be consequently set to zero. Thus we are left with the product of the parameters  $\eta$  and  $T$ . For fixed  $\eta$  the highest ordering is achieved when  $T \rightarrow 1$ , and its limit value is now  $-(1-\eta)/\eta$ . Under the assumption that  $\eta$  and  $T$  are close to one, the ordering of the measured distribution is effectively equal to this limiting value if the difference  $1-T$  is much smaller than  $1-\eta$ . This is a realistic condition for currently existing photodetectors, which have the maximum efficiency about 80% [59]. Thus the highest ordering achievable in our scheme is effectively determined by the photodetector efficiency and is equal to  $-(1-\eta)/\eta$ . It is noteworthy that this is exactly

equal to the ordering of the distribution reconstructed tomographically from data measured in the homodyne detection with imperfect detectors [45].

## 4.4 Multimode approach

So far, we have discussed the experimental scheme assuming that the signal and the probe beams are single-mode fields. We shall now present the full multimode theory of the direct scheme for measuring the quantum optical quasidistribution functions. In the single-mode description it was sufficient to use a pair of annihilation operators  $\hat{a}_S$  and  $\hat{a}_P$ . The spatio-temporal characteristics of these two modes was not important in this approach, and it was implicitly assumed that the modes are matched perfectly at the beam splitter. We shall free our further analysis from these simplifying assumptions.

Let us denote by  $\hat{\mathbf{E}}_{\text{out}}^{(+)}(\mathbf{r}, t)$  the positive-frequency part of the electric field operator at the surface of the detector. This field is a superposition of the signal and the probe fields combined at the beam splitter BS. Mathematical representation of this combination is a slightly delicate matter. If we wanted to express  $\hat{\mathbf{E}}_{\text{out}}^{(+)}(\mathbf{r}, t)$  in terms of the signal and probe field operators before the beam splitter, we would have to introduce appropriate propagators. This would obscure the physical picture of the measurement. Therefore we shall choose another notation for the signal and the probe fields, which will make the discussion much more transparent. We shall denote by  $\hat{\mathbf{E}}_S^{(+)}(\mathbf{r}, t)$  the electric field operator of the signal beam that would fall onto the detector surface *in the absence of the beam splitter BS*. Analogously, let  $\hat{\mathbf{E}}_P^{(+)}(\mathbf{r}, t)$  be the probe field at the detector surface, assuming that the beam splitter BS *was replaced by a perfectly reflecting mirror*. With these definitions, the field  $\hat{\mathbf{E}}_{\text{out}}^{(+)}(\mathbf{r}, t)$  resulting from the interference of the signal and the probe beams is given simply by

$$\hat{\mathbf{E}}_{\text{out}}^{(+)}(\mathbf{r}, t) = \sqrt{T}\hat{\mathbf{E}}_S^{(+)}(\mathbf{r}, t) - \sqrt{1-T}\hat{\mathbf{E}}_P^{(+)}(\mathbf{r}, t). \quad (4.12)$$

We have assumed here that the characteristics of the beam splitter is constant over the spectral and polarization range of the considered fields.

Further, we shall assume that the detected fields are quasi-monochromatic with the central frequency  $\omega_0$ . This will allow us to relate easily the number of photons to the energy of the field absorbed by the detector. Assuming that the direction of propagation of the field  $\hat{\mathbf{E}}_{\text{out}}^{(+)}(\mathbf{r}, t)$  is perpendicular to the detector, the operator of the photon flux through the detector surface is given by

$$\hat{\mathcal{J}}_{\text{out}} = \frac{2\epsilon_0 c}{\hbar\omega_0} \int_{\Delta t} dt \int_D d^2\mathbf{r} \hat{\mathbf{E}}_{\text{out}}^{(-)}(\mathbf{r}, t) \hat{\mathbf{E}}_{\text{out}}^{(+)}(\mathbf{r}, t) \quad (4.13)$$

where  $\hat{\mathbf{E}}_{\text{out}}^{(-)}(\mathbf{r}, t) = [\hat{\mathbf{E}}_{\text{out}}^{(+)}(\mathbf{r}, t)]^\dagger$ , and the temporal and the spatial integrals are performed respectively over the detector opening time  $\Delta t$  and its active surface  $D$ . The probability of registering

$n$  photons is given by

$$p_n = \left\langle : e^{-\eta \hat{J}_{\text{out}}} \frac{(\eta \hat{J}_{\text{out}})^n}{n!} : \right\rangle_{S,P}, \quad (4.14)$$

where  $\eta$  is the detector quantum efficiency.

As before, we will use the count statistics to calculate the average parity of the registered photons. It can be expressed in terms of the photon flux operator as:

$$\sum_{n=0}^{\infty} (-1)^n p_n = \langle : \exp(-2\eta \hat{J}_{\text{out}}) : \rangle_{S,P}. \quad (4.15)$$

If a coherent field is used as the probe, we may immediately evaluate the quantum expectation value over the  $P$  mode and obtain

$$\begin{aligned} \sum_{n=0}^{\infty} (-1)^n p_n &= \left\langle : \exp \left( -\frac{4\eta\epsilon_0 c}{\hbar\omega_0} \int_{\Delta t} dt \int_D d^2\mathbf{r} [\sqrt{T} \hat{\mathbf{E}}_S^{(-)}(\mathbf{r}, t) - \sqrt{1-T} \mathbf{E}_P^*(\mathbf{r}, t)] \right. \right. \\ &\quad \times [\sqrt{T} \hat{\mathbf{E}}_S^{(+)}(\mathbf{r}, t) - \sqrt{1-T} \mathbf{E}_P(\mathbf{r}, t)] \left. \right) : \right\rangle, \end{aligned} \quad (4.16)$$

where  $\mathbf{E}_P(\mathbf{r}, t) = \langle \hat{\mathbf{E}}_P^{(+)}(\mathbf{r}, t) \rangle_P$  is the amplitude of the coherent probe field.

We will now consider the signal field  $\hat{\mathbf{E}}_S^{(+)}(\mathbf{r}, t)$  in which a finite number of  $M$  modes is possibly excited. We shall denote the corresponding annihilation operators by  $\hat{a}_i$ , and the mode functions by  $\mathbf{u}_i(\mathbf{r}, t)$ , where  $i = 1, 2, \dots, M$ . Our goal will be to relate the photon statistics  $p_n$  to the multimode quasidistribution characterizing these modes. Thus we decompose the signal field  $\hat{\mathbf{E}}_S^{(+)}(\mathbf{r}, t)$  in the form

$$\hat{\mathbf{E}}_S^{(+)}(\mathbf{r}, t) = \sum_{i=1}^M \hat{a}_i \mathbf{u}_i(\mathbf{r}, t) + \hat{\mathbf{V}}(\mathbf{r}, t), \quad (4.17)$$

where the operator  $\hat{\mathbf{V}}(\mathbf{r}, t)$  is a sum of all the other modes remaining in the vacuum state. This part of the field does not contribute to the detector counts in the normally ordered expression given in Eq. (4.16), because its normally ordered moments are zero.

Further, we shall assume that virtually all the excited part of the signal field is absorbed by the detector within the gate opening time. This allows us to write orthonormality relations for the mode functions  $\mathbf{u}_i(\mathbf{r}, t)$  in the form

$$\frac{2\epsilon_0 c}{\hbar\omega_0} \int_{\Delta t} dt \int_D d^2\mathbf{r} \mathbf{u}_i^*(\mathbf{r}, t) \mathbf{u}_j(\mathbf{r}, t) = \delta_{ij} \quad (4.18)$$

where the integrals are restricted to the domain defined by the detection process. With these assumptions, we may simplify the exponent of Eq. (4.16). It is convenient to introduce dimensionless amplitudes  $\alpha_i$ , which are projections of the probe field onto the mode functions:

$$\alpha_i = \frac{2\epsilon_0 c}{\hbar\omega_0} \int_{\Delta t} dt \int_D d^2\mathbf{r} \mathbf{u}_i^*(\mathbf{r}, t) \mathbf{E}_P(\mathbf{r}, t). \quad (4.19)$$

Using these amplitudes, we may write the measured quantity as:

$$\begin{aligned} \sum_{n=0}^{\infty} (-1)^n p_n &= \left\langle : \exp \left( -2\eta T \sum_{i=1}^M (\hat{a}_i^\dagger - \sqrt{(1-T)/T} \alpha_i^*) (\hat{a}_i - \sqrt{(1-T)/T} \alpha_i) \right) : \right\rangle \\ &\times \exp \left[ -2\eta(1-T) \left( \frac{2\epsilon_0 c}{\hbar \omega_0} \int_{\Delta t} dt \int_D d^2 \mathbf{r} |\mathbf{E}_P(\mathbf{r}, t)|^2 - \sum_{i=1}^M |\alpha_i|^2 \right) \right]. \end{aligned} \quad (4.20)$$

The exponent appearing in the second line of the above expression results from the part of the probe field that is orthogonal (in the sense of Eq. (4.18)) to the mode functions describing the excited component of the signal field. This exponent is equal to one if the probe field matches the  $M$  signal modes of interest. This condition can be written as:

$$\mathbf{E}_P(\mathbf{r}, t) = \sum_{i=1}^M \alpha_i \mathbf{u}_i(\mathbf{r}, t). \quad (4.21)$$

In this case, we can easily recognize in the quantum expectation value in Eq. (4.20) the multimode quasidistribution function defined in Eq. (2.24), and write:

$$\sum_{n=0}^{\infty} (-1)^n p_n = \left( \frac{\pi}{2\eta T} \right)^M W_S \left( \sqrt{\frac{1-T}{T}} \alpha_1, \dots, \sqrt{\frac{1-T}{T}} \alpha_M; -\frac{1-\eta T}{\eta T} \right). \quad (4.22)$$

Thus, the direct scheme allows one to measure multimode quasidistribution functions, even if the modes cannot be spatially separated. What one needs to do, is to combine the multimode signal field with appropriately chosen probe field, and to measure the count statistics of the resulting superposition. Let us note, that it is not necessary to resolve contributions to the count statistics from each of the modes; the only observable we need to reconstruct the multimode quasidistribution is the parity of the *total* number of photocounts.

The direct scheme for measuring multimode quasidistributions can be also used if some of the modes are spatially separated. In this case, each mode (or group of spatially overlapping modes) has to be displaced in the phase space by combining at a beam splitter with a coherent probe field, and then measured using a photon counting detector. The parity of the number of photocounts obtained on all the detectors yields the value of the quasidistribution function at a point defined by the values of coherent displacements.

## 4.5 Examples of photocount statistics

We will close this chapter by presenting several examples of the photocount statistics for different quantum states of the signal probed by a coherent source of light. The most straightforward case

is when a coherent state  $|\alpha_0\rangle$  enters through the signal port of the beam splitter. Then the statistics of the registered counts is given by the Poisson distribution:

$$p_n^{|\alpha_0\rangle} = \frac{[J(\alpha_0)]^n}{n!} e^{-J(\alpha_0)}, \quad (4.23)$$

where  $J(\alpha_0) = \eta T |\beta - \alpha_0|^2$  is the average number of registered photons, and  $\beta = \sqrt{(1-T)/T}\alpha$  denotes the point of the phase space at which the value of the quasidistribution is measured. When the measurement is performed at the point where the quasidistribution of the signal field is centered, i.e.,  $\beta = \alpha_0$ , the fields interfere destructively and no photons are detected. In general, for an arbitrary phase space point, the average number of registered photons is proportional to the squared distance from  $\alpha_0$ . Averaging Eq. (4.23) over an appropriate  $P$  representation yields the photocount statistics for a thermal signal state characterized by an average photon number  $\bar{n}$ :

$$p_n^{\text{th}} = \frac{(\eta T \bar{n})^n}{(1 + \eta T \bar{n})^{n+1}} L_n \left( -\frac{|\beta|^2}{\bar{n}(1 + \eta T \bar{n})} \right) \exp \left( -\frac{\eta T |\beta|^2}{1 + \eta T \bar{n}} \right), \quad (4.24)$$

where  $L_n$  denotes the  $n$ th Laguerre polynomial.

A more interesting case is when the signal field is in a nonclassical state, which cannot be described by a positive definite  $P$  function. Then the interference between the signal and the probe fields cannot be described within the classical theory of radiation. We will consider two nonclassical states: the one photon Fock state and the Schrödinger cat state. The most straightforward way to calculate the photocount statistics is to evaluate explicitly the general quasidistribution function, and to substitute as its parameters  $\sqrt{(1-T)/T}\alpha$  and  $-(1-s-\eta T)/\eta T$  according to Eq. (4.11). Expanding this expression into the powers of  $(s+1)/(s-1)$  yields the photocount statistics, which follows from the first line of Eq. (4.10).

The photocount distribution for the one photon Fock state  $|1\rangle$  can be written as an average of two terms with the weights  $\eta T$  and  $1 - \eta T$ :

$$p_n^{|1\rangle} = \eta T [n - J(0)]^2 \frac{[J(0)]^{n-1}}{n!} e^{-J(0)} + (1 - \eta T) \frac{[J(0)]^n}{n!} e^{-J(0)}. \quad (4.25)$$

The second term corresponds to the detection of the vacuum signal field. Its presence is a result of the detector imperfection and the leakage of the signal field through the unused output port of the beam splitter. This term vanishes in the limit of  $\eta T \rightarrow 1$ , where the Wigner function is measured in the setup. The first term describes the detection of the one photon Fock state. In Fig. 4.3(a) we show the statistics generated by this term for different values of  $\beta$ . If the amplitude of the probe field is zero, we detect the undisturbed signal field and the statistics is nonzero only for  $n = 1$ . The distribution becomes flatter with increasing  $\beta$ . Its characteristic feature is that it vanishes around  $n \approx J(0)$ .

For the Schrödinger cat state defined in Eq. (2.18) the photocount statistics is a sum of three terms:

$$p_n^{|\psi\rangle} = \frac{1}{2(1 + e^{-2|\alpha_0|^2})} \left[ \frac{[J(\alpha_0)]^n}{n!} e^{-J(\alpha_0)} + \frac{[J(-\alpha_0)]^n}{n!} e^{-J(-\alpha_0)} \right]$$

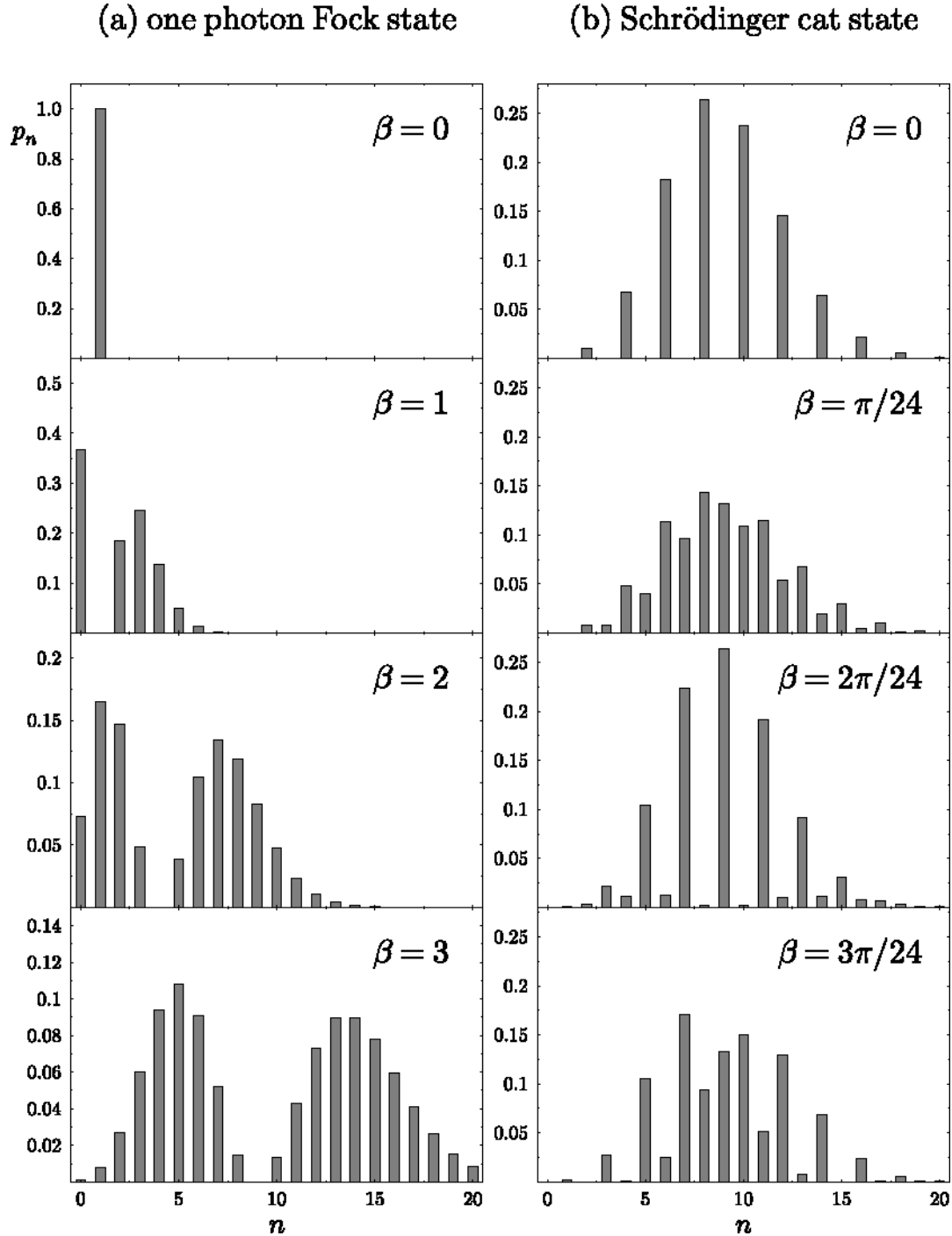


Figure 4.3: The photocount statistics of (a) the one photon Fock state and (b) the Schrödinger cat state for  $\alpha_0 = 3i$ , shown for several values of the rescaled probe field amplitude  $\beta = \sqrt{(1 - T)/T}\alpha$  in the limit  $\eta T = 1$ .

$$+2\text{Re} \left( \frac{[\eta T(\beta^* - \alpha_0^*)(\beta + \alpha_0)]^n}{n!} e^{\eta T(\alpha_0^*\beta - \alpha_0\beta^*)} \right) e^{-(2-\eta T)|\alpha_0|^2 - \eta T|\beta|^2} \right]. \quad (4.26)$$

The first two terms describe the two coherent components of the cat state, whereas the last one contributes to the quantum interference structure. In Fig. 4.3(b) we plot the photocount statistics for different values of  $\beta$  probing this structure, in the limit  $\eta T \rightarrow 1$ . The four values of  $\beta$  correspond to the cosine function in Eq. (2.19) equal to 1, 0,  $-1$ , and 0, respectively, for  $t = 0$ . It is seen that the form of the statistics changes very rapidly with  $\beta$ . This behavior becomes clear if we recall that the Wigner function is given by the expectation value of the displaced photon number parity operator. Therefore, in order to obtain a large positive (negative) value of the Wigner function, the photocount statistics has to be concentrated in even (odd) values of  $n$ .



# Chapter 5

## Practical aspects

We will now discuss practical aspects of the direct scheme for measuring quasidistributions of a single light mode. An important problem is the role of the statistical noise. The proposed measurement scheme is based on the relation between the quasidistributions and the photocount statistics. In a real experiment the statistics of the detector counts cannot be known with perfect accuracy, as it is determined from a finite sample of  $N$  measurements. This statistical uncertainty affects the experimental value of the quasidistribution. Theoretical analysis of the statistical error is important for two reasons. First, we need an estimate for the number of the measurements required to determine the quasidistribution with a given accuracy. Such an estimate is needed when designing an experiment. The total number of measurements is usually limited by various factors, such as temporal stability of the optical setup. Estimation of the statistical error tells us, how precise result can be expected in a realistic scheme. Secondly, we have seen in Sec. 4.3 that one may attempt to compensate the imperfection of the detector and the non-unit transmission of the beam splitter by appropriate numerical processing of the measured statistics. However, a preliminary qualitative discussion of the statistical noise strongly indicated that such a procedure may amplify the statistical noise. Our present calculations will provide a detailed, quantitative analysis of this problem. In Sec. 5.1 we define the observable whose statistical properties will be studied. In Sec. 5.2 we derive expressions for the mean value and the statistical variance. The basic element of this derivation is the multinomial distribution, which defines the probability of obtaining a specific photocount statistics from a series of  $N$  measurements. The behaviour of the mean value and statistical variance is discussed in Sec. 5.3. Particular attention is paid to the possibility of loss compensation. We present a collection of pathological cases, where the compensation leads to an explosion of the statistical uncertainty. These cases show clearly that in a general case the compensation of detector losses is not possible.

In Sec. 5.4 we discuss effects of the mode-mismatch between the signal and the probe fields. In practice, the fields superposed at a beam splitter never exhibit 100% visibility of interference. This fact has to be taken into account, when we analyse the result of a real experiment. The effects of the mode-mismatch will be discussed using the multimode theory developed in

Sec. 4.4.

## 5.1 Photon count generating function

In order to make our discussion more transparent, we shall redefine the quantity evaluated from the photocount statistics  $p_n$  to the form:

$$\Pi(s) = \sum_{n=0}^{\infty} \left( \frac{s+1}{s-1} \right)^n p_n. \quad (5.1)$$

Thus,  $\Pi(s)$  corresponds to the observable defined in Eq. (4.10) without the front normalization factor. We shall call  $\Pi(s)$  the *photon count generating function (PCGF)*, as the full photon statistics can be retrieved from  $\Pi(s)$  as an analytical function of  $s$ . In our scheme, the PCGF is given by the expectation value

$$\Pi(s) = \left\langle : \exp \left( -\frac{2\eta\hat{\mathcal{J}}_{\text{out}}}{1-s} \right) : \right\rangle, \quad (5.2)$$

where  $\hat{\mathcal{J}}_{\text{out}}$  is the operator of the time-integrated flux of the light incident onto the surface of the detector. This operator can be expressed in terms of the signal and probe fields as

$$\hat{\mathcal{J}}_{\text{out}} = (\sqrt{T}\hat{a}_S^\dagger - \sqrt{1-T}\hat{a}_P^\dagger)(\sqrt{T}\hat{a}_S - \sqrt{1-T}\hat{a}_P), \quad (5.3)$$

with  $T$  being the beam splitter power transmission. When a coherent state  $|\alpha\rangle_P$  is used as a probe, we have

$$\Pi(s) = \frac{\pi(1-s)}{2\eta T} W_S \left( \sqrt{\frac{1-T}{T}}\alpha; -\frac{1-s-\eta T}{\eta T} \right), \quad (5.4)$$

and the PCGF is proportional to the quasidistribution function of the signal mode.

## 5.2 Statistical error

In a real experiment, the photon statistics is obtained from a finite series of  $N$  measurements. The result of these measurements has the form of a histogram  $\{k_n\}$ , where  $k_n$  denotes the number of measurements when  $n$  photons have been detected. Dividing  $k_n$  by the total number of measurements, we obtain an estimate for the photon distribution  $p_n$ . This estimate is subsequently used to evaluate the PCGF defined in Eq. (5.1). In the analysis of the statistical properties of the PCGF, we shall introduce a cut-off parameter  $K$  for the maximum photon number. In this way, the analysed quantity will depend on a finite number of variables  $k_n$ , where  $n = 0, 1, \dots, K$ . Thus, we consider an experimental estimate for  $\Pi(s)$  in the form:

$$\Pi_{\text{exp}}(s) = \frac{1}{N} \sum_{n=0}^K \left( \frac{s+1}{s-1} \right)^n k_n. \quad (5.5)$$

Our goal is to see how well this estimate approximates the ideal quantity  $\Pi(s)$ . Due to extreme simplicity of the relation between the count statistics the quasidistributions, it is possible to perform a rigorous analysis of the statistical error and to obtain an exact expression for the uncertainty of the final result. The basic tool in our analysis is the probability distribution for the histograms  $\{k_n\}$  which can be obtained from  $N$  experimental runs. Because all the runs are statistically independent, the set of  $k_n$ s obeys the multinomial distribution [60]:

$$\mathcal{P}(k_0, k_1, \dots, k_K) = \frac{N!}{k_0! k_1! \dots (N - \sum_{n=0}^K k_n)!} p_0^{k_0} p_1^{k_1} \dots p_K^{k_K} \left(1 - \sum_{n=0}^K p_n\right)^{N - \sum_{n=0}^K k_n}. \quad (5.6)$$

In this formula,  $p_n$  is the ideal, noise-free photocount distribution that would be obtained in the limit of the infinite number of measurements.

Using the distribution given in Eq. (5.6), we may calculate quantities characterizing statistical properties of the experimental PCGF. In order to see how well  $\Pi_{\text{exp}}(s)$  approximates the ideal quantity we will find its mean value and its variance. This task is quite easy, since the only expressions we need in the calculations are the following moments:

$$\begin{aligned} \overline{k_n} &= Np_n, \\ \overline{k_l k_n} &= N(N-1)p_l p_n + \delta_{ln} Np_n. \end{aligned} \quad (5.7)$$

We use the bar to denote the statistical average with respect to the distribution  $\mathcal{P}(k_0, \dots, k_K)$ . Given this result, it is straightforward to obtain:

$$\overline{\Pi_{\text{exp}}(s)} = \sum_{n=0}^K \left( \frac{s+1}{s-1} \right)^n p_n, \quad (5.8)$$

and

$$\begin{aligned} \delta \Pi_{\text{exp}}^2(s) &= \overline{(\Pi_{\text{exp}}(s) - \overline{\Pi_{\text{exp}}(s)})^2} \\ &= \frac{1}{N} \left[ \sum_{n=0}^K \left( \frac{s+1}{s-1} \right)^{2n} p_n - \left( \sum_{n=0}^K \left( \frac{s+1}{s-1} \right)^n p_n \right)^2 \right]. \end{aligned} \quad (5.9)$$

The error introduced by the cut-off of the photocount statistics can be estimated by

$$|\overline{\Pi_{\text{exp}}(s)} - \Pi(s)| = \left| \sum_{n=K+1}^{\infty} \left( \frac{s+1}{s-1} \right)^n p_n \right| \leq \sum_{n=K+1}^{\infty} \left| \frac{s+1}{s-1} \right|^n p_n. \quad (5.10)$$

The variance  $\delta \Pi_{\text{exp}}^2$ , derived in Eq. (5.9), is a difference of two terms. The second one is simply the squared average of  $\Pi_{\text{exp}}$ . The first term is a sum over the count statistics multiplied by the

powers of a *positive* factor  $[(s+1)(s-1)]^2$ . If  $s > 0$ , this factor is greater than one and the sum may be arbitrarily large. In the case when the contribution from the cut tail of the statistics is negligible, i.e., if  $K \rightarrow \infty$ , it can be estimated by the average number of registered photons:

$$\sum_{n=0}^{\infty} \left( \frac{s+1}{s-1} \right)^{2n} p_n \geq 1 + \frac{4s}{(s-1)^2} \langle \eta \hat{\mathcal{J}}_{\text{out}} \rangle. \quad (5.11)$$

Thus, the variance grows unlimited as we probe phase space points far from the area where the quasidistribution is localized. Several examples in the next section will demonstrate that the variance usually explodes much more rapidly, exponentially rather than linearly. This makes the compensation of the detector inefficiency a very subtle matter. It can be successful only for very restricted regions of the phase space, where the count statistics is concentrated for a small number of counts and vanishes sufficiently quickly for larger  $n$ 's.

Therefore, in order to ensure that the statistical error remains bounded over the whole phase space, we have to impose the condition  $s \leq 0$ . Since we are interested in achieving the highest possible ordering of the measured quasidistribution, we should consequently set  $s = 0$ . For this particular value the estimations for the uncertainty of  $\Pi_{\text{exp}}$  take a much simpler form. The error caused by the cut-off of the count distribution can be estimated by the “lacking” part of the probability:

$$|\Pi_{\text{exp}}(0) - \Pi(0)| \leq 1 - \sum_{n=0}^K p_n, \quad (5.12)$$

which shows that the cut-off is unimportant as long as the probability of registering more than  $K$  photons is negligible. The variance of  $\Pi_{\text{exp}}$  is given by

$$\delta \Pi_{\text{exp}}^2(0) = \frac{1}{N} \left[ \sum_{n=0}^K p_n - \left( \overline{\Pi_{\text{exp}}(0)} \right)^2 \right] \leq \frac{1}{N} \left[ 1 - \left( \overline{\Pi_{\text{exp}}(0)} \right)^2 \right] \leq \frac{1}{N}. \quad (5.13)$$

Thus, the statistical uncertainty of the measured quasidistribution can be simply estimated as  $1/\sqrt{N}$  multiplied by the proportionality constant given in Eq. (5.4). It is also seen that the uncertainty is smaller for the phase space points where the magnitude of the quasidistribution is large.

### 5.3 Compensation of detector losses

We will now consider several examples of the reconstruction of the quasidistributions from the data collected in a photon counting experiment. Our discussion will be based on Monte Carlo simulations compared with the analytical results obtained in the previous section.

First, let us note that the huge statistical error is not the only problem in compensating the detector inefficiency. If  $s > 0$ , the sum (5.8) does not even have to converge in the limit of

$K \rightarrow \infty$ . An example of this pathological behaviour is provided by a thermal state, which has been calculated in Eq. (4.24). For the zero probe field we obtain

$$\overline{\Pi_{\text{exp}}^{\text{th}}(s)} = \frac{1}{1 + \eta T \bar{n}} \sum_{n=0}^K \left( \frac{s+1}{s-1} \right)^n \left( \frac{\eta T \bar{n}}{1 + \eta T \bar{n}} \right)^n, \quad (5.14)$$

which shows that if  $s > 0$ , then for a sufficiently intense thermal state the magnitude of the summand is larger than one and consequently the sum diverges, when  $K \rightarrow \infty$ . This behaviour is due to the very slowly vanishing count distribution for large  $n$ , and it does not appear for the other examples of the count statistics derived in Sec. 4.5.

In Fig. 5.1 we plot the reconstructed quasidistributions for the coherent state  $|\alpha_0 = 1\rangle$  and the one photon Fock state. Due to the symmetry of these states, it is sufficient to discuss the behaviour of the reconstructed quasidistribution on the real axis of the phase space. The cut-off parameter is set high enough to make the contribution from the cut tail of the statistics negligibly small. The quasidistributions are determined at each phase space point from the Monte Carlo simulations of  $N = 1000$  events. The grey areas denote the statistical uncertainty calculated according to Eq. (5.9). The two top graphs show the reconstruction of the Wigner function in the ideal case  $\eta T = 1$ . It is seen that the statistical error is smaller, where the magnitude of the Wigner function is large. In the outer regions it approaches its maximum value  $1/\sqrt{N}$ . The effect of the nonunit  $\eta T$  is shown in the center graphs. The measured quasidistributions become wider and the negative dip in the case of the Fock state is shallower. In the bottom graphs we depict the result of compensating the nonunit value of  $\eta T$  by setting  $s = 1 - \eta T$ . The compensation works quite well in the central region, where the average number of detected photons is small, but outside of this region the statistical error explodes exponentially. Of course, the statistical error can be in principle suppressed by increasing the number of measurements. However, this is not a practical method, since the statistical error decreases with the size of the sample only as  $1/\sqrt{N}$ .

The reconstruction of the interference structure of the Schrödinger cat state is plotted in Fig. 5.2. We have used the state defined in Eq. (2.18) with  $\alpha_0 = 3i$ . The interference structure is very fragile, and its precise measurement requires a large sample of events. In the case of the presented plot,  $N = 5000$  simulations were performed at each phase space point. Comparison of the top and the center graphs shows how even relatively small imperfection destroys the interference pattern. The data collected in a non-ideal setup can be processed to recover the Wigner function, but at the cost of a significantly larger statistical error, as it is shown in the bottom graph. Outside the interference structure, we again observe the exponential explosion of the dispersion due to the increasing intensity of the detected light.

From the above examples we clearly see, that compensation of any efficiency lower than 100% is a delicate matter. This conclusion may be quite puzzling, if we compare it with recently published results on compensation of losses in photodetection [15]. It was shown there that the true photon distribution can be reconstructed from data measured by an imperfect detector,

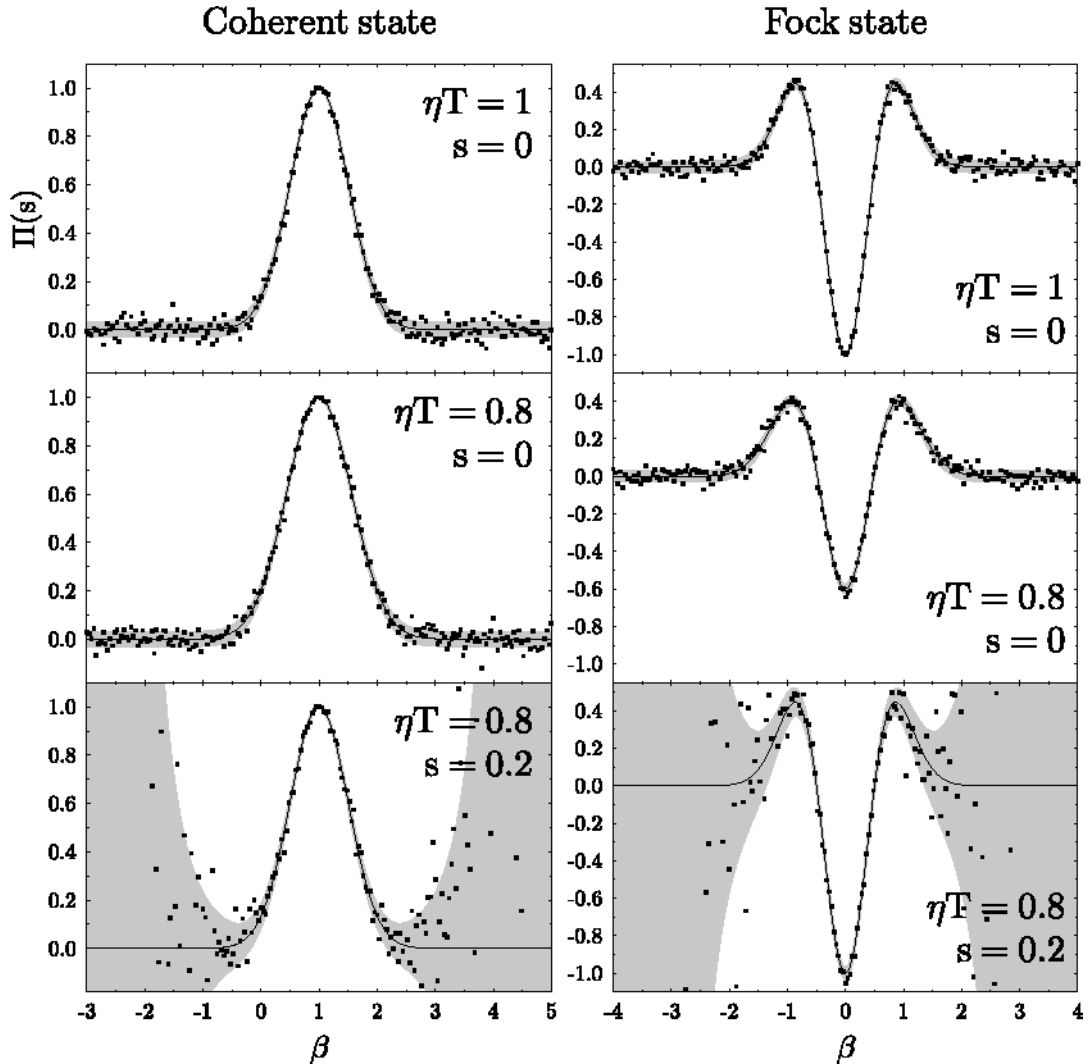


Figure 5.1: Reconstruction of the quasiprobability distributions of the coherent state  $|\alpha_0 = 1\rangle$  (left) and the one photon Fock state (right) from  $N = 1000$  events. The solid lines are the analytical quasidistributions and the grey areas mark the statistical dispersion. The plots are parameterized with the rescaled probe field amplitude  $\beta = \sqrt{(1 - T)/T}\alpha$ .

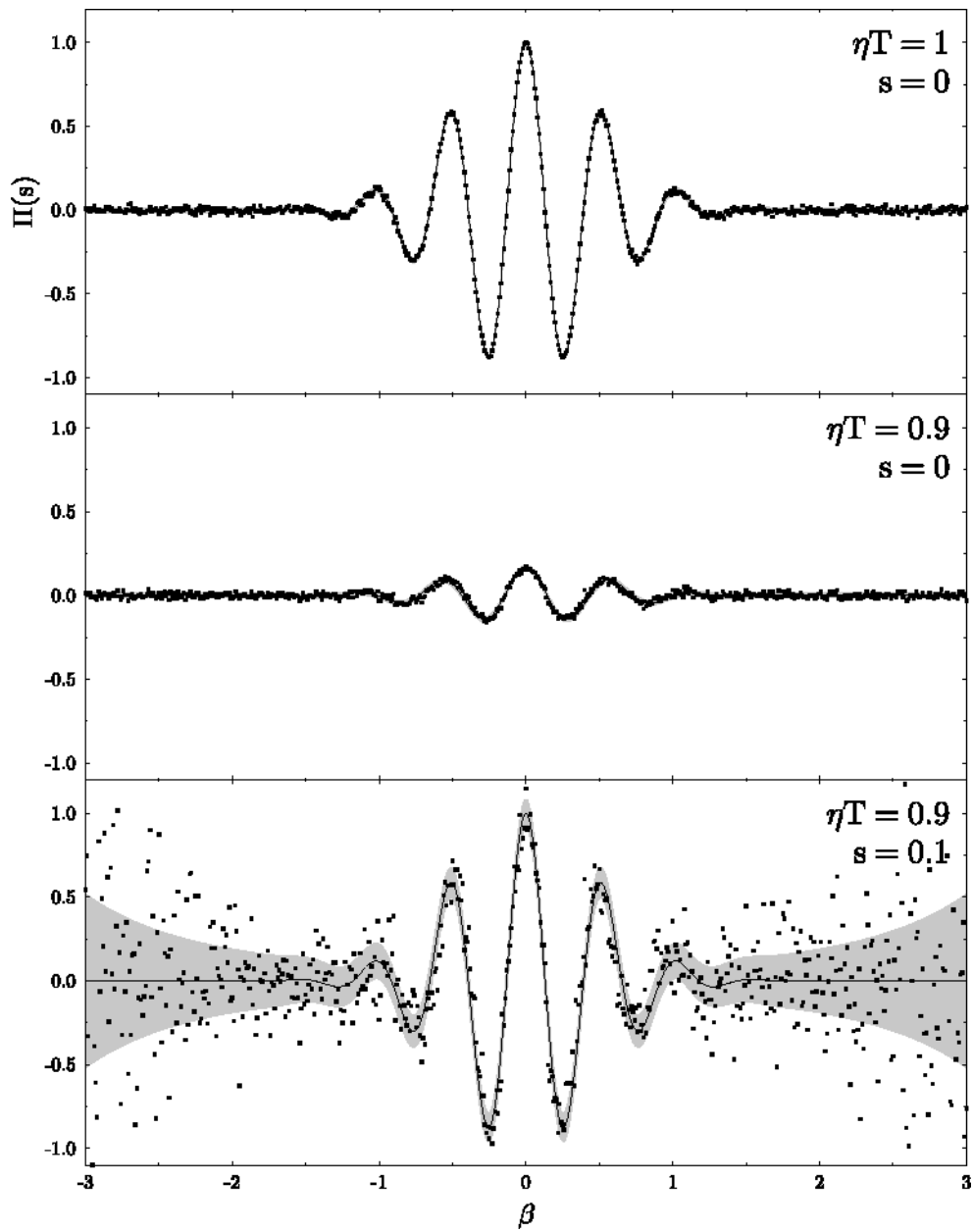


Figure 5.2: Reconstruction of the interference structure of the Schrödinger cat state for  $\alpha_0 = 3i$  from  $N = 5000$  events at each point.

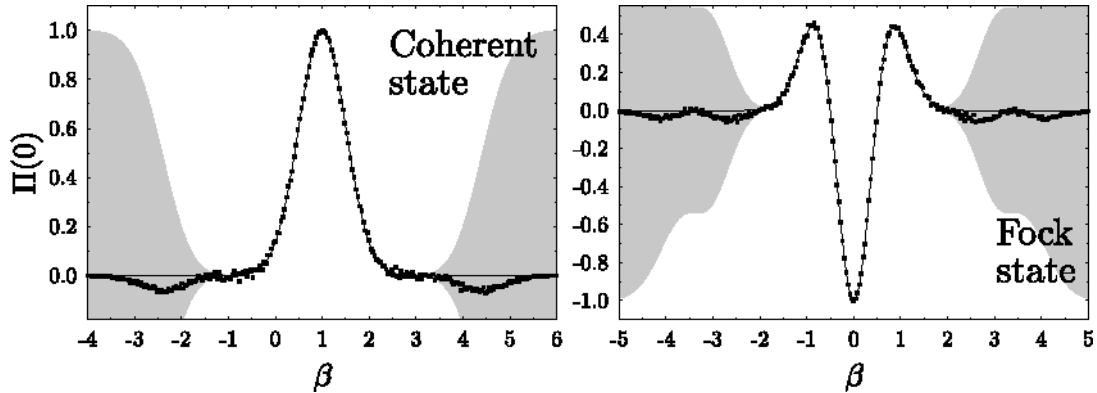


Figure 5.3: Reconstruction of the Wigner function of the coherent state and the one photon Fock state from the count statistics cut at  $K = 11$ , for  $\eta T = 1$  and  $s = 0$ . The number of events is  $N = 10^4$ .

provided that its efficiency is greater than 50%. If this condition is fulfilled, the photon distribution can be obtained from experimental data via the so-called inverse Bernoulli transformation, and the statistical properties of such reconstruction have been shown to behave regularly. One could think of using this recipe in our scheme for measuring quasidistribution functions: first, application of the inverse Bernoulli transformation would yield the loss-free photon distribution, and then evaluation of the alternating series would yield the unblurred Wigner function. However, a simple calculation shows that such a two-step method is completely equivalent to setting  $s = 1 - \eta T$  in the PCGF, and we end up with all the difficulties discussed above. Explanation of this seeming contradiction is simple: quantities obtained from the inverse Bernoulli transformation have strongly correlated statistical errors, which accumulate when evaluating the alternating series. We shall discuss this issue in detail in Sec. 7.2, using the general theory of statistical uncertainty in photodetection measurements.

Finally, let us look at the effect of cutting the statistics at a finite value. Fig. 5.3 shows the Wigner functions for the one photon coherent and Fock states reconstructed from the count distributions cut at  $K = 11$ . We performed a large number of  $N = 10^4$  simulations in order to get the pure effect of the cut-off that is not spoiled by the statistical uncertainty. The grey areas show the cut-off error, estimated using Eq. (5.12). The reconstruction works well as long as the probability of detecting more than  $K$  photons is negligible. When the average number of incident photons starts to be comparable with the cut-off parameter, “ghost” structures appear. When we go even further, the Wigner function again tends to zero, but this is a purely artificial effect due to the virtually vanishing count distribution below  $K$ . This kind of “ghost” structures resulting from the cut-off were observed in the characterization of the motional state of a trapped ion [11]. In this experiment, the analog of photon statistics  $p_n$  was reconstructed in an indirect way by monitoring the fluorescence [61], and it was necessary to truncate the statistics  $p_n$  in order to

keep the error on a reasonably low level. We have seen that in the regions of the phase space where a substantial part of the statistics  $p_n$  is lost by the truncation, we do not have sufficient data to determine the value of the Wigner function.

## 5.4 Mode mismatch

Another experimental imperfection that occurs in a realistic setup is the non-unit matching of the modes interfered at the high-transmission beam splitter BS. In order to analyse consequences of the mode mismatch, we will use the multimode approach developed in Sec. 4.4. Let us take the signal field and the coherent probe field to be of the form

$$\begin{aligned}\hat{\mathbf{E}}_S^{(+)}(\mathbf{r}, t) &= \hat{a}_S \mathbf{u}_S(\mathbf{r}, t) + \hat{\mathbf{V}}(\mathbf{r}, t), \\ \mathbf{E}_P(\mathbf{r}, t) &= \alpha \mathbf{u}_P(\mathbf{r}, t)\end{aligned}\quad (5.15)$$

where  $\mathbf{u}_S(\mathbf{r}, t)$  and  $\mathbf{u}_P(\mathbf{r}, t)$  are the corresponding normalized mode functions, and the operator  $\hat{\mathbf{V}}(\mathbf{r}, t)$  is the sum of all other signal modes remaining in the vacuum state. We will assume that the support of these mode functions lies within the domain defined by the detector surface and the gate opening time. This allows us to write the normalization of the mode functions as

$$\int_{\Delta t} dt \int_D d^2\mathbf{r} |\mathbf{u}_S(\mathbf{r}, t)|^2 = \int_{\Delta t} dt \int_D d^2\mathbf{r} |\mathbf{u}_P(\mathbf{r}, t)|^2 = \frac{\hbar\omega_0}{2\epsilon_0 c} \quad (5.16)$$

Further, we will assume that the overlap of the functions  $\mathbf{u}_S(\mathbf{r}, t)$  and  $\mathbf{u}_P(\mathbf{r}, t)$  is real and positive. This can be always achieved by multiplying  $\mathbf{u}_P(\mathbf{r}, t)$  and  $\alpha$  by appropriate conjugated phase factors. We will denote

$$\frac{2\epsilon_0 c}{\hbar\omega_0} \int_{\Delta t} dt \int_D d^2\mathbf{r} \mathbf{u}_S^*(\mathbf{r}, t) \mathbf{u}_P(\mathbf{r}, t) = \sqrt{\xi}. \quad (5.17)$$

Under these assumptions, we may represent the PCGF calculated from the count statistics given by Eq. (4.14) in the form:

$$\Pi(s) = \left\langle : \exp \left( -\frac{2\eta}{1-s} [\hat{T}\hat{a}_S^\dagger \hat{a}_S - \sqrt{\xi T(1-T)}(\hat{a}_S^\dagger \alpha + \hat{a}_S \alpha^*) + (1-T)|\alpha|^2] \right) : \right\rangle \quad (5.18)$$

Rearranging the terms in the exponent yields:

$$\Pi(s) = \frac{\pi(1-s)}{2\eta T} W_S \left( \sqrt{\frac{\xi(1-T)}{T}} \alpha; -\frac{1-s-\eta T}{\eta T} \right) \exp \left( -\frac{2\eta(1-T)(1-\xi)}{1-s} |\alpha|^2 \right). \quad (5.19)$$

Thus, if the signal and the probe modes are not matched perfectly, the PCGF is given by the quasidistribution function of the signal, but multiplied by a Gaussian envelope  $\exp[-2\eta(1-$

$T)(1 - \xi)|\alpha|^2/(1 - s)$ . This envelope is centered at the origin of the phase space, and the faster it decays, the larger is the mode mismatch, characterized by the difference  $1 - \xi$ . Additionally, the parameterization of the signal quasidistribution is rescaled by  $\sqrt{\xi}$ .

The effect of the mode-mismatch is more severe in outer regions of the phase space. It is not important if the quasidistribution is localized around the center of the phase space within the width of the Gaussian envelope. In particular, for the vacuum signal state we obtain:

$$\Pi(s) = \exp\left(-\frac{2\eta(1-T)}{1-s}|\alpha|^2\right). \quad (5.20)$$

This result does not depend at all on the mode overlap parameter  $\xi$ , simply because with the vacuum signal field no interference occurs at the beam splitter BS and all the recorded photons come from the probe beam. The above expression can be interpreted as the quasidistribution function of the signal mode characterized by the mode function  $\mathbf{u}_P(\mathbf{r}, t)$ , which perfectly overlaps with the probe field.

In a general case, we may rewrite Eq. (5.19) to the form:

$$\begin{aligned} \Pi(s) = & \frac{\pi(1-s)}{2\eta T} W_S \left( \sqrt{\frac{\xi(1-T)}{T}}\alpha; -\frac{1-s-\eta T}{\eta T} \right) \\ & \times \frac{\pi(1-s)}{2\eta T} W_{\text{vac}} \left( \sqrt{\frac{(1-\xi)(1-T)}{T}}\alpha; -\frac{1-s-\eta T}{\eta T} \right), \end{aligned} \quad (5.21)$$

where  $W_{\text{vac}}(\beta; s)$  is the vacuum quasidistribution function. This representation allows us to interpret Eq. (5.19) as a two-mode quasidistribution which is a product of the signal mode quasidistribution and an additional vacuum quasidistribution. These two modes are probed at the phase space points proportional to  $\sqrt{\xi}\alpha$  and  $\sqrt{1-\xi}\alpha$ . The amplitude  $\sqrt{\xi}\alpha$  describes the part of the probe field that overlaps perfectly with the signal field, whereas  $\sqrt{1-\xi}\alpha$  corresponds to the orthogonal remainder (orthogonality is understood here in the sense of the scalar product between the mode functions).

The parameter  $\xi$  characterizing the overlap of the signal and the probe modes can be related to the visibility of the interference. This expression will be useful in the discussion of the practical realization of the scheme. Let us assume that the signal mode is in a coherent state  $|\alpha_0\rangle$ . The intensity of the field measured by the photodetector is given by

$$I = |\sqrt{1-T}\alpha - \sqrt{\xi T}\alpha_0|^2 + (1-\xi)T|\alpha_0|^2, \quad (5.22)$$

where  $\alpha$  is the amplitude of the coherent probe mode. It is seen that for given  $\alpha_0$  the minimum intensity is obtained for  $\sqrt{1-T}\alpha = \sqrt{\xi T}\alpha_0$ , and it equals to:

$$I_{\min} = (1-\xi)T|\alpha_0|^2. \quad (5.23)$$

When we now vary with the phase of  $\alpha$ , keeping its absolute value fixed, the maximum intensity is achieved for  $\sqrt{1-T}\alpha = -\sqrt{\xi T}\alpha_0$ , and its value is:

$$I_{\max} = 4\xi T|\alpha_0|^2 + (1 - \xi)T|\alpha_0|^2. \quad (5.24)$$

A simple calculation shows that the interference visibility  $v$  can be expressed using the overlap parameter  $\xi$  as:

$$v = \frac{I_{\max} - I_{\min}}{I_{\max} + I_{\min}} = \frac{4\xi}{2 + 2\xi}. \quad (5.25)$$

Inverting this relation, we obtain that  $\xi = v/(2 - v)$ .

Finally, let us note that the effect of mode-mismatch in our scheme is quite different from balanced homodyne detection, where it can be simply included in the overall detection efficiency parameter. In our scheme, it generates a Gaussian envelope multiplying the measured quasidistribution function, and its importance depends on the probed point of the phase space.



# Chapter 6

## Experiment

We shall now present direct measurement of the Wigner function by photon counting, using the method presented in Chap. 4. Previous measurements of the Wigner function of light, performed at the University of Oregon [7] and Universität Konstanz [10], were realizations of optical homodyne tomography. In our experiment, the Wigner function is determined directly from the statistics of photocounts. Apart from the different principle of the measurement, we use a different technique for light detection. As we discussed in Chap. 3, optical homodyne tomography is based on detection of the signal light superposed on a strong, classical local oscillator. The light incident on photodetectors has macroscopic intensity, and it is converted into an electronic current with the help of *p-i-n* photodiodes. At this level of intensity, it is not possible to resolve contributions from single photons, and the electric current is practically a continuous variable. Information on the quantum state of the measured light is contained in fluctuations of the difference signal between two detectors. This signal is recorded using an analog-to-digital converter.

In our scheme, the intensity of the detected light is comparable with the intensity of the signal field itself. Therefore, we need to use a detector that is sensitive to single optical photons. Currently, the most efficient commercially available detectors on single-photon level are avalanche photodiodes operated in the so-called Geiger mode. The Geiger mode of operation consists in biasing the diode slightly above breakdown. Absorption of a photon triggers the breakdown, which is a macroscopic, recordable event. The diode is placed in a circuit which quenches the breakdown by lowering the voltage, and after a while restores the higher bias thus preparing the diode for the detection of a next photon. The electronic signal obtained from the diode has the form of pulses of uniform height and duration, which correspond to single detection events. These pulses, after shaping, can be counted using a standard digital logic device.

We open this chapter with a review of the principle of the measurement in Sec. 6.1. The experimental setup is described in Sec. 6.2, and the results of the measurements are reported in Sec. 6.3. In Sec. 6.4 we discuss the effect of various experimental factors, and summarize the presentation of the experiment.

## 6.1 Principle

In order to make the presentation of the experiment self-contained, let us start with a brief review of the principle of the measurement. The Wigner function at a given phase space point is itself a well defined quantum observable. Furthermore, the measurement of this observable can be implemented for optical fields using an arrangement employing an auxiliary coherent probe beam. The amplitude and the phase of the probe field define the point in the phase space at which the Wigner function is measured. This allows one to scan the phase space point-by-point, simply by changing the parameters of the probe field.

Our experiment is based on the representation of the Wigner function at a complex phase space point denoted by  $\alpha$  as the expectation value of the following operator:

$$\hat{W}(\alpha) = \frac{2}{\pi} \sum_{n=0}^{\infty} (-1)^n \hat{D}(\alpha) |n\rangle \langle n| \hat{D}^\dagger(\alpha), \quad (6.1)$$

where  $\hat{D}(\alpha)$  is the displacement operator and  $|n\rangle$  denote Fock states,  $\hat{n}|n\rangle = n|n\rangle$ . Thus,  $\hat{W}(\alpha)$  has two eigenvalues:  $2/\pi$  and  $-2/\pi$ , corresponding to degenerate subspaces spanned respectively by even and odd displaced Fock states. Practical means to translate this formula into an optical arrangement are quite simple. The displacement transformation can be realized by superposing the measured field at a low-reflection beam splitter with a strong coherent probe beam. The value of the displacement  $\alpha$  is equal in this setup to the reflected amplitude of the probe field. Furthermore, the projections on Fock states can be obtained by photon counting assuming unit quantum efficiency. These two procedures, combined together, provide a practical way to measure the Wigner function at an arbitrarily selected phase space point  $\alpha$ .

## 6.2 Setup

The experimental setup we used to measure the Wigner function is shown schematically in Fig. 6.1. In principle, it is a Mach-Zender interferometric scheme with the beams in two arms of the interferometer serving as the signal and the probe fields. An attenuated, linearly polarized (in the plane of Fig. 4.1) 632.8 nm beam from a frequency-stabilized single-mode He:Ne laser is divided by a low-reflection beam splitter BS1. The weak reflected beam is used to generate the signal field whose Wigner function will be measured. The state preparation stage consists of a neutral density filter ND and a mirror mounted on a piezoelectric translator PZT. With this arrangement, we are able to create pure coherent states with variable phase as well as their incoherent mixtures. Though these states do not exhibit nonclassical properties, they constitute a nontrivial family to demonstrate the principle of the method, which provides complete characterization of both quantum and classical field fluctuations.

The strong beam leaving the beam splitter BS1 plays the role of the probe field with which we perform the displacement transformation  $\hat{D}(\alpha)$ . In order to scan the phase space one should

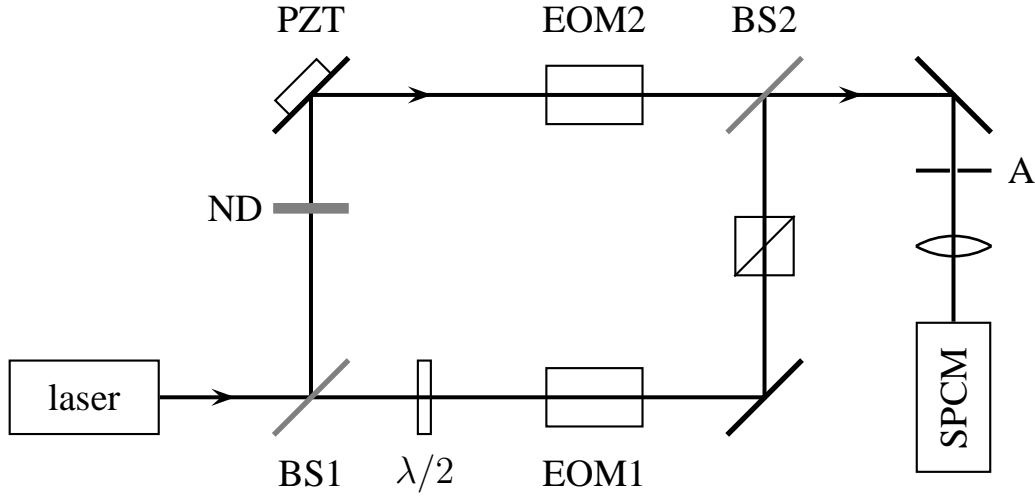


Figure 6.1: The experimental setup for measuring the Wigner function. BS1 and BS2 are quartz plates serving as low-reflection beam splitters. The quantum state is prepared using the neutral density filter ND and a mirror mounted on a piezoelectric translator PZT. The electrooptic modulators EOM1 and EOM2 control respectively the amplitude and the phase of the point at which the Wigner function is measured. The signal field, after removing spurious reflections using the aperture A, is focused on a single photon counting module SPCM.

be able to set freely its amplitude and phase, which define respectively the radial and angular coordinate in the phase space. The amplitude modulation is achieved with a half-wave plate, a longitudinal Pockels cell EOM1, and a polarizer oriented parallel to the initial direction of polarization. The phase modulation is done with the help of an ADP crystal electrooptic phase modulator EOM2 on the signal field. This is completely equivalent to modulating the probe field phase, but more convenient for technical reasons: in this arrangement optical paths in both the arms of the Mach-Zender interferometer are approximately the same, and better overlap of the signal and the probe modes is achieved at the output of the interferometer.

The signal and the probe fields are interfered at a nearly completely transmitting beam splitter BS2 with the power transmission  $T = 98.6\%$ . In this regime, the transmitted signal field effectively undergoes the required displacement transformation. Spurious reflections that accompany the beam leaving the interferometer are removed using the aperture A. Finally, the transmitted signal is focused on an EG&G photon counting module SPCM-AQ-CD2749, whose photosensitive element is a silicon avalanche diode operated in the Geiger regime. The overall quantum efficiency of the module specified by the manufacturer is  $\eta \geq 70\%$ . The count rate is kept low in the experiment, so that the chance of two or more photons triggering a single avalanche signal is very small, and the probability of another photon arriving during the detector dead time can be neglected. Under these assumptions, each pulse generated by the module corresponds to the

detection of a single photon<sup>1</sup>. The pulses are acquired by a computer, which also controls the voltages applied to the electrooptic modulators. The interference visibility in our setup has been measured to be  $v \geq 98.5\%$ , and the phase difference between the two arms was stable up to few percent over times of the order of ten minutes.

### 6.3 Results

The voltages applied to electrooptic modulators were generated by high-voltage power supplies controlled by analog output ports of a multifunction I/O card (National Instruments PCI-MIO-16E-4). A typical scan of the phase space consisted of sampling a sequence of circles with increasing radius. This was because changing the voltage applied to the amplitude modulator required a settling time of the order of 1 s. For a fixed amplitude the phase could be scanned much faster, as the phase modulator driver had the bandwidth up to 10 kHz. For a selected point of the phase space, the photon statistics was collected using a digital counter on the same I/O card, operated in the buffered event counting mode.

In Fig. 6.2 we depict the measured Wigner functions of the vacuum, a weak coherent state, and a phase diffused coherent state. Phase fluctuations were obtained by applying a 400 Hz sine waveform to the piezoelectric translator. For all the plots, the phase space was scanned on a grid defined by 20 amplitudes and 40 phases. The scaling of the radial coordinate is obtained from the average number of photons  $n_{\text{vac}}$  detected for the blocked signal path. Thus the graphs are parameterized with the complex variable  $\beta = e^{i\varphi} n_{\text{vac}}^{1/2}$ , where  $\varphi$  is the phase shift generated by the phase modulator EOM2. At each selected point of the phase space, the photocount statistics  $p_n(\beta)$  was determined from a sequence of  $N = 8000$  counting intervals, each  $\tau = 30\mu\text{s}$  long. The duration of the counting interval  $\tau$  defines the temporal envelope of the measured mode. The count statistics was used to evaluate the alternating sum<sup>2</sup>

$$\Pi(\beta) = \sum_{n=0}^{\infty} (-1)^n p_n(\beta), \quad (6.2)$$

which, up to the normalization factor  $2/\pi$  is equal to the Wigner function of the measured state. Statistical variance of this result can be estimated by  $\text{Var}[\Pi(\beta)] = \{1 - [\Pi(\beta)]^2\}/N$ , according to the discussion in Sec. 5.2. Thus, the statistical error of our measurement reaches its maximum value, equal to  $1/N^{1/2} \approx 1.1\%$ , when the value of the Wigner function is close to zero.

<sup>1</sup>The operating mode of the SPCM results in a certain amount of extraneous pulses originating from dark counts and afterpulsing. The dark count rate of our module is less than  $100 \text{ s}^{-1}$ . This gives on average  $< 3 \cdot 10^{-3}$  during a single counting interval, which is  $30 \mu\text{s}$  long. The typical afterpulsing probability is 0.2%. Thus, both these effects give a negligible contribution to the measured count statistics.

<sup>2</sup>Here we explicitly write dependence of  $\Pi$  on the phase space point  $\beta$ . The number  $s$  used in the previous chapter as a parameter of  $\Pi$  is now fixed and equal to zero. The operational phase space point  $\beta$  can be expressed by the amplitude  $\alpha$  of the probe field as  $\beta = \sqrt{\eta(1-T)}\alpha$ .

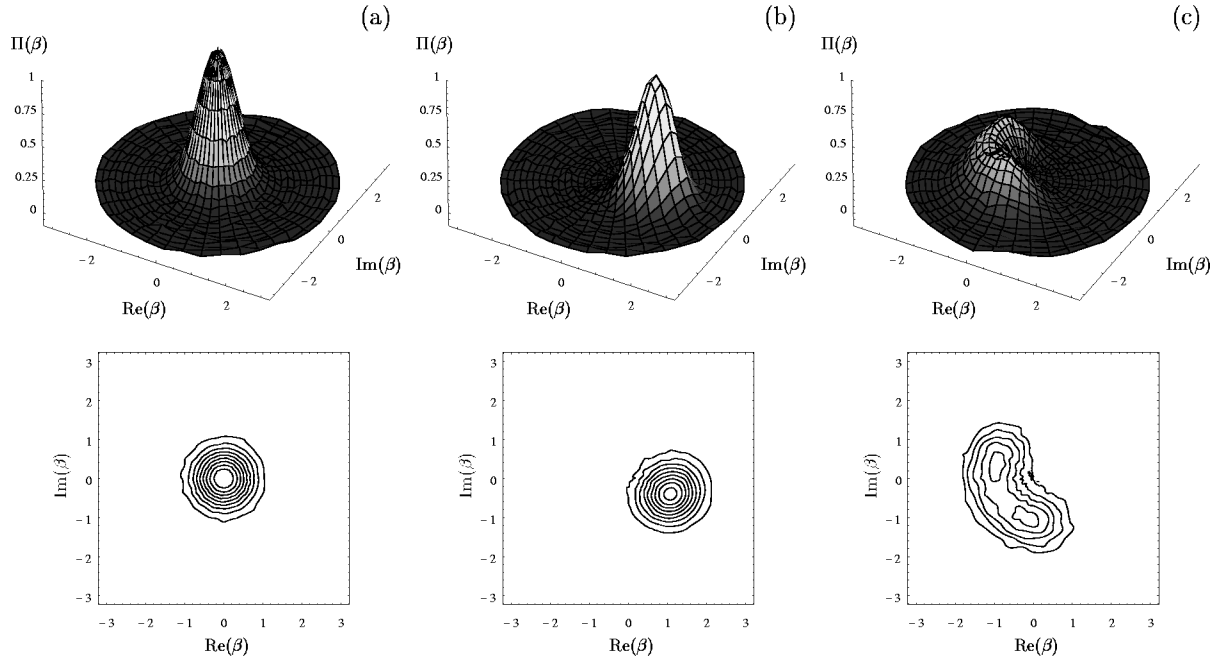


Figure 6.2: The measured Wigner functions of (a) the vacuum, (b) a weak coherent state, and (c) a phase diffused coherent state. The contour plots depict interpolated heights given by multiples of 0.1 for the plots (a) and (b), and by 0.08, 0.14, 0.20, 0.26, 0.32 for the plot (c).

The Wigner functions of the vacuum and of the coherent state are Gaussians centered at the average complex amplitude of the field, and their widths characterize quantum fluctuations. It can be noticed that the measured Wigner function of the coherent state is slightly lower than that of the vacuum state. In the following, when discussing experimental imperfections, we shall explain this as a result of non-unit interference visibility. In the plot of the Wigner function of the phase diffused coherent state, one can clearly distinguish two outer peaks corresponding to the turning points of the harmonically modulated phase. Another set of results is presented in a colour plate at the end of this chapter.

## 6.4 Discussion

There are several experimental factors whose impact on the result of the measurement needs to be analyzed. First, there are losses of the signal field resulting from two main sources: the reflection from the beam splitter BS2 and, what is more important, imperfect photodetection characterized by the quantum efficiency  $\eta$ . Analysis of these losses performed in Sec. 4.3 shows, that in such a case the alternating series evaluated from photocount statistics is proportional to a generalized,  $s$ -ordered quasidistribution function  $W(\alpha; s)$ , with the ordering parameter equal  $s = -(1 - \eta T)/\eta T$ .

In addition, the two modes interfered at the beam splitter BS2 are never matched perfectly. The effects of the mode mismatch have been analysed in Sec. 5.4. We will now apply this analysis to the experimental results, but first let us recall briefly the physical picture of mode mismatch. For this purpose, we need to consider the normalized mode functions describing the transmitted signal field and the reflected probe field. The squared overlap  $\xi$  of these two mode functions can be related to the interference visibility  $v$  as  $\xi = v/(2 - v)$ . In order to describe the effects of the mode mismatch, we need to decompose the probe mode function into a part that precisely overlaps with the signal, and the orthogonal remainder. The amplitude of the probe field effectively interfering with the signal is thus multiplied by  $\xi^{1/2}$ , and the remaining part of the probe field contributes to independent Poissonian counts with the average number of detected photons equal  $(1 - \xi)|\beta|^2$ . Consequently, the full count statistics is given by a convolution of the statistics generated by the interfering fields, and the Poissonian statistics of mismatched photons. A simple calculation shows, that the alternating sum evaluated from such a convolution can be represented as a product of the contributions corresponding to the two components of the probe field:

$$\begin{aligned} \Pi(\beta) &= \exp[-2(1 - \xi)|\beta|^2] \\ &\times \frac{\pi}{2\eta T} W \left( \sqrt{\frac{\xi}{\eta T}} \beta; -\frac{1 - \eta T}{\eta T} \right). \end{aligned} \quad (6.3)$$

Here on the right-hand side we have made use of the theoretical results for imperfect detection obtained in Secs. 4.3 and 5.4. Specializing the above result to a coherent signal state  $|\alpha_0\rangle$  with the amplitude  $\alpha_0$ , yields:

$$\Pi(\beta) = \exp[-2|\beta - \sqrt{\xi\eta T}\alpha_0|^2 - 2(1 - \xi)\eta T|\alpha_0|^2]. \quad (6.4)$$

Thus, in a realistic case  $\Pi(\beta)$  represents a Gaussian centered at the attenuated amplitude  $\sqrt{\xi\eta T}\alpha_0$ , and the width remains unchanged. This Gaussian function is multiplied by the constant factor  $\exp[-2(1 - \xi)\eta T|\alpha_0|^2]$ . For our measurement,  $\xi \approx 97\%$  and  $\eta T|\alpha_0|^2 \approx 1.34$ , which gives the value of this factor equal 0.92. This result agrees with the height of the experimentally measured Wigner function of a coherent state.

In Fig. 6.3 we compare the phase-averaged measured Wigner function for the vacuum state with theoretical predictions. Agreement between the experimental points and the Gaussian curve is very good. This plot can be used to estimate the amount of excess thermal noise in the laser radiation. Let us assume that from the average  $n_{\text{vac}} = |\beta|^2$  registered photons a constant fraction  $\varkappa_{\text{th}}$  originates from thermal noise. The  $P$ -representation of the field that is effectively detected is given by

$$P(\gamma) = \frac{1}{\pi\varkappa_{\text{th}}|\beta|^2} \exp \left( -\frac{|\gamma - \sqrt{1 - \varkappa_{\text{th}}}\beta|^2}{\varkappa_{\text{th}}|\beta|^2} \right). \quad (6.5)$$

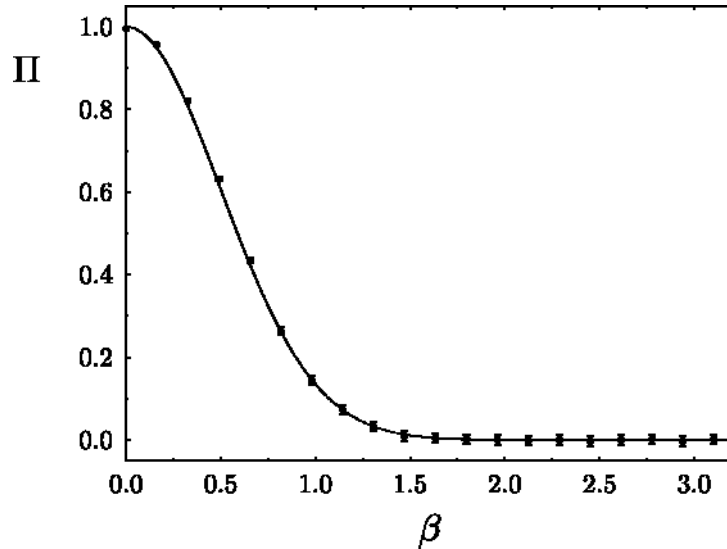


Figure 6.3: Comparison of the phase-averaged experimental Wigner function for the vacuum state (points with error bars) with the theoretical prediction (line), given by the Gaussian  $\exp(-2|\beta|^2)$ .

The average photon number parity measured for such a field reads:

$$\Pi(\beta) = \frac{1}{2\kappa_{\text{th}}|\beta|^2 + 1} \exp\left(-\frac{2(1 - \kappa_{\text{th}})|\beta|^2}{2\kappa_{\text{th}}|\beta|^2 + 1}\right) \quad (6.6)$$

and in the presence of thermal noise exhibits departure from a pure Gaussian shape. The perfect agreement observed in Fig. 6.3 confirms that the contribution of thermal noise is negligibly small.

Concluding, let us compare the demonstrated direct method for measuring the Wigner function with the optical homodyne tomography approach. An important parameter in experimental quantum state reconstruction is the detection efficiency. Here better figures are exhibited by the homodyne technique, which detects quantum fluctuations as a difference between two rather intense fields. Such fields can be efficiently converted into photocurrent signals with the help of *p-i-n* diodes. It should be also noted that an avalanche photodiode is not capable of resolving the number of simultaneously absorbed photons, and that it delivers a signal proportional to the light intensity only in the regime used in our experiment. However, continuous progress in single photon detection technology gives hope to overcome current limitations of photon counting [59]. Alternatively, the displacement transformation implemented in the photon counting technique can be combined with efficient random phase homodyne detection. This yields the recently proposed scheme for cascaded homodyning [62].

The simplicity of the relation (6.1) linking the count statistics with quasidistribution functions allows one to determine the Wigner function at a given point from a relatively small sample of experimental data. This feature becomes particularly advantageous, when we consider detection of multimode light. Optical homodyne tomography requires substantial numerical effort to

reconstruct the multimode Wigner function. In contrast, the photon counting method has a very elegant generalization to the multimode case: after applying the displacement to each of the involved modes, the Wigner function at the selected point is simply given by the average parity of the total number of detected photons. Moreover, the dichotomic outcome of such a measurement provides a novel way of testing quantum nonlocality exhibited by correlated states of optical radiation [63].

# Chapter 7

## Statistical uncertainty in photodetection measurements

In this chapter, we shall study the problem of statistical uncertainty from a more general point of view. Over recent years, the set of tools for measuring quantum statistical properties of optical radiation has substantially enlarged. In addition to the techniques discussed in this thesis: double homodyne detection, optical homodyne tomography, and the direct method for measuring quasidistribution functions, other novel schemes have been proposed [64, 65, 66, 67, 68]. The quantum optical “toolbox” for measuring light contains now experimentally established schemes for reconstructing various representations of its quantum state: the  $Q$  function, the Wigner function, and the density matrix in the quadrature and the Fock bases. A device that is used in most of quantum optical schemes to convert the quantum signal to a macroscopic level is the photodetector. Thus, photodetection is a basic ingredient of quantum optical measurements.

The quantum state can be characterized using various representations: quasidistribution functions or a density matrix in a specific basis. From a theoretical point of view, all these forms are equivalent. Each representation contains complete information on the quantum state, and they can be transformed from one to another. Any observable related to the measured systems can be evaluated from an arbitrary representation using an appropriate expression [69].

This simple picture becomes much more complicated when we deal with real experimental data rather than analytical formulae. Each quantity determined from a finite number of experimental runs is affected by a statistical error. Consequently, the density matrix or the quasidistribution function reconstructed from the experimental data is known only with some statistical uncertainty. This uncertainty is important when we further use the reconstructed information to calculate other observables or to pass to another representation. The crucial question is, whether determination of a certain representation with sufficient accuracy guarantees that arbitrary observable can be calculated from these data with a reasonably low statistical error. If this is not the case, the reconstructed information on the quantum state of the measured system turns out to be somewhat incomplete. Furthermore, transformation between various representations of the

quantum state becomes a delicate matter.

These and related problems call for a rigorous statistical analysis of quantum optical measurements. We shall provide here complete statistical description of a measurement of quantum observables in optical schemes based on photodetection. This approach fully characterizes statistical properties of quantities determined in a realistic measurement from a finite number of experimental runs. It can be applied either to determination of a single quantum observable, or to the reconstruction of the quantum state in a specific representation. Within the presented framework we study, using a simple example, the completeness of the experimentally reconstructed information on the quantum state. We demonstrate the pathological behavior suggested above, when the reconstructed data cannot be used to calculate certain observables due to rapidly exploding statistical errors. Our example is motivated by the direct scheme for measuring quasidistribution functions of light.

Compared to previous works on statistical noise, our attention will be focused here on two important statistical aspects of quantum state measurement. First, we shall go beyond the minimum second-order treatment of the statistical error [50, 51, 52] and provide, in a closed mathematical form, a complete statistical description of quantum observables determined from realistic measurements. This result, derived from the first principles without using any approximations, is an exact analytical solution to the problem which so far has been approached only by means of Monte Carlo simulations [46, 49]. The second problem discussed here will be the feasibility of reconstructing the quantum state from realistic, finite data collected in a specific experimental scheme. It is generally believed that a sufficient condition for successful reconstruction is the existence of the covariance matrix with finite elements [15, 16, 17]. We point out that this belief misses an important issue resulting from statistical uncertainty. Suppose we have reconstructed a family of observables with finite statistical variances. In order to be sure that the reconstructed information on the quantum state is accurate and complete, we should ask the following question: can we always use these observables to evaluate any quantum property of the measured system that can be expressed in terms of the reconstructed family? We shall give a clear negative answer to this question, based on a detailed discussion of carefully selected counterexamples. Although all observables involved in these examples are represented by bounded, well-defined operators, statistical fluctuations are shown to be arbitrarily huge, when the reconstructed family is further used to evaluate certain quantum expectation values. This singular behaviour is quantitatively explained as a result of strong statistical correlations between observables reconstructed from the same sample of experimental data. Consequently, the discussed examples clearly demonstrate that statistical properties of reconstructed observables depend in an essential way on a specific experimental scheme, which effectively limits available information on the measured system.

This chapter is organized as follows. The starting point of our analysis is the probability distribution of obtaining a specific histogram from  $N$  runs of the experimental setup. This basic quantity determines all statistical properties of quantum observables reconstructed from a finite sample of experimental data. We characterize these properties using the generating function,

for which we derive an exact expression directly from the probability distribution of the experimental outcomes. These general results are presented in Sec. 7.1. Then, in Sec. 7.2, we use the developed formalism to discuss the reconstruction of the photon number distribution of a single light mode, and its subsequent utilization to evaluate the parity operator  $\hat{\Pi}$ . We consider two experimental schemes: direct photon counting using an imperfect detector, and homodyne detection with random phase. In both the cases we find that the evaluation of the parity operator from the reconstructed photon statistics is a very delicate matter. For photon counting of a thermal state, we show that neither the statistical mean value of  $\hat{\Pi}$  nor its variance have to exist when we take into account arbitrarily high count numbers. For random phase homodyne detection, the statistical error of the parity operator is an interplay of the number of runs  $N$  and the specific regularization method used for its evaluation. The example of the parity operator illustrates difficulties related to the transformations between various experimentally determined representations of the quantum state, as the parity operator yields, up to a multiplicative constant, the Wigner function at the phase space origin. Finally, in Sec. 7.3 we discuss consequences of statistical uncertainty in the measurements of the quantum state.

## 7.1 Statistical analysis of experiment

In photodetection measurements, the raw quantity delivered by a single experimental run is the number of photoelectrons ejected from the active material of the detectors. The data recorded for further processing depends on a specific scheme. It may be just the number of counts on a single detector, or a difference of photocounts on a pair of photodetectors, which is the case of balanced homodyne detection. It may also be a finite sequence of integer numbers, e.g. for double homodyne detection. We will denote in general this data by  $n$ , keeping in mind all the possibilities.

The experimental scheme may have some external parameters  $\theta$ , for example the phase of the local oscillator in homodyne detection. The series of measurements are repeated for various settings  $\theta_i$  of these parameters. Thus, what is eventually obtained from the experiment, is a set of histograms  $\{k_n\}_{\theta_i}$ , telling in how many runs with the settings  $\theta_i$  the outcome  $n$  has been recorded. We assume that for each setting the same total number of  $N$  runs has been performed.

The theoretical probability  $p_n(\theta_i)$  of obtaining the outcome  $n$  in a run with settings  $\theta_i$  is given by the expectation value of a positive operator-valued measure (POVM)  $\hat{p}_n(\theta_i)$  acting in the Hilbert space of the measured system. The reconstruction of an observable  $\hat{A}$  is possible, if it can be represented as a linear combination of the POVMs for the settings used in the experiment:

$$\hat{A} = \sum_i \sum_n a_n(\theta_i) \hat{p}_n(\theta_i), \quad (7.1)$$

where  $a_n(\theta_i)$  are the kernel functions. The above formula allows one to compute the quantum expectation value  $\langle \hat{A} \rangle$  from the probability distributions  $p_n(\theta_i) = \langle \hat{p}_n(\theta_i) \rangle$ .

This theoretical relation has to be applied now to the experimental data. The simplest and the most commonly used strategy is to estimate the probability distributions  $p_n(\theta_i)$  by experimental relative frequencies  $(k_n/N)_{\theta_i}$ . The relative frequencies integrated with the appropriate kernel functions yield an estimate for the expectation value of the operator  $\hat{A}$ . For simplicity, we will denote this estimate just by  $A$ . Thus, the recipe for reconstructing the observable  $A$  from experimental data is given by the counterpart of Eq. (7.1):

$$A = \sum_i \sum_n a_n(\theta_i) \left( \frac{k_n}{N} \right)_{\theta_i}. \quad (7.2)$$

We will now analyse statistical properties of the observable  $A$  evaluated according to Eq. (7.2) from data collected in a finite number of experimental runs. Our goal is to characterize the statistical distribution  $w(A)$  defining the probability that the experiment yields a specific result  $A$ . The fundamental object in this analysis is the probability  $\mathcal{P}(\{k_n\}; \theta)$  of obtaining a specific histogram  $\{k_n\}$  for the settings  $\theta$ . In order to avoid convergence problems, we will restrict the possible values of  $n$  to a finite set by introducing a cut-off. The probability  $\mathcal{P}(\{k_n\}; \theta)$  is then given by the multinomial distribution [60]:

$$\mathcal{P}(\{k_n\}; \theta) = \frac{N!}{(N - \sum_n' k_n)!} \left( 1 - \sum_n' p_n(\theta) \right)^{N - \sum_n' k_n} \prod_n' \frac{1}{k_n!} [p_n(\theta)]^{k_n}, \quad (7.3)$$

where prim in sums and products denotes the cut-off. This distribution describing experimental histograms is derived from an assumption that all the detection events are statistically independent.

Let us first consider a contribution  $A_i$  to the observable  $A$  calculated from the histogram  $\theta_i$ :

$$A_i = \sum_n' a_n(\theta_i) \left( \frac{k_n}{N} \right)_{\theta_i}. \quad (7.4)$$

Its statistical distribution  $w(A_i; \theta_i)$  is given by the following sum over all possible histograms that can be obtained from  $N$  experimental runs:

$$w(A_i; \theta_i) = \sum_{\{k_n\}} \mathcal{P}(\{k_n\}; \theta_i) \delta \left( A_i - \frac{1}{N} \sum_n' a_n(\theta_i) k_n \right). \quad (7.5)$$

Equivalently, the statistics of  $A_i$  can be characterized by the generating function  $\tilde{w}(\lambda; \theta_i)$  for the moments, which is the Fourier transform of the distribution  $w(A_i; \theta_i)$ :

$$\begin{aligned} \tilde{w}(\lambda; \theta_i) &= \int dA_i e^{i\lambda A_i} w(A_i; \theta_i) \\ &= \sum_{\{k_n\}} \mathcal{P}(\{k_n\}; \theta_i) \exp \left( \frac{i\lambda}{N} \sum_n' a_n(\theta_i) k_n \right). \end{aligned} \quad (7.6)$$

An easy calculation yields the explicit form of the generating function:

$$\tilde{w}(\lambda; \theta_i) = \left( 1 + \sum_n' p_n(\theta_i) (e^{i\lambda a_n(\theta_i)/N} - 1) \right)^N. \quad (7.7)$$

The observable  $A$  is obtained via summation of the components  $A_i$  corresponding to all settings of the external parameters  $\theta_i$ . As these components are determined from disjoint subsets of the experimental data, they are statistically independent. Consequently, the generating function  $\tilde{w}(\lambda)$  for the moments of the observable  $A$  is given by the product:

$$\begin{aligned} \tilde{w}(\lambda) &= \int dA e^{i\lambda A} w(A) = \prod_i \tilde{w}(\lambda; \theta_i) \\ &= \prod_i \left( 1 + \sum_n' p_n(\theta_i) (e^{i\lambda a_n(\theta_i)/N} - 1) \right)^N. \end{aligned} \quad (7.8)$$

This expression contains the complete statistical information on determination of the observable  $A$  from a finite number of runs of a specific experimental setup. The measuring apparatus is included in this expression in the form of a family of POVMs  $\hat{p}_n(\theta_i)$ . The quantum expectation value of these POVMs over the state of the measured system yields the probability distributions  $p_n(\theta_i)$ . Finally, the coefficients  $a_n(\theta_i)$  are given by the computational recipe for reconstructing the observable  $A$  from the measured distributions. The analytical expression for the generating function given in Eq. (7.8), derived from the exact description of raw experimental outcomes, provides a complete characterization of statistical fluctuations in realistic measurements of quantum observables. Let us note that in general the generating function  $\tilde{w}(\lambda)$  cannot be expressed by the operator  $\hat{A}$  alone. Both the POVMs  $\hat{p}_n(\theta_i)$  and the kernel functions  $a_n(\theta_i)$  enter Eq. (7.8) in a nontrivial way, which clearly shows that statistical properties of the reconstructed observable depend essentially on the specific measurement scheme.

The basic characteristics of statistical properties of the observable  $A$  is provided by the mean value  $E(A)$  and the variance  $\text{Var}(A)$ . These two quantities can be easily found by differentiating the logarithm of the generating operator:

$$E(A) := \frac{1}{i} \frac{d}{d\lambda} \log \tilde{w}(\lambda) \Big|_{\lambda=0} = \sum_i \sum_n' a_n(\theta_i) p_n(\theta_i), \quad (7.9)$$

$$\begin{aligned} \text{Var}(A) &:= \frac{1}{i^2} \frac{d^2}{d\lambda^2} \log \tilde{w}(\lambda) \Big|_{\lambda=0} \\ &= \frac{1}{N} \left[ \sum_i \sum_n' a_n^2(\theta_i) p_n(\theta_i) - \sum_i \left( \sum_n' a_n(\theta_i) p_n(\theta_i) \right)^2 \right]. \end{aligned} \quad (7.10)$$

The statistical error is scaled with the inverse of the square root of the number of runs  $N$ . Let us note that the second component in the derived formula for  $\text{Var}(A)$  differs from that used in the

discussions of homodyne tomography in Refs. [50, 52], where it was equal just to  $[\mathbb{E}(A)]^2$ . This difference results from different assumptions about the local oscillator phase: in Refs. [50, 52] it was considered to be a uniformly distributed stochastic variable in order to avoid systematic errors, whereas we have assumed that the number of runs is fixed for each selected setting of the external parameters.

The goal of quantum state measurements is to retrieve the maximum amount of information on the quantum state available from the experimental data. Therefore the experimental histograms are usually processed many times in order to reconstruct a family of observables characterizing the quantum state. Of course, quantities determined from the same set of experimental data are not statistically independent, but in general exhibit correlations. The analysis presented above can be easily extended to the evaluation of any number of observables from the same sample of experimental data. If we restrict our attention to the basic, second-order characterization of these correlations, it is sufficient to discuss simultaneous determination of two observables. Let us suppose that in addition to  $A$ , another observable  $B$  has been calculated from the histograms  $\{k_n\}_{\theta_i}$  according to the formula:

$$B = \sum_i \sum_n' b_n(\theta_i) \left( \frac{k_n}{N} \right)_{\theta_i}. \quad (7.11)$$

The generating function  $\tilde{w}(\lambda, \mu)$  corresponding to the joint probability distribution  $w(A, B)$  can be found analogously to the calculations presented above. The final result is:

$$\begin{aligned} \tilde{w}(\lambda, \mu) &= \int dA dB e^{i\lambda A + i\mu B} w(A, B) \\ &= \prod_i \left( 1 + \sum_n' p_n(\theta_i) (e^{i\lambda a_n(\theta_i)/N + i\mu b_n(\theta_i)/N} - 1) \right)^N. \end{aligned} \quad (7.12)$$

The covariance between the experimentally determined values of  $A$  and  $B$  is given by:

$$\begin{aligned} \text{Cov}(A, B) &:= \frac{1}{i^2} \frac{d^2}{d\lambda d\mu} \log \tilde{w}(\lambda, \mu) \Big|_{\lambda, \mu=0} \\ &= \frac{1}{N} \sum_i \left[ \sum_n' a_n(\theta_i) b_n(\theta_i) p_n(\theta_i) - \left( \sum_n' a_n(\theta_i) p_n(\theta_i) \right) \left( \sum_m' b_m(\theta_i) p_m(\theta_i) \right) \right]. \end{aligned} \quad (7.13)$$

The covariance can be normalized to the interval  $[-1, 1]$  using  $\text{Var}(A)$  and  $\text{Var}(B)$ , which yields the correlation coefficient for the pair of observables  $A$  and  $B$ :

$$\text{Corr}(A, B) := \frac{\text{Cov}(A, B)}{\sqrt{\text{Var}(A)\text{Var}(B)}}. \quad (7.14)$$

This quantity defines whether the statistical deviations of  $A$  and  $B$  tend to have the same or opposite sign, which corresponds respectively to the positive or negative value of  $\text{Corr}(A, B)$ .

We have assumed that the histograms  $k_n$  have been measured for a finite number of external parameters settings  $\theta_i$ , which is always the case in an experiment. However, in some schemes the measurement of histograms is in principle necessary for all values of a continuous parameter. For example, in optical homodyne tomography the full information on the quantum state is contained in a family of quadrature distributions for all local oscillator phases. Restriction to a finite set of phases introduces a systematic error to the measurement [50, 70].

## 7.2 Phase-insensitive detection of a light mode

We will now apply the general formalism developed in the preceding section to the reconstruction of phase-independent properties of a single light mode. The basic advantage of this exemplary system is that it will allow us to discuss, in a very transparent way, pathologies resulting from the statistical uncertainty. All phase-independent properties of a single light mode are fully characterized by its photon number distribution  $\rho_\nu$ . Therefore, it is sufficient to apply a phase-insensitive technique to measure the photon statistics of the field. We will consider two measurement schemes that can be used for this purpose: direct photon counting and random phase homodyne detection.

The photon number distribution is given by the expectation value of a family of projection operators  $\hat{\rho}_\nu = |\nu\rangle\langle\nu|$ , where  $|\nu\rangle$  is the  $\nu$ th Fock state. In principle, knowledge of this distribution enables us to evaluate any phase-independent observable related to the measured field. A simple yet nontrivial observable, which we will use to point out difficulties with the completeness of the reconstructed information on the quantum state, is the parity operator:

$$\hat{\Pi} = \sum_{\nu=0}^{\infty} (-1)^\nu |\nu\rangle\langle\nu|. \quad (7.15)$$

This operator is bounded, and well defined on the complete Hilbert space of a single light mode. Its expectation value is given by the alternating series of the photon number distribution:

$$\langle \hat{\Pi} \rangle = \sum_{\nu=0}^{\infty} (-1)^\nu \langle \hat{\rho}_\nu \rangle, \quad (7.16)$$

which is absolutely convergent for any quantum state. Therefore, any pathologies connected to its determination from experimental data, if there appear any, cannot be ascribed to its singular analytical properties.

### 7.2.1 Direct photon counting

First, we will consider the reconstruction of phase insensitive properties of a single light mode from data measured using a realistic, imperfect photodetector. The positive operator-valued measure  $\hat{p}_n$  describing the probability of ejecting  $n$  photoelectrons from the detector is given by [71]:

$$\hat{p}_n = : \frac{(\eta \hat{a}^\dagger \hat{a})^n}{n!} \exp(-\eta \hat{a}^\dagger \hat{a}) :, \quad (7.17)$$

where  $\hat{a}$  is the annihilation operator of the light mode, and  $\eta$  is the quantum efficiency of the photodetector. In the limit  $\eta \rightarrow 1$  we get directly  $\hat{p}_n = |n\rangle\langle n|$ . In a general case, the probability distribution for the photoelectron number is related to the photon statistics via the Bernoulli transformation. This relation can be analytically inverted [15], which yields the expression:

$$\hat{\rho}_\nu = \sum_{n=0}^{\infty} r_{\nu n}^{(\eta)} \hat{p}_n, \quad (7.18)$$

where the kernel functions  $r_{\nu n}^{(\eta)}$  are given by:

$$r_{\nu n}^{(\eta)} = \begin{cases} 0, & n < \nu, \\ \frac{1}{\eta^\nu} \binom{n}{\nu} \left(1 - \frac{1}{\eta}\right)^{n-\nu}, & n \geq \nu. \end{cases} \quad (7.19)$$

The inversion formula has a remarkable property that  $\rho_\nu$  depends only on the “tail” of the photocount statistics for  $n \geq \nu$ . It has been shown that the inverse transformation can be applied to experimentally determined photocount statistics for an arbitrary state of the field, provided that the detection efficiency is higher than 50% [15].

We will now discuss statistical properties of the photon number distribution determined by photon counting within the general framework developed in Sec. 7.1. The case of perfect detection is trivial for statistical analysis. Therefore we will consider nonunit detection efficiency, which is numerically compensated in the reconstruction process using the inverse Bernoulli transformation according to Eq. (7.18). For all examples presented here, the efficiency is  $\eta = 80\%$ , which is well above the 50% stability limit.

In Fig. 7.1 we depict the reconstructed photon number distributions for a coherent state, a thermal state, and a squeezed vacuum state. The mean values  $E(\rho_\nu)$  along with their statistical errors  $[\text{Var}(\rho_\nu)]^{1/2}$  are compared with Monte Carlo realizations of a photon counting experiment, with the number of runs  $N = 4000$ . It is seen that for a thermal state and a squeezed vacuum state, the statistical error of the probabilities  $\rho_\nu$  grows unlimitedly with the photon number  $\nu$ . However, any experimental histogram obtained from a finite number of runs ends up for a certain count number, and therefore the reconstructed photon statistics is zero above this number. An important feature that is evidently seen in the Monte Carlo simulations, are correlations between the consecutive matrix elements. The reconstructed photon number distribution clearly

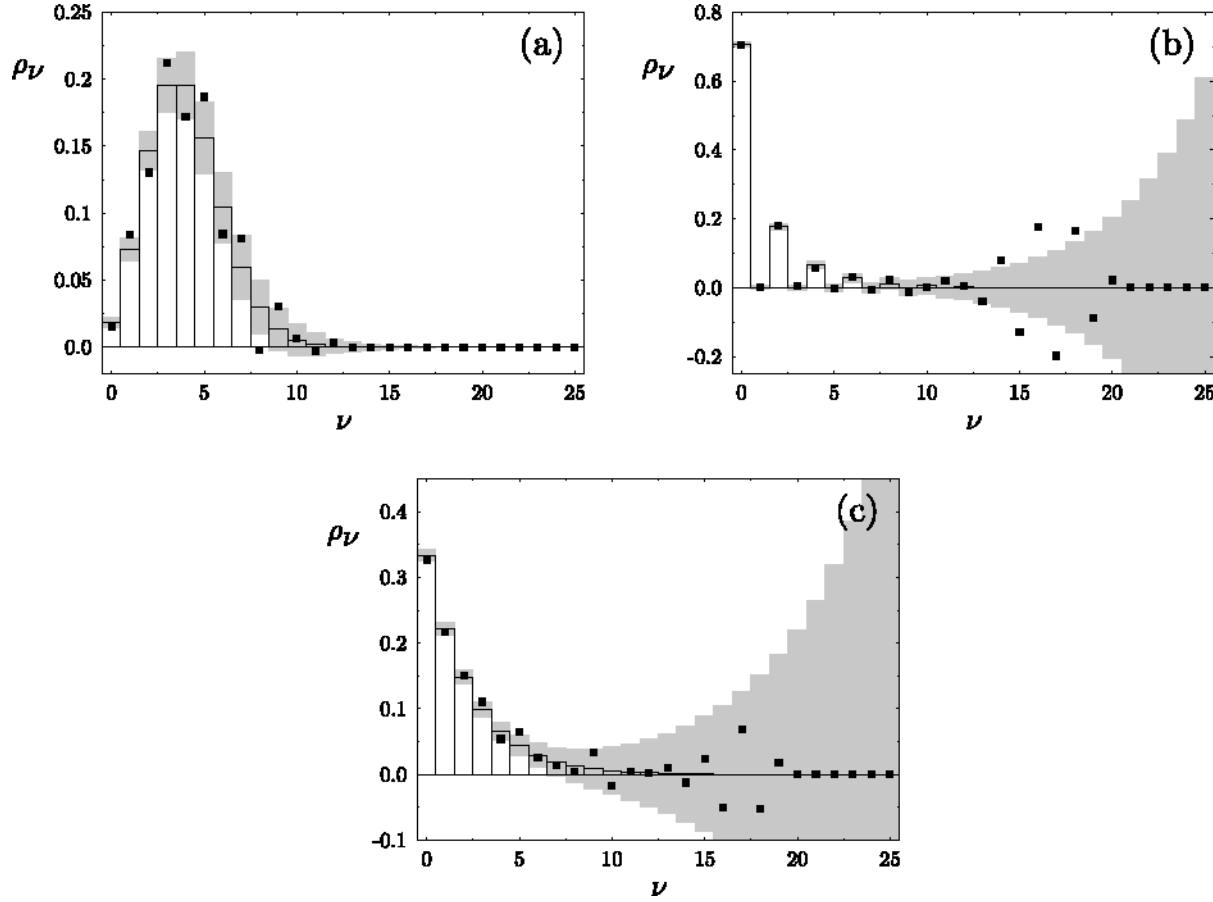


Figure 7.1: Reconstruction of the photon number distribution from photon counting for (a) a coherent state with  $\langle \hat{n} \rangle = 4$ , (b) a squeezed vacuum state with  $\langle \hat{n} \rangle = 1$ , and (c) a thermal state with  $\langle \hat{n} \rangle = 2$ , from  $N = 4000$  runs in each case. Monte Carlo simulations of a photon counting experiment, depicted with points, are compared with exact values (solid lines), with the statistical errors  $[\text{Var}(\rho_\nu)]^{1/2}$  marked as grey areas. The detection efficiency is  $\eta = 80\%$ .

exhibits oscillations around the true values. This property can be quantified using the correlation coefficient defined in Eq. (7.14), which we plot for all three states in Fig. 7.2. For large  $\nu$ 's,  $\text{Corr}(\rho_\nu, \rho_{\nu+1})$  is close to its minimum allowed value  $-1$ , which acknowledges that statistical correlations are indeed significant.

These correlations affect any quantity computed from the reconstructed photon number distribution. The parity operator is here a good example: since in Eq. (7.16) we sum up consecutive  $\rho_\nu$ 's with opposite signs, their statistical deviations do not add randomly, but rather contribute with the same sign. Consequently, the statistical error of the evaluated parity operator may be huge. It is therefore interesting to study this case in detail. In principle, we could obtain statistical properties of the reconstructed parity using the covariance matrix for the photon distribution.

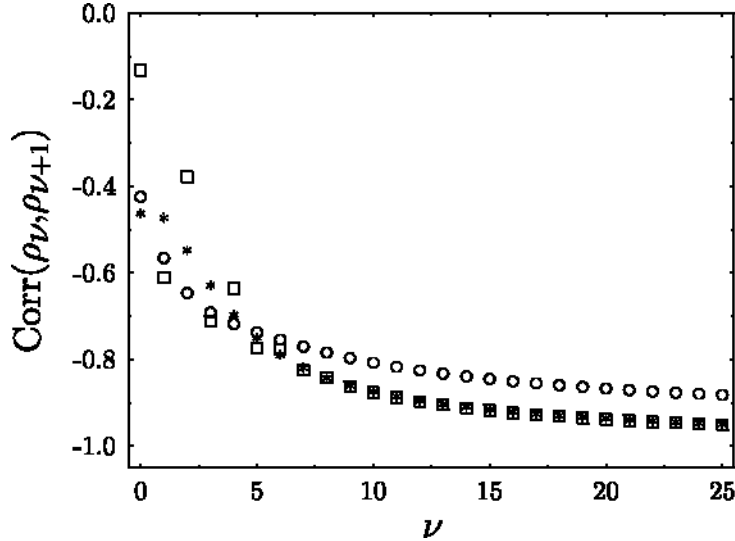


Figure 7.2: The correlation coefficient between the consecutive density matrix elements  $\text{Corr}(\rho_\nu, \rho_{\nu+1})$ , depicted for the coherent state ( $\circ$ ), the squeezed state ( $\square$ ), and the thermal state ( $*$ ) from Fig. 7.1.

However, it will be more instructive to express the parity directly in terms of the photocount statistics, and then to apply the statistical analysis to this reconstruction recipe. This route is completely equivalent to studying evaluation of the parity via the photon number distribution, as all transformations of the experimental data, which we consider here, are linear.

A simple calculation combining Eqs. (7.15) and (7.18) shows that:

$$\hat{\Pi} = \sum_{n=0}^K \left(1 - \frac{2}{\eta}\right)^n \hat{p}_n, \quad (7.20)$$

where we have introduced in the upper summation limit a cut-off parameter  $K$  for the photocount number. This formula clearly demonstrates pathologies related to the determination of the parity operator. For any  $\eta < 1$ , the factor  $(1 - 2/\eta)^n$  is not bounded, which makes the convergence of the whole series questionable in the limit  $K \rightarrow \infty$ . Of course, for an experimental histogram the summation is always finite, but the exploding factor amplifies contribution from the “tail” of the histogram, where usually only few events are recorded, and consequently statistical errors are significant.

Let us study these pathologies more closely using examples of a coherent state and a thermal state. For a coherent state  $|\alpha\rangle$ , both the expressions for  $E(\Pi)$  and  $\text{Var}(\Pi)$  are convergent with  $K \rightarrow \infty$ . However, the variance, given by the formula:

$$\text{Var}(\Pi^{\text{coh}}) = \frac{1}{N} \left[ \exp\left(\frac{4(1-\eta)}{\eta} |\alpha|^2\right) - \exp(-4|\alpha|^2) \right], \quad (7.21)$$

grows very rapidly with the coherent state amplitude  $\alpha$ , when the number of runs  $N$  is fixed. For a thermal state with the average photon number  $\bar{n}$ , the matter becomes more delicate. When

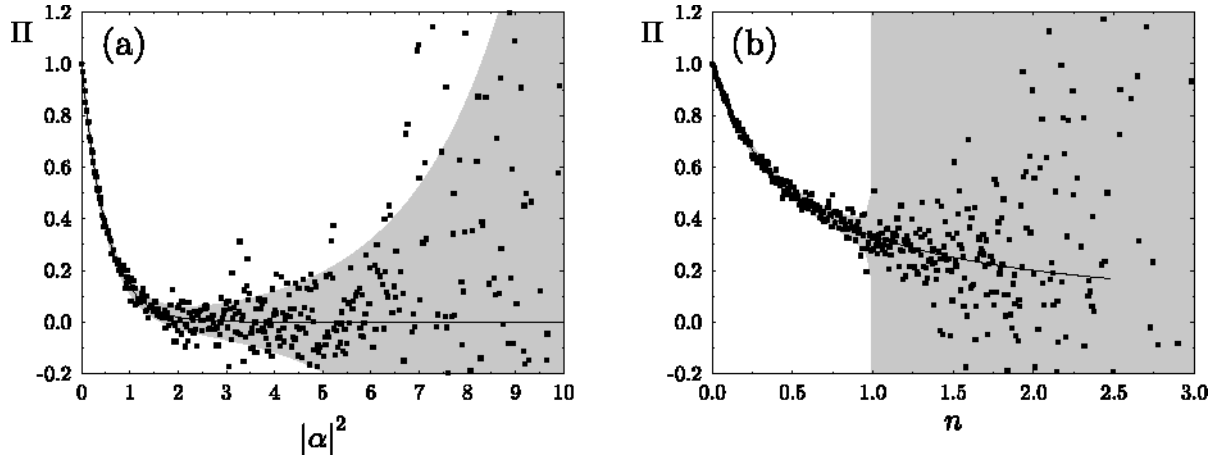


Figure 7.3: Determination of the parity operator for (a) coherent states and (b) thermal states with the increasing average photon number, assuming the photodetector efficiency  $\eta = 80\%$ . Each square represents the parity evaluated from Monte Carlo simulated photon statistics with  $N = 4000$  runs for a given average photon number. The solid lines and the grey areas depict the mean value  $E(\Pi)$  and the error  $[\text{Var}(\Pi)]^{1/2}$ . For thermal states, the variance diverges to infinity when  $\bar{n} \geq 1$ , and the mean value  $E(\Pi)$  does not exist above  $\bar{n} \geq 2.5$ .

$K \rightarrow \infty$ , the series (7.20) is convergent only for  $\bar{n} < 1/[2(1-\eta)]$ , which for  $\eta = 80\%$  gives just 2.5 photons. Even when the mean value exists, the variance is finite only for  $\bar{n} < \eta/[4(1-\eta)]$  and equals:

$$\text{Var}(\Pi^{\text{th}}) = \frac{1}{N} \left( \frac{\eta}{\eta - 4\bar{n}(1-\eta)} - \frac{1}{(1+2\bar{n})^2} \right). \quad (7.22)$$

We illustrate these results with Fig. 7.3, depicting Monte Carlo simulations for various average photon numbers. For coherent states, statistical fluctuations can in principle be suppressed by increasing the number of runs. For thermal states, the situation is worse: when  $\bar{n} \geq 1$ , the variance cannot even be used as a measure of statistical uncertainty.

Let us recall that the bound  $\eta > 50\%$  for the stability of the inverse Bernoulli transformation is independent of the state to be measured. It has been obtained from the requirement that in the limit  $K \rightarrow \infty$  both  $E(\rho_\nu)$  and  $\text{Var}(\rho_\nu)$  should converge [15]. The example with the parity operator clearly shows, that the condition  $\eta > 50\%$  does not guarantee that the reconstructed photon number distribution can be safely used to determine an arbitrary well-behaved phase independent observable. Thus, imperfect detection is inevitably connected with some loss of the information on the measured quantum state.

We have noted that as long as finite, experimental data are concerned, evaluation of observables via intermediate quantities is equivalent to expressing them directly in terms of the measured probability distributions. One might try to circumvent the  $\eta > 50\%$  bound for reconstructing the photon statistics by applying the inverse Bernoulli transformation in two or more

steps, and compensating in each step only a fraction of its inefficiency. Of course, such a strategy must fail, as for any finite sample of experimental data this treatment is equivalent to a single transformation which is unstable. In many-step processing this instability would be reflected in increasing correlations and statistical errors exploding to infinity.

### 7.2.2 Random phase homodyne detection

As we discussed in Sec. 3.4, random phase homodyne detection is a recently developed technique for measuring phase-independent properties of optical radiation, which goes beyond certain limitations of plain photon counting [55]. Data recorded in this scheme is the difference of counts on two photodetectors measuring superposition of the signal field with a strong coherent local oscillator. The count difference is rescaled by the local oscillator amplitude, and the resulting stochastic variable  $x$  can be treated with a good approximation as a continuous one. The photon number distribution is reconstructed from the random phase homodyne statistics  $p_{\mathcal{R}}(x)$  by integrating it with pattern functions  $f_{\nu}(x)$  [46, 47, 48]:

$$\langle \hat{\rho}_{\nu} \rangle = \int_{-\infty}^{\infty} dx f_{\nu}(x) p_{\mathcal{R}}(x). \quad (7.23)$$

A convenient method for numerical evaluation of the pattern functions has been described in Ref. [51].

Let us now discuss statistical properties of the homodyne scheme in its discretized version used in experiments, when the rescaled count difference is divided into finite width bins. As the local oscillator phase is random, the setup has no controllable parameters, and the statistics of the observables is fully determined by  $p_{\mathcal{R}}(x)$ . Statistical errors of the density matrix in the Fock basis reconstructed via homodyne detection have been studied in Ref. [50]. Here we will focus our attention on statistical correlations exhibited by the diagonal density matrix elements, and their further utilization for evaluating phase-independent observables.

We will consider the unit detection efficiency  $\eta = 1$ , with no compensation in the processing of the experimental data. This is the most regular case from the numerical point of view. When  $\eta < 1$  and the compensation is employed, the statistical errors are known to increase dramatically [50]. In Fig. 7.4 we depict the homodyne reconstruction of the photon number distribution for the three states discussed in the previous subsection. For large  $\nu$ , the statistical errors tend to a fixed value  $\sqrt{2/N}$ , which has been explained by D'Ariano *et al.* using the asymptotic form of the pattern functions [50]. Again, Monte Carlo simulations suggest that the reconstructed density matrix elements are correlated, which is confirmed by the correlation coefficient for the consecutive photon number probabilities, plotted in Fig. 7.5. A simple analytical calculation involving the asymptotic form of the pattern functions shows, that for large  $\nu$  this coefficient tends to its minimum value  $-1$ .

One may now expect that no subtleties can be hidden in using the reconstructed photon number distribution to evaluate the parity operator according to Eq. (7.16). However, let us

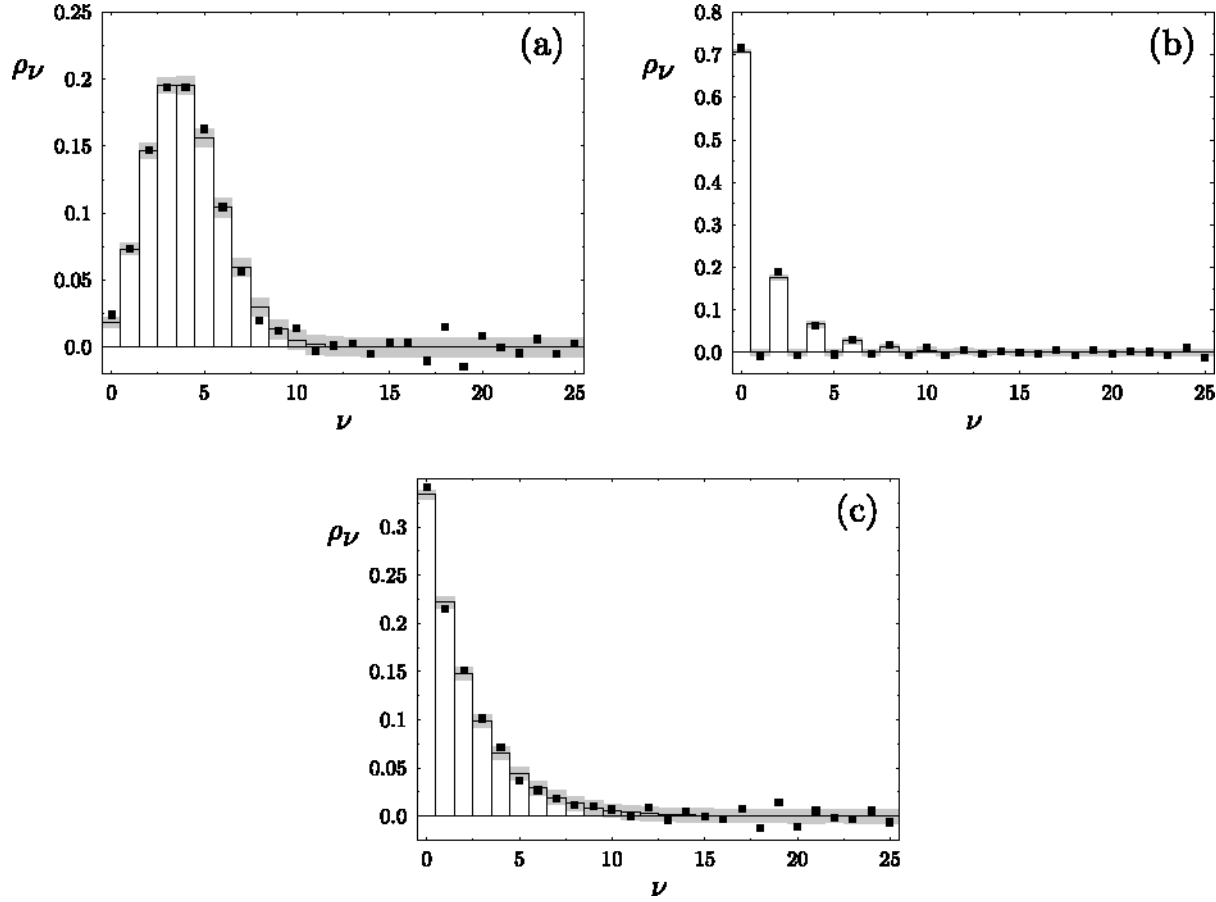


Figure 7.4: Random phase homodyne reconstruction of the photon number distribution for (a) the coherent state (b) the squeezed state and (c) the thermal state, all states with the same photon numbers as in Fig. 7.1. The range of the homodyne variable is restricted to the interval  $-6 \leq x \leq 6$  divided into 1200 bins. The simulated homodyne statistics is obtained from  $N = 4 \cdot 10^4$  Monte Carlo events.

recall that the parity operator is equal, up to a multiplicative constant, to the Wigner function at the phase space origin. The Wigner function is related to the homodyne statistics via the inverse Radon transformation, which is singular. In particular, applying this transformation for the phase space point  $(0, 0)$  we obtain the following expression for the parity operator in terms of the homodyne statistics [72]:

$$\langle \hat{\Pi} \rangle = \frac{1}{2} \int_{-\infty}^{\infty} dx p_{\mathcal{R}}(x) \frac{d}{dx} P \frac{1}{x}, \quad (7.24)$$

where  $P$  denotes the principal value. Due to the singularity of the inverse Radon transform, its application to experimental data has to be preceded by a special filtering procedure. This feature must somehow show up, when we evaluate the parity operator from the reconstructed photon

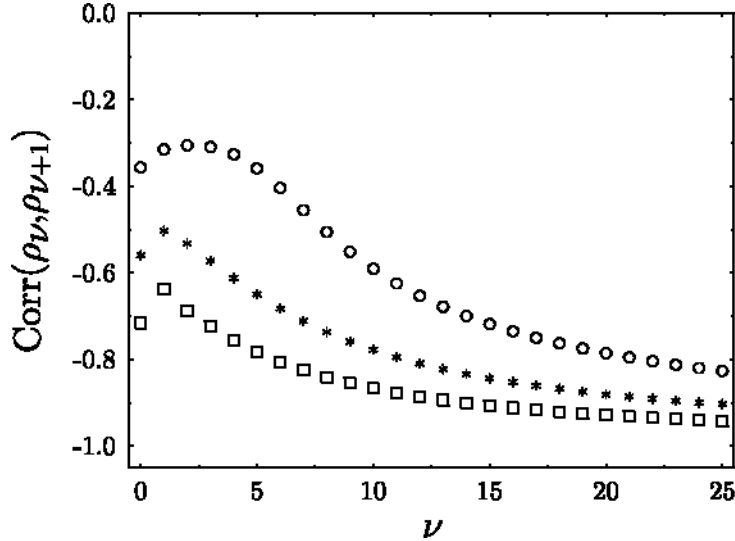


Figure 7.5: The correlation coefficient for the consecutive photon number probabilities for the coherent state ( $\circ$ ), the squeezed state ( $\square$ ) and the thermal state ( $*$ ).

statistics. In order to analyse this problem in detail let us discuss evaluation of the truncated parity operator  $\hat{\Pi}_K$  from a finite part of the photon number distribution:

$$\langle \hat{\Pi}_K \rangle = \sum_{\nu=0}^K (-1)^\nu \langle \hat{\rho}_\nu \rangle = \int_{-\infty}^{\infty} g_K(x) p(x), \quad (7.25)$$

where

$$g_K(x) = \sum_{\nu=0}^K (-1)^\nu f_\nu(x) \quad (7.26)$$

can be considered to be a regularized kernel function for the parity operator. In Fig. 7.6 we plot this function for increasing values of the cut-off parameter  $K$ . It is seen that the singularity of the kernel function in the limit  $K \rightarrow \infty$  is reflected by an oscillatory behaviour around  $x = 0$  with growing both the amplitude and the frequency. This amplifies the statistical uncertainty of the experimental homodyne data. In Fig. 7.7 we show determination of the parity operator for the three states discussed before, using increasing values of the cut-off parameter  $K$ . Though we are in the region where the true photon number distribution is negligibly small, addition of subsequent matrix elements increases the statistical error in an approximately linear manner. This is easily understood, if we look again at the reconstructed photon number distributions: increasing  $K$  by one means a contribution of the order of  $\sqrt{2/N}$  added to the statistical uncertainty, and, moreover, these contributions tend to have the same sign due to correlations between the consecutive matrix elements. Thus, determination of the parity operator from homodyne statistics requires an application of a certain regularization procedure. It may be either the filtering

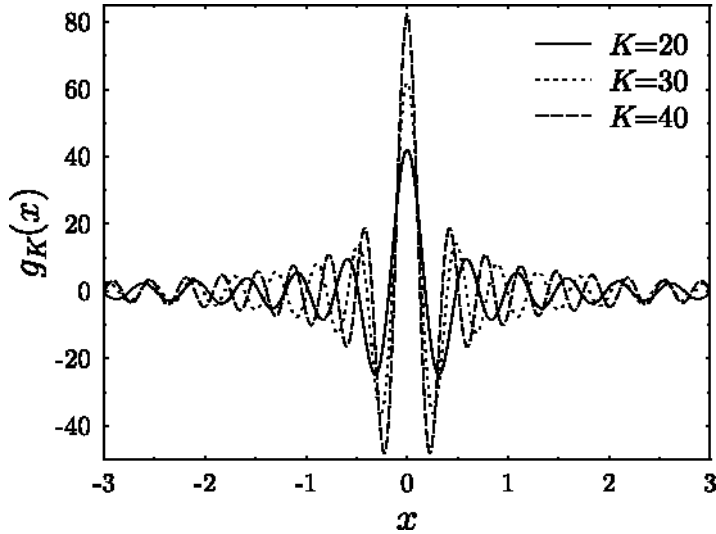


Figure 7.6: Regularized kernel functions for the parity operator  $g_K(x)$  evaluated as a finite sum of the Fock states pattern functions, for increasing values of the cut-off parameter  $K$ .

used in tomographic back-projection algorithms, or the cut-off of the photon number distribution. The statistical uncertainty of the final outcome is eventually a result of an interplay between the number of experimental runs and the applied regularization scheme.

Finally, let us briefly comment on the compensation for the nonunit efficiency of the homodyne detector. First, one might think of applying a two-mode inverse Bernoulli transformation directly to the joint count statistics on the detectors. However, it is impossible in the homodyne scheme to resolve contributions from single absorbed photons due to high intensity of the detected fields. The inverse Bernoulli transformation has no continuous limit, as consecutive count probabilities are added with opposite signs. Nevertheless, the nonunit detection efficiency can be taken into account in the pattern functions [47, 48]. In this case the statistical errors increase dramatically, and explode with  $\nu \rightarrow \infty$ , which makes determination of the parity operator even more problematic. This is easily understood within the phase space picture: the distributions measured by an imperfect homodyne detector are smeared-out by a convolution with a Gaussian function [35, 45]. Evaluation of the parity operator, or equivalently, the Wigner function at the phase space origin requires application of a deconvolution procedure, which enormously amplifies the statistical error [73].

### 7.3 Consequences for quantum state measurement

We have presented a complete statistical analysis of determining quantum observables in optical measurement schemes based on photodetection. We have derived an exact expression for the

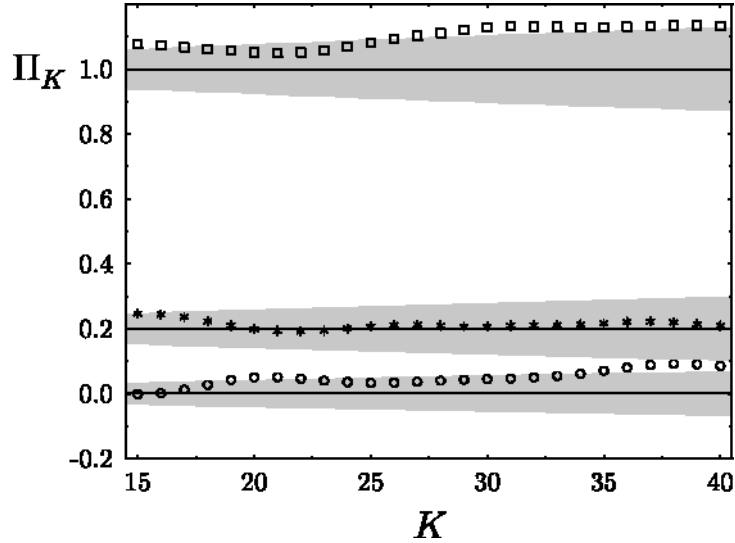


Figure 7.7: Reconstruction of the truncated parity operator  $\hat{\Pi}_K$  for the coherent state ( $\circ$ ), the squeezed state ( $\square$ ), and the thermal state ( $*$ ) with various values of the cut-off parameter  $K$ , using the same Monte Carlo homodyne statistics as in Fig. 7.4. The simulations are compared with the corresponding mean values  $E(\Pi_K)$  and errors  $[\text{Var}(\Pi_K)]^{1/2}$  plotted as solid lines surrounded by grey areas.

generating function characterizing statistical moments of the reconstructed observables, which, in particular, provides formulae for statistical errors and correlations between the determined quantities. These general results have been applied to the detection of phase-independent properties of a single light mode using two schemes: direct photon counting, and random phase homodyne detection. This study has revealed difficulties related to the completeness of the reconstructed information on the quantum state: in some cases the parity observable, which is a well-behaved bounded operator, effectively cannot be evaluated from the reconstructed data due to the exploding statistical error.

We have recalled that the parity operator is directly related to the value of the Wigner function at the phase space origin. Thus, our example can also be interpreted as a particular case of the transformation between two representations of the quantum state: in fact, we have considered evaluation of the Wigner function at a specific point  $(0, 0)$  from the relevant elements of the density matrix in the Fock basis. Therefore, our discussion exemplifies subtleties related to the transition between various quantum state representations, when we deal with data reconstructed in experiments. Though a certain representation can be determined with the statistical uncertainty which seems to be reasonably small, it effectively cannot be converted to another one due to accumulating statistical errors.

The presented study suggests that the notion of completeness in quantum state measurements should inherently take into account the statistical uncertainty. From a theoretical point of view, the quantum state can be characterized in many different ways which are equivalent as long as

expectation values of quantum operators are known with perfect accuracy. In a real experiment, however, we always have to keep in mind the specific experimental scheme used to perform the measurement. This scheme defines statistical properties of the reconstructed quantities, and may effectively limit the available information on the quantum state. Determination of a family of observables does not automatically guarantee the feasibility of reconstructing the expectation value of an arbitrary well behaved operator. Reconstruction of any observable should be preceded by an analysis how significantly the final result is affected by statistical noise corrupting the raw experimental data.



# Chapter 8

## Conclusions

In this thesis, we have developed a direct method for measuring quasidistribution functions of light. Quasidistribution functions provide a complete characterization of the quantum state in the form which is analogous to a classical phase space distribution. We have shown that quasidistributions, in particular the Wigner function, can be determined using an optical scheme based on photon counting. We have reported an experimental realisation of this scheme, and presented measurements of the Wigner function for several classical-like states.

There is a wide range of problems arising from a closer look at various aspects of the proposed scheme. We have discussed the deleterious effects of imperfect detection, and shown that they cannot be in general compensated in numerical processing of the experimental data. Further, we have developed a general multimode theory of the scheme, and extended the principle of the measurement to multimode quasidistributions. The developed multimode theory has been a useful tool in studying the role of experimental imperfections. We have also seen that in order to analyse the feasibility of the measurement, it is necessary to take into account the statistical uncertainty. We have derived estimates for the statistical error, and shown that in some cases the statistical noise effectively limits available information on the quantum state.

The field of quantum state measurement is continuously developing. Currently, an interesting direction of research is related to fundamental aspects of retrieving information on the quantum state. Generally, our source of information on the quantum state is the result of a measurement performed on an ensemble of a finite number of copies. From these data we want to infer the quantum state of the ensemble. The inference can be performed in different ways, based on various statistical methodologies. Throughout this thesis, we have used the linear approach, where quantum probability distributions are estimated by relative frequency histograms. This is the most straightforward and so far the most commonly used strategy, but it is not necessarily the most efficient one. Recently, other approaches to data processing have been proposed, based on the maximum entropy principle [74], the least-squares inversion [75], and the maximum-likelihood estimation [76, 57, 77, 78]. These methods enhance the amount of information which can be obtained from a realistic measurement. From a more fundamental point of view, one

may ask what is the ultimate bound for estimating the quantum state from finite ensembles. This question can be reformulated as a problem of designing the optimal quantum state measurement on finite ensembles. Such a problem is in general extremely difficult, and so far it has been studied only in selected yet highly nontrivial cases [79, 80, 81]. The optimal strategy has been shown to be of the form of a collective measurement performed jointly on all the available copies.

The research on quantum state measurement significantly contributes to the understanding of the foundations of quantum theory. Quantum mechanics still unveils surprising consequences of its principles. An important recent example is the observation that quantum mechanics opens up completely new ways of processing, storing, and transmitting information. Exploration of these possibilities can result in novel information technologies, such as quantum computing [6] and quantum cryptography [82, 83]. Some issues in quantum state measurement are shared with the quantum information theory, for example methods of quantum estimation and the effect of decoherence. On the other hand, quantum information technologies need carefully prepared quantum systems, and measuring the quantum state is here an indispensable diagnostic tool. With no doubt, the field of quantum state measurement plays a prominent role at the forefront of contemporary physics.

# Bibliography

- [1] M. Born, *Quantenmechanik der Stossvorgänge*, Z. Phys. **38**, 803 (1926).
- [2] W. Heisenberg, *The Physical Properties of the Quantum Theory* (Dover, New York, 1930).
- [3] W. K. Wootters and W. H. Zurek, *A single quantum cannot be cloned*, Nature **299**, 802 (1982).
- [4] R. N. Zare, *Laser control of chemical reactions*, Science **279**, 1875 (1998).
- [5] D. F. Walls and G. J. Milburn, *Quantum Optics* (Springer Verlag, Berlin, 1994), Chap. 8.
- [6] D. Deutsch and A. Ekert, *Quantum computation*, Phys. World **11**(3), 47 (1998).
- [7] D. T. Smithey, M. Beck, M. G. Raymer, and A. Faridani, *Measurement of the Wigner Distribution and the Density Matrix of a Light Mode Using Optical Homodyne Tomography: Application to Squeezed States and the Vacuum*, Phys. Rev. Lett. **70**, 1244 (1993).
- [8] M. Freyberger, P. Bardroff, C. Leichtle, G. Schrade, and W. Schleich, *The art of measuring quantum states*, Phys. World **10**(11), 14 (1997).
- [9] T. J. Dunn, I. A. Walmsley, and S. Mukamel, *Experimental determination of the quantum-mechanical state of a molecular vibrational mode using fluorescence tomography*, Phys. Rev. Lett. **74**, 884 (1995).
- [10] G. Breitenbach, S. Schiller, and J. Mlynek, *Measurement of the quantum states of squeezed light*, Nature **387**, 471 (1997).
- [11] D. Leibfried, D. M. Meekhof, B. E. King, C. Monroe, W. M. Itano, and D. J. Wineland, *Experimental determination of the motional quantum state of a trapped atom*, Phys. Rev. Lett. **77**, 4281 (1996).
- [12] C. Kurtsiefer, T. Pfau, and J. Mlynek, *Measurement of the Wigner function of an ensemble of helium atoms*, Nature **386**, 150 (1997).

- [13] E. P. Wigner, *On the quantum correction for thermodynamic equilibrium*, Phys. Rev. **40**, 749 (1932).
- [14] M. Hillery, R. F. O'Connell, M. O. Scully, and E. P. Wigner, *Distribution functions in physics: Fundamentals*, Phys. Rep. **106**, 121 (1984).
- [15] T. Kiss, U. Herzog, and U. Leonhardt, *Compensation of losses in photodetection and in quantum-state measurements*, Phys. Rev. A **52**, 2433 (1995).
- [16] G. M. D'Ariano and C. Macchiavello, *Loss-error compensation in quantum-state measurements*, Phys. Rev. A **57**, 3131 (1998).
- [17] T. Kiss, U. Herzog, and U. Leonhardt, *Reply to “Loss-error compensation in quantum-state measurements”*, Phys. Rev. A **57**, 3134 (1998).
- [18] L. G. Lutterbach and L. Davidovich, *Method for direct measurement of the Wigner function in cavity QED and ion traps*, Phys. Rev. Lett. **78**, 2547 (1997).
- [19] L. Davidovich, M. Orszag, and N. Zagury, *Quantum diagnosis of molecules: A method for measuring directly the Wigner function of a molecular vibrational state*, Phys. Rev. A **57**, 2544 (1998).
- [20] H. Weyl, *Quantenmechanik and Gruppentheorie*, Z. Phys. **46**, 1 (1927).
- [21] K. E. Cahill and R. J. Glauber, *Density Operators and Quasiprobability Distributions*, Phys. Rev. **177**, 1882 (1969).
- [22] R. J. Glauber, *Photon correlations*, Phys. Rev. Lett. **10**, 84 (1963).
- [23] E. C. G. Sudarshan, *Equivalence of semiclassical and quantum mechanical descriptions of statistical light beams*, Phys. Rev. Lett. **10**, 277 (1963).
- [24] K. Husimi, Proc. Phys. Math. Soc. Japan **22**, 264 (1940).
- [25] Y. Kano, *A new phase-space distribution function in the statistical theory of the electromagnetic field*, J. Math. Phys. **6**, 1913 (1965).
- [26] C. L. Mehta and E. C. G. Sudarshan, *Relation between quantum and semiclassical description of optical coherence*, Phys. Rev. **138**, B274 (1965).
- [27] W. H. Louisell, *Quantum Statistical Properties of Radiation* (Wiley, New York, 1973), Chap. 3.
- [28] B.-G. Englert, *On the operator bases underlying Wigner's, Kirkwood's and Glauber's phase space functions*, J. Phys. A **22**, 625 (1989).

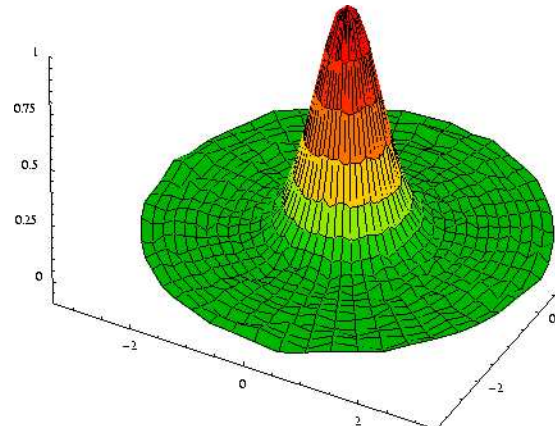
- [29] H. Moya-Cessa and P. L. Knight, *Series representation of quantum-field quasiprobabilities*, Phys. Rev. A **48**, 2479 (1993).
- [30] L. Mandel, *Photoelectric counting measurement as a test for the existence of photons*, J. Opt. Soc. Am. **67**, 1101 (1977).
- [31] W. Schleich, M. Pernigo, and F. L. Kien, *Nonclassical state from two pseudoclassical states*, Phys. Rev. A **44**, 2172 (1991).
- [32] V. Bužek and P. L. Knight, in *Progress in Optics XXXIV*, edited by E. Wolf (North-Holland, Amsterdam, 1995).
- [33] N. G. Walker and J. E. Carroll, *Multiport homodyne detection near the quantum noise limit*, Opt. Quant. Electron. **18**, 355 (1986).
- [34] S. L. Braunstein, *Homodyne statistics*, Phys. Rev. A **42**, 474 (1990).
- [35] W. Vogel and J. Grabow, *Statistics of difference events in homodyne detection*, Phys. Rev. A **47**, 4227 (1993).
- [36] K. Banaszek and K. Wódkiewicz, *Operational theory of homodyne detection*, Phys. Rev. A **55**, 3117 (1997).
- [37] W. Vogel and D.-G. Welsch, *Lectures on Quantum Optics* (Akademie Verlag, Berlin, 1994), Chap. 6.
- [38] K. Wódkiewicz, *Operational approach to phase-space measurements in quantum mechanics*, Phys. Rev. Lett. **52**, 1064 (1984).
- [39] S. Stenholm, *Simultaneous measurement of conjugate variables*, Ann. Phys. (N.Y.) **218**, 233 (1992).
- [40] N. G. Walker, *Quantum theory of multiport optical homodyning*, J. Mod. Opt. **34**, 15 (1987).
- [41] J. W. Noh, A. Fougères, and L. Mandel, *Measurement of the quantum phase by photon counting*, Phys. Rev. Lett. **67**, 1426 (1991).
- [42] M. Freyberger and W. Schleich, *Photon counting, quantum phase, and phase-space distributions*, Phys. Rev. A **47**, R30 (1993).
- [43] U. Leonhardt and H. Paul, *Phase measurement and Q function*, Phys. Rev. A **47**, R2460 (1993).
- [44] H. H. Barrett, in *Progress in Optics XXI*, edited by E. Wolf (North-Holland, Amsterdam, 1984).

- [45] U. Leonhardt and H. Paul, *Realistic optical homodyne measurements and quasiprobability distributions*, Phys. Rev. A **48**, 4598 (1993).
- [46] G. M. D'Ariano, C. Macchiavello, and M. G. A. Paris, *Detection of the density matrix through optical homodyne tomography without filtered back projection*, Phys. Rev. A **50**, 4298 (1994).
- [47] G. M. D'Ariano, U. Leonhardt, and H. Paul, *Homodyne detection of the density matrix of the radiation field*, Phys. Rev. A **52**, R1801 (1995).
- [48] U. Leonhardt, H. Paul, and G. M. D'Ariano, *Tomographic reconstruction of the density matrix via pattern functions*, Phys. Rev. A **52**, 4899 (1995).
- [49] G. M. D'Ariano, C. Macchiavello, and M. G. A. Paris, *Precision of quantum tomographic detection of radiation*, Phys. Lett. **A195**, 31 (1994).
- [50] G. M. D'Ariano, C. Macchiavello, and N. Sterpi, *Systematic and statistical errors in homodyne measurements of the density matrix*, Quantum Semiclass. Opt. **9**, 929 (1997).
- [51] U. Leonhardt, M. Munroe, T. Kiss, T. Richter, and M. G. Raymer, *Sampling of photon statistics and density matrix using homodyne detection*, Opt. Comm. **127**, 144 (1996).
- [52] G. M. D'Ariano and M. G. A. Paris, *Added noise in homodyne measurement of field observables*, Phys. Lett. **A233**, 49 (1997).
- [53] G. Breitenbach, T. Müller, S. F. Pereira, J.-P. Poizat, S. Schiller, and J. Mlynek, *Squeezed vacuum from a monolithic optical parametric oscillator*, J. Opt. Soc. Am. B **12**, 2304 (1995).
- [54] B. Eppich, *Complete characterization of partially coherent 2D beams*, preprint.
- [55] M. Munroe, D. Boggavarapu, M. E. Anderson, and M. G. Raymer, *Photon-number statistics from phase-averaged quadrature-field distribution: Theory and ultrafast measurement*, Phys. Rev. A **52**, R924 (1995).
- [56] S. Schiller, G. Breitenbach, S. F. Pereira, T. Müller, and J. Mlynek, *Quantum Statistics of the Squeezed Vacuum by Measurement of the Density Matrix in the Number State Representation*, Phys. Rev. Lett. **77**, 2933 (1996).
- [57] K. Banaszek, *Maximum-likelihood estimation of photon number distribution from homodyne statistics*, Phys. Rev. A **57**, 5013 (1998).
- [58] A. Royer, *Wigner function as the expectation value of a parity operator*, Phys. Rev. A **15**, 449 (1977).

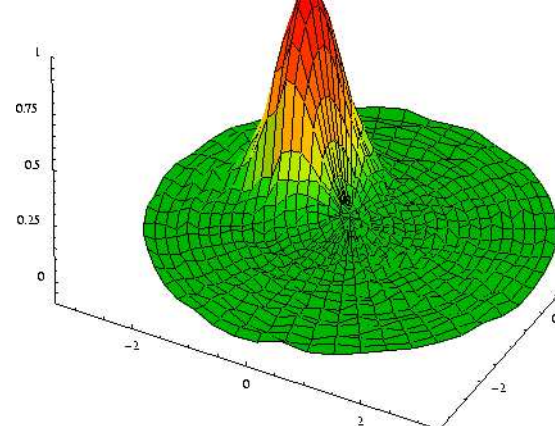
- [59] P. G. Kwiat, A. M. Steiberg, R. Y. Chiao, P. H. Eberhard, and M. D. Petroff, *High-efficiency single-photon detectors*, Phys. Rev. A **48**, R867 (1993).
- [60] W. T. Eadie, D. Drijard, F. E. James, M. Roos, and B. Sadoulet, *Statistical Methods in Experimental Physics* (North-Holland, Amsterdam, 1971), Chap. 4.
- [61] D. M. Meekhof, C. Monroe, B. E. King, W. M. Itano, and D. J. Wineland, *Generation of Nonclassical Motional States of a Trapped Atom*, Phys. Rev. Lett. **76**, 1796 (1996).
- [62] Z. Kis, T. Kiss, J. Janszky, P. Adam, S. Wallentowitz, and W. Vogel, *Local sampling of phase-space distributions by cascaded optical homodyning*, Phys. Rev. A **59**, R39 (1999).
- [63] K. Banaszek and K. Wódkiewicz, *Testing Quantum Nonlocality in Phase Space*, Phys. Rev. Lett. **82**, 2009 (1999).
- [64] P. J. Bardsroff, E. Mayr, and W. P. Schleich, *Quantum state endoscopy: Measurement of the quantum state in a cavity*, Phys. Rev. A **51**, 4963 (1995).
- [65] H. Paul, P. Törmä, T. Kiss, and I. Jex, *Photon chopping: new way to measure the quantum state of light*, Phys. Rev. Lett. **76**, 2464 (1996).
- [66] A. Zucchetti, W. Vogel, M. Tasche, and D.-G. Welsch, *Direct sampling of density matrices in field-strength bases*, Phys. Rev. A **54**, 1678 (1996).
- [67] M. G. Raymer, D. F. McAlister, and U. Leonhardt, *Two-mode quantum-optical state measurement: Sampling the joint density matrix*, Phys. Rev. A **54**, 2397 (1996).
- [68] K. Jacobs, P. L. Knight, and V. Vedral, *Determining the state of a single cavity mode from photon statistics*, J. Mod. Opt **44**, 2427 (1997).
- [69] W. Vogel and D.-G. Welsch, *Lectures on Quantum Optics* (Akademie Verlag, Berlin, 1994).
- [70] U. Leonhardt and M. Munroe, *Number of phases required to determine a quantum state in optical homodyne tomography*, Phys. Rev. A **54**, 3682 (1996).
- [71] P. L. Kelley and W. H. Kleiner, *Theory of Electromagnetic Field Measurement and Photo-electron Counting*, Phys. Rev. **136**, A316 (1964).
- [72] U. Leonhardt and I. Jex, *Wigner functions and quadrature distributions for quantum-oscillator states with random phase*, Phys. Rev. A **49**, R1555 (1994).
- [73] U. Leonhardt and H. Paul, *Can a Wigner function be reconstructed from experimentally determined distributions?*, J. Mod. Opt. **41**, 1427 (1994).

- [74] V. Bužek, G. Adam, and G. Drobny, *Quantum state reconstruction and detection of quantum coherences on different observation levels*, Phys. Rev. A **54**, 804 (1996).
- [75] T. Opatrný, D.-G. Welsch, and W. Vogel, *Least-squares inversion for density-matrix reconstruction*, Phys. Rev. A **56**, 1788 (1997).
- [76] Z. Hradil, *Quantum-state estimation*, Phys. Rev. A **55**, R1561 (1997).
- [77] K. Banaszek, *Quantum homodyne tomography with a priori constraints*, Phys. Rev. A **59**, 4797 (1999).
- [78] K. Banaszek, G. M. D'Ariano, M. G. A. Paris, and M. F. Sacchi, *Maximum-likelihood estimation of the density matrix*, preprint quant-ph/9909052.
- [79] S. Massar and S. Popescu, *Optimal extraction of information from finite quantum ensembles*, Phys. Rev. Lett. **74**, 1259 (1995).
- [80] R. Derka, V. Bužek, and A. K. Ekert, *Universal algorithm for optimal estimation of quantum states from finite ensembles via realizable generalized measurement*, Phys. Rev. Lett. **80**, 1571 (1998).
- [81] G. Vidal, J. I. Latorre, P. Pascual, and R. Tarrach, *Optimal minimal measurements of mixed states*, Phys. Rev. A **60**, 126 (1999).
- [82] R. J. Hughes, D. M. Alde, P. Dyer, G. G. Luther, G. L. Morgan, and M. Schauer, *Quantum cryptography*, Contemporary Physics **36**, 149 (1995).
- [83] S. J. D. Phoenix and P. D. Townsend, *Quantum cryptography: how to beat the code breakers using quantum mechanics*, Contemporary Physics **36**, 165 (1995).

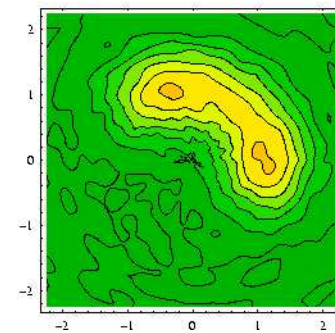
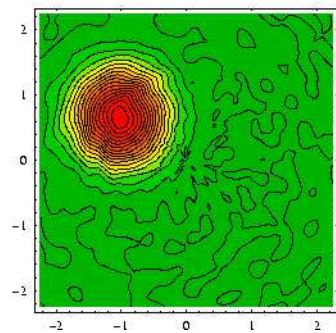
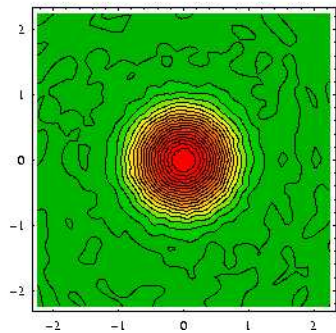
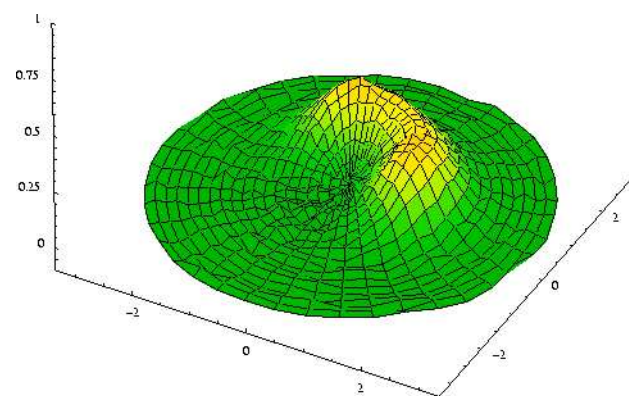
**(a) Vacuum state**



**(b) Coherent state**



**(c) Phase diffused coherent state**



The measured Wigner functions for (a) the vacuum, (b) a weak coherent state with approximately one photon, and (c) a phase diffused coherent state. The photon statistics was collected on a polar grid spanned by 20 amplitudes, and 50 phases for the plots (a) and (b), or 40 phases for the plot (c). The duration of a single counting interval was  $40 \mu\text{s}$  for (a) and (b) and  $30 \mu\text{s}$  for (c). The measurements were performed for slightly different laser intensities, and the radial coordinate for each of the graphs was scaled separately.